ANL/EBR-070

POSTIRRADIATION EXAMINATION OF HIGHER-WORTH CONTROL RODS L-4008S and L-4009S

by

L. C. Walters, M. T. Laug, W. E. Ruther, and H. A. Taylor, Jr.

EBR-II Project
Argonne National Laboratory
Argonne, Illinois - Idaho Falls, Idaho

May 1973

TABLE OF CONTENTS

LIST OF FIGURES

LIST OF TABLES

POSTIRRADIATION EXAMINATION OF HIGHER-WORTH CONTROL RODS L-4008S and L-4009S

by

L. C. Walters, M. T. Laug, W. E. Ruther, and H. A. Taylor

ABSTRACT

Two higher-worth control rods (HWCR's) whose Mark-IA fuel had reached maximum burnups of 1.44 and 1.80 at.% were examined as part of the program for qualifying future use of HWCR's to a Mark-IA fuel burnup limit of 1.8 at.% in EBR-II. No galling or chafing was found on the capsules containing the B_4C pellets, no additional stress was imposed on the capsule cladding by swelling of the pellets, and no significant interaction of the pellets and the cladding took place. The pellets retained most of the helium generated by ^{10}B burnup, so the additional stress produced from release of helium was negligible.

I. INTRODUCTION

The EBR-II reactor was originally designed to use 12 control rods. In the design configuration, the 12 control rods alternated with driver-fuel subassemblies in the 24 core positions of row 5. A drive mechanism for each control rod penetrates the primary-tank cover and the reactor-vessel cover. Since these penetrations offer the only direct access to the core, the control-rod positions have become attractive locations for instrumented subassemblies and other special equipment that requires external monitoring and control.

To satisfy the EBR-II operating limits, at least 10 control rods of the original design must be in the core. In order to free more control-rod positions for use with instrumented subassemblies, a new higher-worth control rod (HWCR) was designed[1]. The main requirement for the new higher-worth control rod was to provide a greater variation in reactivity between

the full-in and full-out positions. The design that fulfilled this requirement has a lower section of 61 Mark-IA fuel elements and an upper section of seven capsules containing B_4C pellets. This design for a higher-worth control rod has the advantage over an all-poison control rod of causing a smaller perturbation in neutron flux for the adjacent subassemblies.

The operating limit of the higher-worth control rod is fixed by the burnup limit for the Mark-IA fuel, which is 1.8 at.%. Thus, all components of the HWCR must be proven to perform satisfactorily at least to the Mark-IA fuel burnup limit. Two prototype HWCR's were fabricated and inserted sequentially into the core of EBR-II. The first HWCR, designated L-4008S, was put into the reactor on Oct. 7, 1970, in grid position 5A3. On Feb. 2, 1971, this HWCR was moved to grid position 5C1, and on July 13, 1971, it was removed from the reactor core. The total exposure was 5,472 MWd with a maximum Mark-IA fuel burnup of 1.44 at.%. The second HWCR, designated L-4009S, was put in grid position 5C1 on July 13, 1971, and was removed from the reactor core on March 27, 1972. The total exposure was 6,804 MWd with a maximum Mark-IA fuel burnup of 1.80 at.%.

The in-reactor operating-temperature profiles for the B_4C portion of an HWCR have been calculated[2]. For the bottoms of the capsules that contained the B_4C pellets (i.e., the region nearest the core center) the cladding inside-diameter temperature, the B_4C pellet surface temperature, and the B_4C pellet centerline temperature were 1010°F, 1070°F, and 1120°F, respectively. For the tops of the capsules (i.e., the region farthest from the core center) the cladding inside-diameter temperature, the B_4C pellet surface temperature, and the B_4C pellet centerline temperature were 1006°F, 1017°F, and 1027°F, respectively.

The objective of the postirradiation examinations of HWCR's L-4008S and L-4009S was to gain the information required to qualify future use of HWCR's in EBR-II up to the Mark-IA fuel burnup limit of 1.8 at.%. For this goal, the following examinations were essential:

(1) A careful visual examination of the Type 304L stainless steel capsules that contained the B_4C pellets. The anticipated result of this observation was to determine if galling or chafing of the capsules had occurred.

(2) A determination of the increase in helium pressure in the Type 304L stainless steel capsules that contained the B_4C pellets. The reason for this determination was to ascertain if the increase in helium pressure would impose unacceptable stresses on the capsules.

(3) A determination of the dimensional change of the B_4C pellets due to irradiation-induced swelling. These measurements would show whether or not the B_4C swelling was sufficient to close the gap between the B_4C pellet and the capsule wall and thus produce additional stresses on the capsules.

(4) An examination of metallographic specimens from the Type 304L stainless steel capsule to determine the extent of interaction between the B_4C and the stainless steel. The reason for this study was to ascertain if the cladding integrity was maintained during irradiation.

(5) An examination of the compatibility of the irradiated B_4C pellets with liquid sodium. The purpose was to ascertain the extent to which B_4C could be transferred to the primary sodium in the event of a capsule breach.

The procedures and results obtained from the above examinations are discussed in detail in this report. Capsules that contained the B_4C pellets from HWCR L-4008S were also shipped to WADCO and ORNL for examination. The results obtained by these laboratories are discussed and compared with those obtained by ANL. One reason for the amount of detail in the present report is to serve as an aid in future surveillance examinations of HWCR's.

II. DESCRIPTION OF HIGHER-WORTH CONTROL RODS

Figure 1 is a drawing of the higher-worth control-rod subassembly. The fueled portion of the control rod contains 61 Mark-IA fuel elements arranged in a hexagonal array. The space above the fuel contains seven Type 304L stainless steel capsules that are 36-3/32 in. long. Each of the seven capsules contains a 14-in. stack of 1-in.-long natural-B_4C pellets. Figure 2 shows details of the capsule that contains the B_4C. Above the B_4C pellets is a 1-3/8-in.-long Inconel spring, and above the spring is an 8-in.-long stainless steel shield plug. The shield plug is welded in place

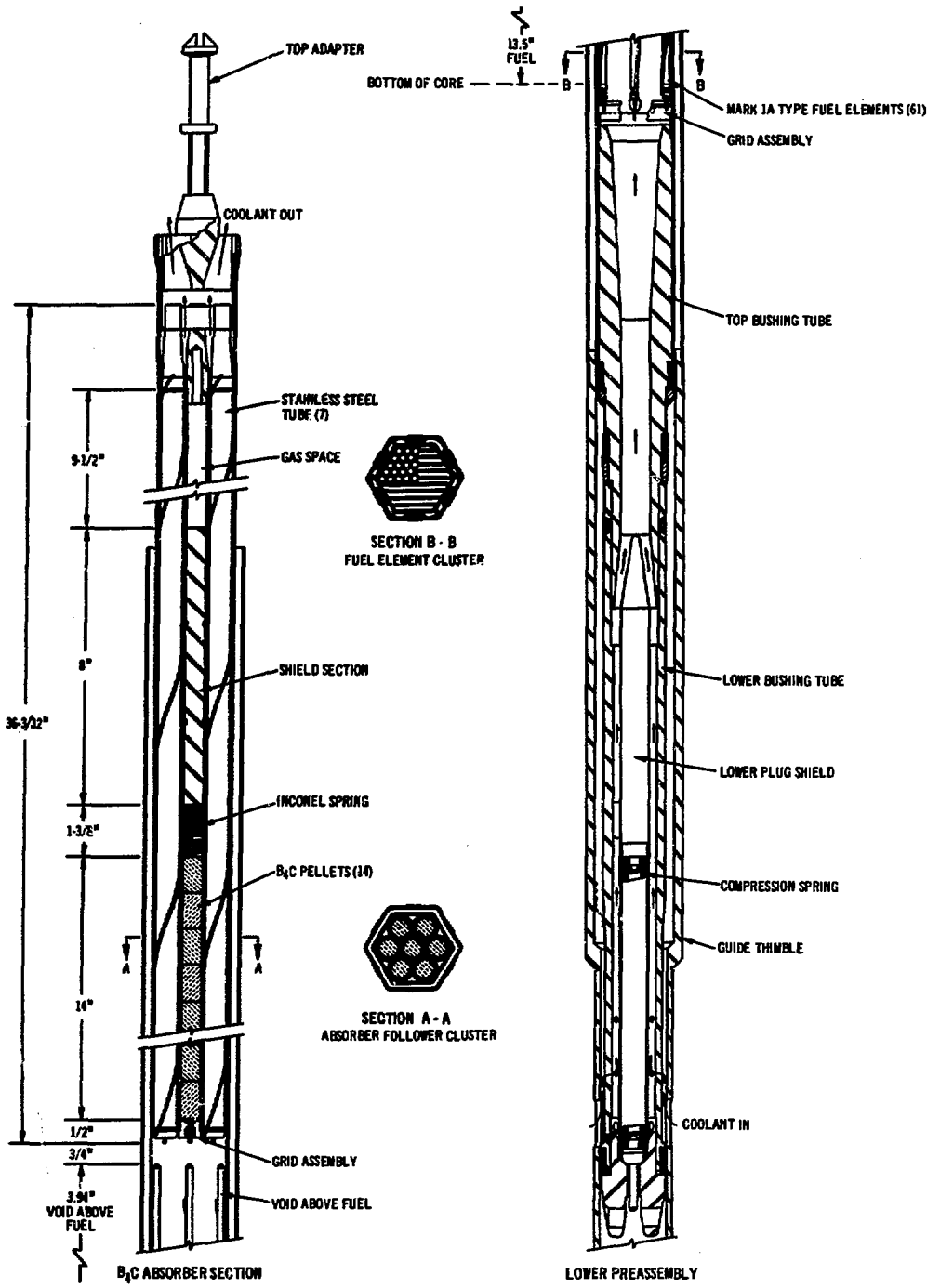

Fig. 1. Higher-worth Control Rod Subassembly

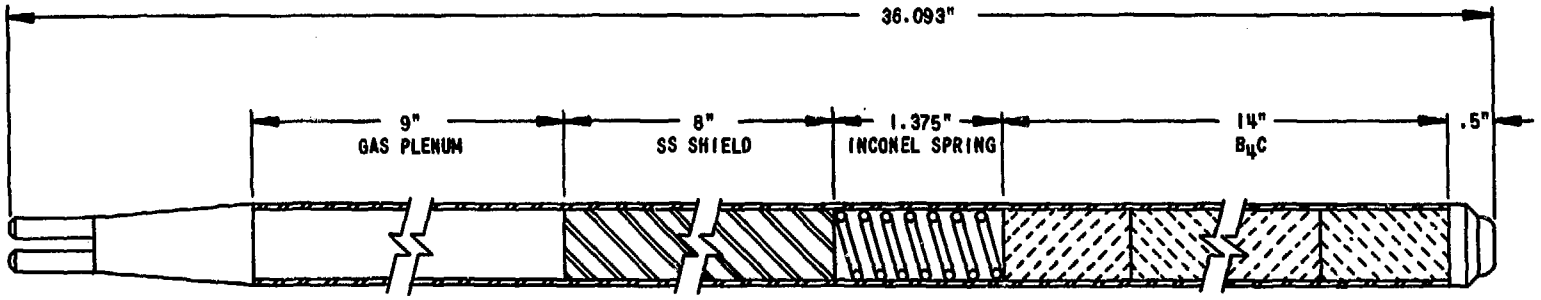

LENGTH		36.093"
TUBING	OD	.625"
	ID	.555"
	WALL THICKNESS	.035"
	MATERIAL	304LSS
PELLET	DIAMETER	.549
	LENGTH	1.000
	MATERIAL	B_4C
WIRE WRAP	DIAMETER	.030"
	HELICAL PITCH	6"

Fig. 2. B_4C Capsule for HWCR

and forms a seat for the spring. The spring prevents the B_4C pellets from shifting during control rod motion and allows for axial expansion of the B_4C column. The stainless steel shield plug contains three axial grooves that permit the helium released in the (n, α) reaction with ^{10}B to escape to the plenum volume at the top of the capsule. The capsule is sealed with 1 atm of helium when fabricated.

The B_4C pellets were manufactured by Cerac Inc., Silver Spring Road, Menomonee Falls, Wisconsin. The details of the manufacturing process are considered proprietary information by Cerac; however, it is customary to hot-press this product in graphite tooling at a temperature of about 2100°C. The results of a preirradiation characterization study of the B_4C pellets used in the two prototype HWCR's was reported by D. E. Walker[3].

Figure 3 shows the positions of the B_4C capsules in subassemblies L-4008S and L-4009S. Figure 4 shows the location of reactor grid positions 5A3 and 5C1 with respect to the center of the core. By noting the location of the identification notches in Figs. 3 and 4, the location of the individual B_4C capsules can be determined in Fig. 4.

III. RESULTS OF POSTIRRADIATION EXAMINATIONS

A. Disassembly and Visual Examination

A well-defined procedure has been established for dismantling and examining higher-worth control rod subassemblies, particularly to the point where the individual B_4C capsules are separated from the subassembly hardware and each other. The HWCR's L-4008S and L-4009S were handled and dismantled as follows:

After the subassembly was removed from EBR-II, it was transferred to Hot Fuel Examination Facility, South (HFEF/S) in the interbuilding coffin (IBC). Sodium and sodium products were removed from the subassembly while it was in the IBC. The cleaned and dried subassembly then was transferred into the HFEF/S air cell, where it was examined visually for any anomalous characteristics. Subassemblies L-4008S and L-4009S showed no unusual features on the external surfaces of the hardware.

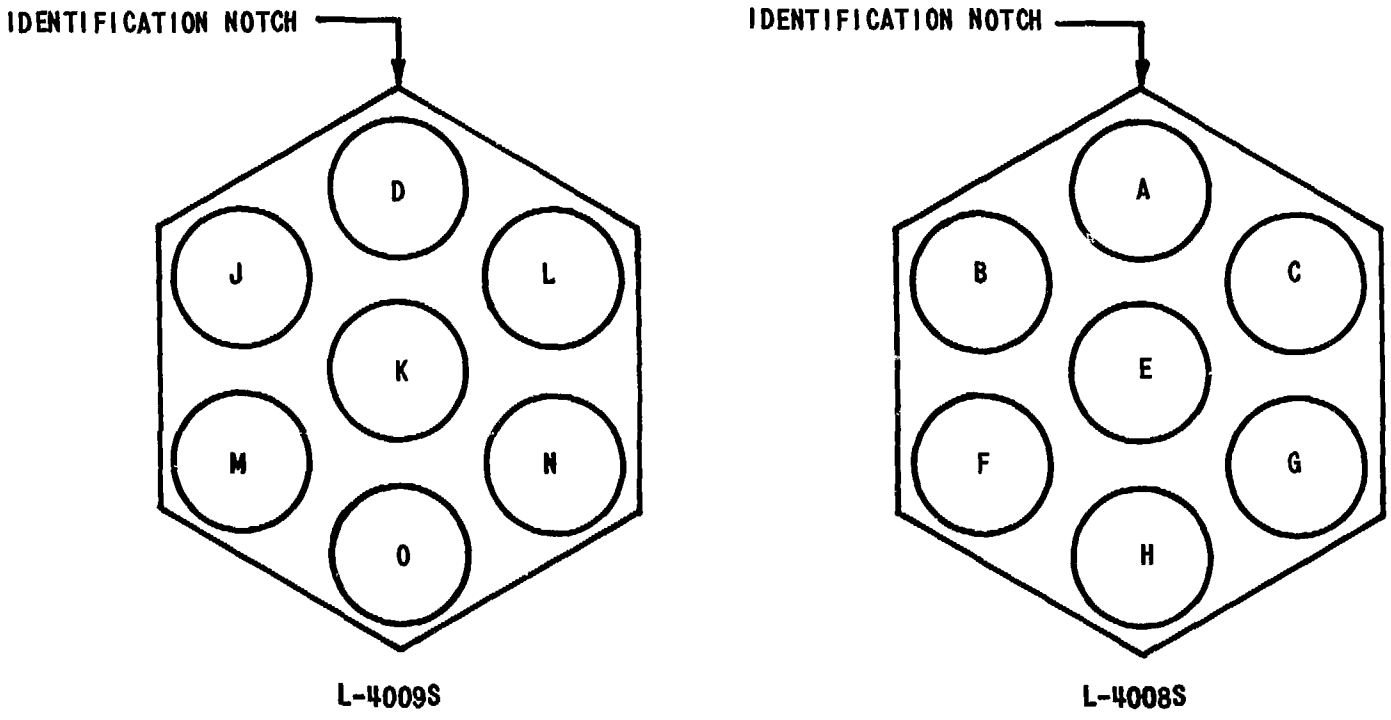

Fig. 3. Positions of B_4C Capsules in HWCR's L-4008S and L-4009S

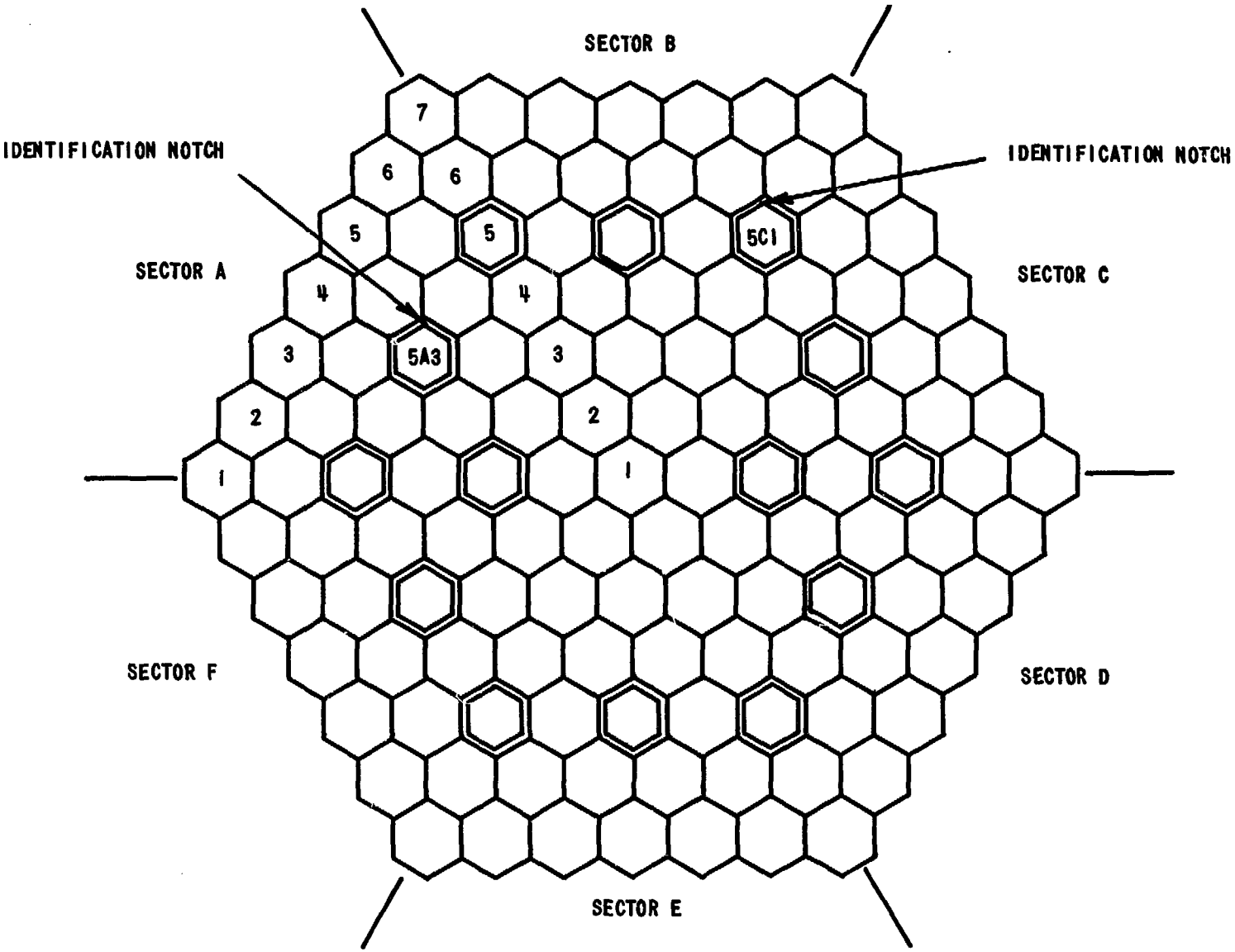

Fig. 4. Location of Reactor Grid Positions 5A3 and 5C1 in Core

Each subassembly was dismantled in HFEF/S using the vertical assembly-disassembly machine. The hexagonal tube was cut just above the spot welds that attach it to the subassembly lower adapter. This permitted the hexagonal tube, containing the seven B_4C capsules, to be drawn upwards from the fuel portion of the subassembly. The 61 fuel elements were removed from the T-bar grids and stored for processing at a later date.

The hexagonal tube with the seven B_4C capsules was moved to a power-hacksaw station for sectioning. First, the hexagonal tube was cut transversely with the power hacksaw at a point 42 in. below the top edge of the hexagonal portion of the subassembly top-end fixture. This cut removed excess (empty) hexagonal tubing and revealed the lower ends of the B_4C capsules. A second transverse cut through the hexagonal tube was made at a point 1-5/8 in. below the top edge of the hexagonal portion of the top-end fixture. This cut exposed the upper ends of the capsules where they were welded to their grid fixture so that their positions in the hexagonal tube could be gauged accurately. A third transverse cut was made with the power hacksaw at a point 3/8 in. below the top surface of the capsules' top-end caps. This cut released each capsule, one from the other, and made it possible to push and slide the capsules out of the hexagonal tube. The capsules were removed by pushing on their top ends only.

Each capsule was identified according to its position in the subassembly and the identification letter stamped on it.

Prior to sectioning of selected capsules to remove the B_4C pellets and examine the capsule cladding metallographically, all the capsules were examined as follows:

- Visual examination -- Each capsule was examined with a Kollmorgen hot-cell periscope after the spacer-wire wrap had been removed. No unusual features were noted on any of the capsules. Figure 5 typifies the condition of the capsules and shows that minute amounts of residual sodium products remained on the surface of the cladding along a line portraying the path of the wire wrap.

- Neutron radiography -- The capsules were radiographed for carbide-pellet outline and penetration in an attempt to show pellet cracking, displacement, growth and swelling, and density

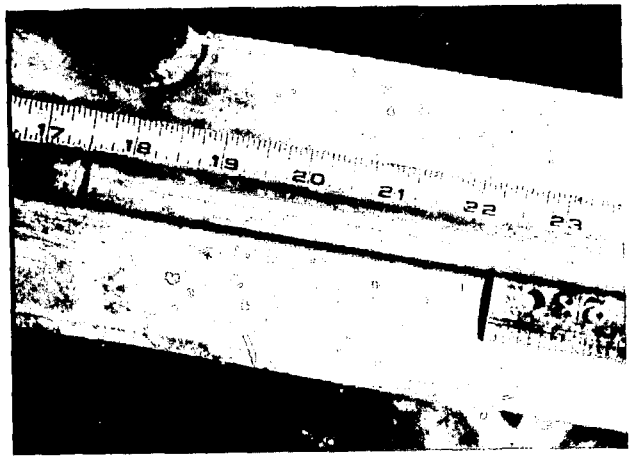

a. Medium View of Capsule 0

b. Closeup of Capsule 0

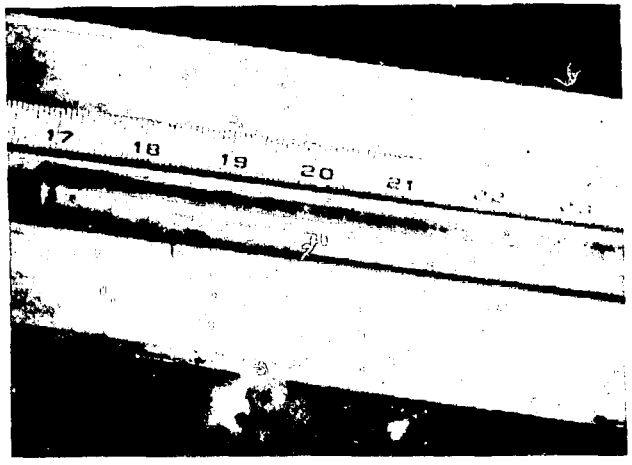

Medium View of Capsule K

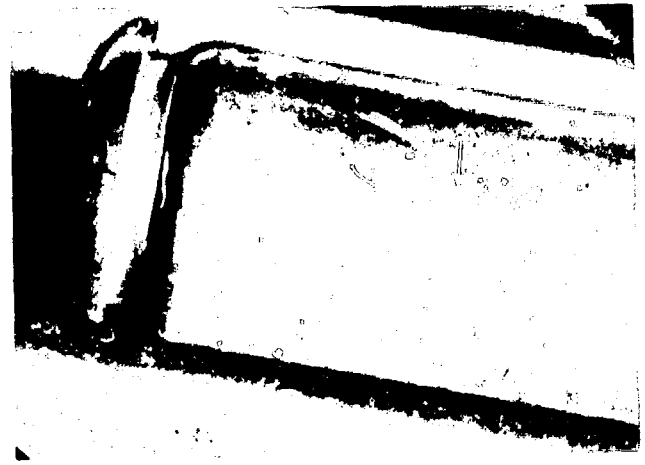

d. Closeup of Capsule K

Fig. 5. Typical Exterior Views of Capsules Containing B_4C Pellets from HWCR L-4009S.

variation. However, the B_4C pellets were so "black" to neutrons that meaningful definition could not be taken from the radiographs.

- Capsule diameter and length measurements -- Preirradiation diameter measurements taken with a Bausch and Lomb DR-25 optical gauge were duplicated in the postirradiation measurements. Overall length measurements of the capsules, also duplicating preirradiation methods, were made remotely on the irradiated capsules.

- Capsule bow measurements -- Each capsule was measured for bowing while supported in a vertical position near the top and bottom ends so that the capsule could assume a normal, unrestrained configuration. Horizontal (x and y) coordinates of the capsule were determined (with respect to an established reference on the machine) at several positions along the length of the capsule. The machine had electrically instrumented probes that stopped when they contacted the capsule cladding; the bow coordinates were then displayed and recorded. These coordinates were used to calculate the capsule's deviation from a straight line. This relative bow was established at each of the measured axial locations.

The internal portion of each capsule (see Fig. 2) consisted of four basic regions:

(1) Pellet region, approximately 14 in. long, containing the 14 B_4C pellets at the bottom of the capsule.

(2) Compression-spring region, approximately 1-3/8 in. long, at the top of the B_4C pellets.

(3) Shield-rod region, approximately 8 in. long, above the compression spring.

(4) Plenum region, approximately 9 in. long, above the shield rod.

In order to remove the B_4C pellets for subsequent examination steps and to provide samples of the cladding from the pellet region, the capsules

were sectioned using a carbide-wheel cutoff saw. A circumferential cut was made through the cladding only in the shield-rod region. This permitted the lower portion of the capsule containing the pellets and the compression spring to slide off of the shield rod. By slightly tilting the severed lower portion of the capsule, it was possible to slide out first the compression spring and then the pellets. As each pellet was removed, the cutoff saw was used to nick the top edge of the pellet for the purpose of marking the pellet orientation in the capsule. Each pellet was placed in a container marked with the capsule letter identification and pellet number in the pellet stack (pellet No. 1 was at the top of the stack, pellet No. 14 at the bottom).

Two transverse sections of cladding about 3/8 in. long were cut from the cladding of selected capsules for metallographic examination. One sample was taken from a position adjacent to pellet 14 and the other from a position adjacent to pellet 6. The metallographic samples were placed in small containers to maintain sample location and identification.

B. Capsule-diameter Profiles, Length Measurements, and Bow Measurements

The diameter profiles of the capsules that contained the B_4C pellets were measured at 0° and 90° orientation before and after irradiation. These measurements were done on the Bausch and Lomb-DR-25 remote optical gauge (±0.0002-in. measurement error). The results of these measurements are shown in Figs. 12 through 39 of Appendix A. A comparison of the pre- and postirradiation diameter profiles indicated that no significant irradiation-induced swelling had occurred.

The pre- and postirradiation length measurements of the capsules (see Table I) indicated that no significant length changes had taken place.

Figures 40 through 55 of Appendix A show the results of the post-irradiation bow measurements of all the capsules from the two HWCR's. The discussion at the beginning of Appendix A explains the interpretation. The overall results shown in these figures indicate that minimal bow occurred during irradiation.

TABLE I. Length Measurements of B_4C Capsules from HWCR's

Subassembly	Capsule	Length with Adapter On, in. Pre	Post	Change
L-4008S	C	36.442	36.423	- .019
	G	36.419	36.411	- .008
	A	36.436	36.423	- .013
	E	36.441	36.430	- .011
	H	36.440	36.426	- .014
	F	36.440	36.425	- .015
	B	36.448	36.433	- .015
L-4009S	J	36.415	36.527	.112
	N	36.447	36.436	- .011
	M	36.403	36.505	.102
	D	36.432	36.512	.080
	L	36.440	36.471	.031
	O	36.405	36.397	- .008
	K	36.387	36.423	.036

C. Capsule Plenum-volume and Pressure Measurements

1. Laser Gas-sampling System

A laser gas-sampling system (LGSS) was designed to sample the plenum gas in HWCR capsules. This LGSS was required to measure the pressure and the volume of the gas in the capsule plenums as well as remove a portion of the gas for analysis of its composition by mass spectrometry. The activity levels of the stainless steel HWCR capsules required that gas sampling be carried out in the Argonne-West Analytical Laboratory Hot Cell.

The LGSS consists of four basic components as follows:

(a) A high-vacuum system

(b) A vacuum chamber to contain the HWCR capsule to be sampled

(c) A laser system

(d) A precise pressure-measuring device.

All the major components of the LGSS are conveniently excluded from the necessity of being within the hot cell except for the sample chamber and its vacuum line. Figure 6 is a schematic diagram of this LGSS.

A portable high-vacuum system, consisting of an 80-liter/sec mercury diffusion pump and a liquid-nitrogen cold trap, is used to evacuate the LGSS. This system routinely achieves 1×10^{-6} Torr, as measured by a Bayard Alpert type of ionization gauge. A 1/4-in.-dia stainless steel tube connects this vacuum system from valve 1 (see Fig. 6) to the capsule-sampling chamber. A 3-in.-dia plug is removed from the hot-cell wall for installation of this vacuum line. Valve 1 is used as an isolation valve for the vacuum station and as a convenient point for disconnecting the sample chamber when exchanging capsules after sampling.

The vacuum-sampling chamber is constructed from Type 304L stainless steel tubing 1 in. in diameter by 50 in. long, sealed at the bottom end and fitted with two flanges, as shown in Figs. 7 and 8. A quartz window 1.5 in. in diameter by 1/4 in. thick is located in one flange so that the optical axis of the laser system will impinge upon the HWCR capsule plenum. A lens mount is provided to place a 100-mm-focal-length quartz lens on the same optical axis as the quartz window. Viton O-rings are used in the flanges for vacuum integrity. The halves of the upper flange are doweled in a manner to permit only one correct position for mating, so that

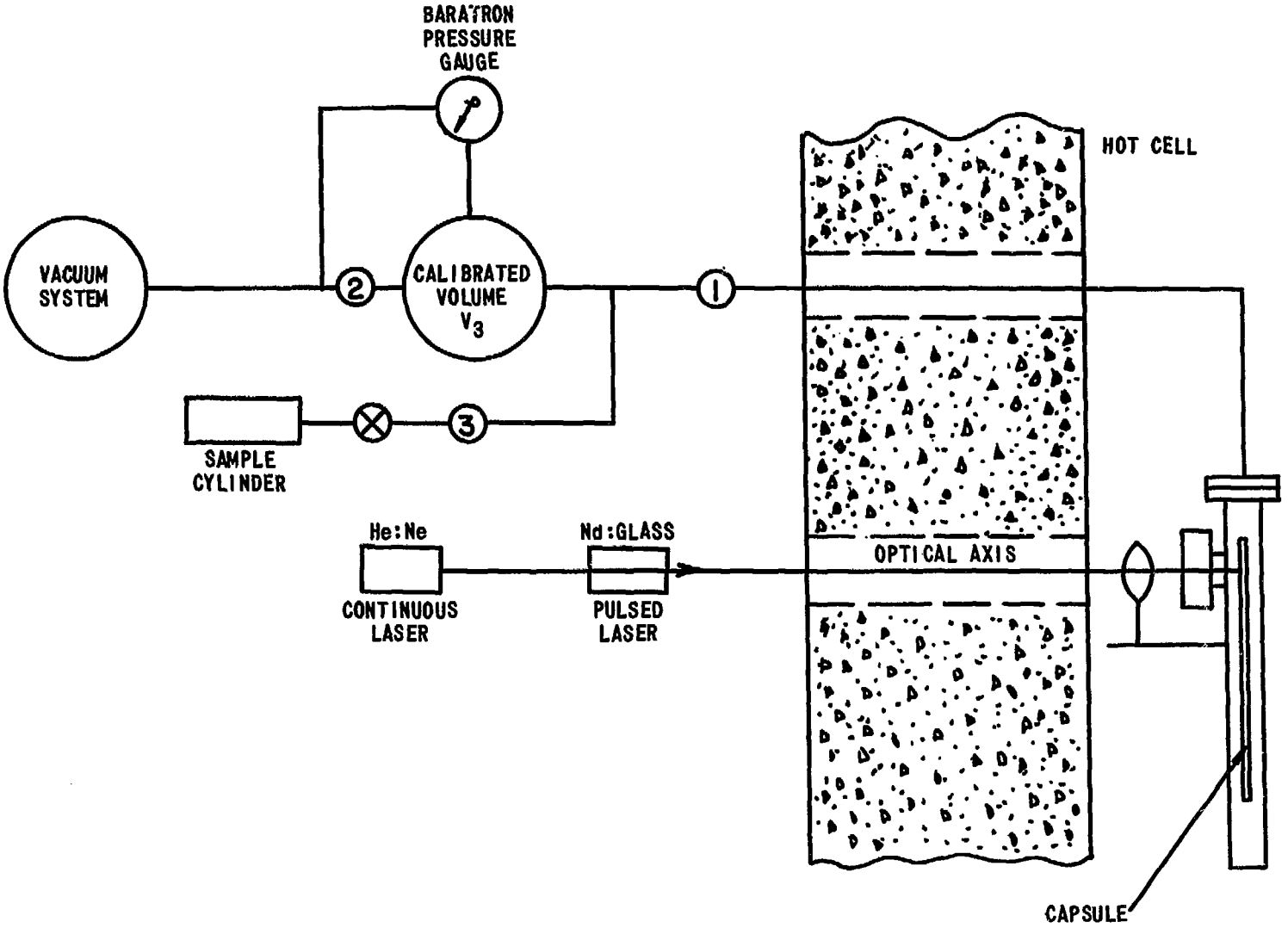

Fig. 6. Laser Gas-sampling System for Sampling of HWCR Capsules

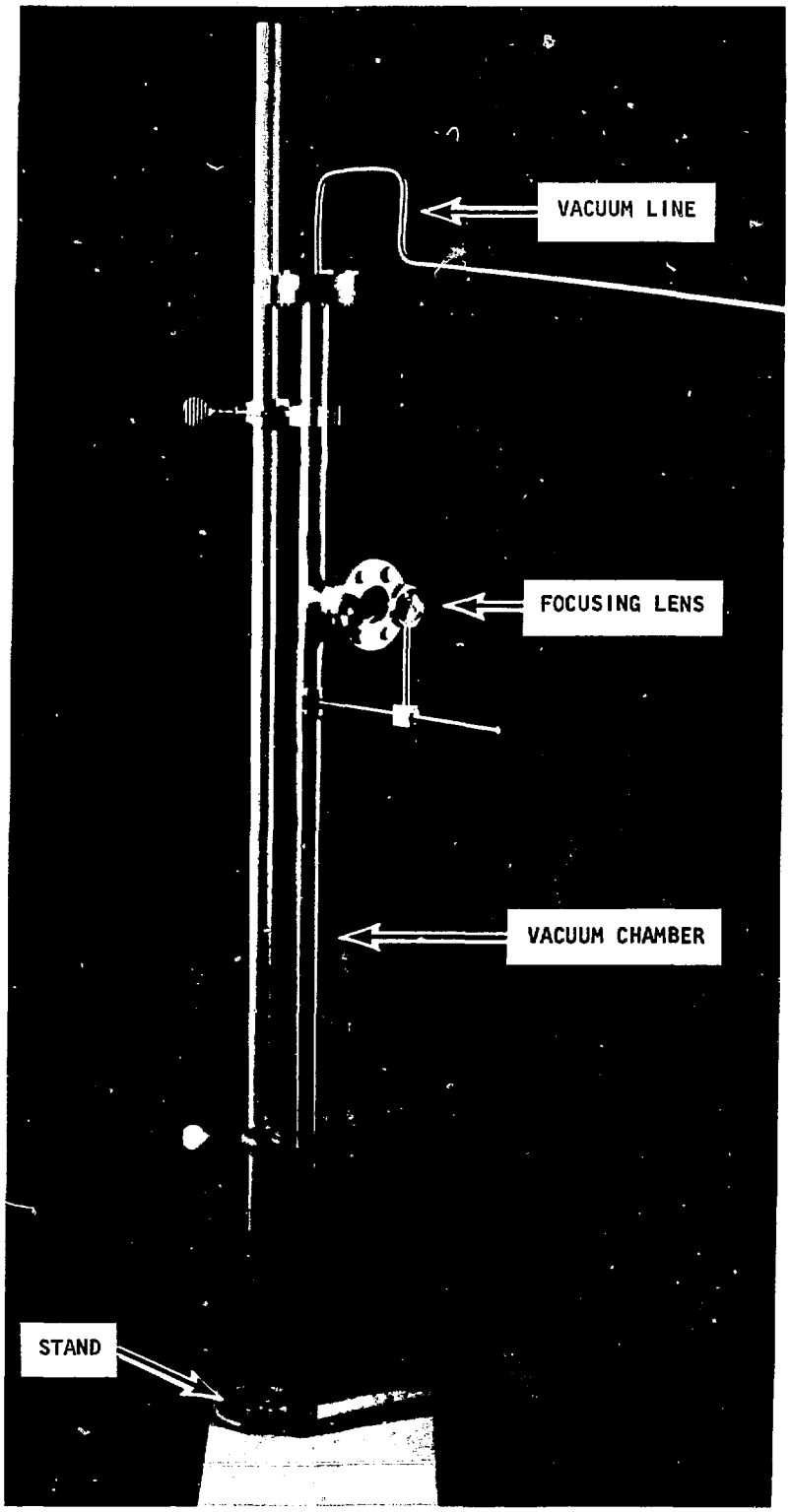

Fig. 7. Vacuum Chamber for Gas Sampling of HWCR Capsules, Assembled

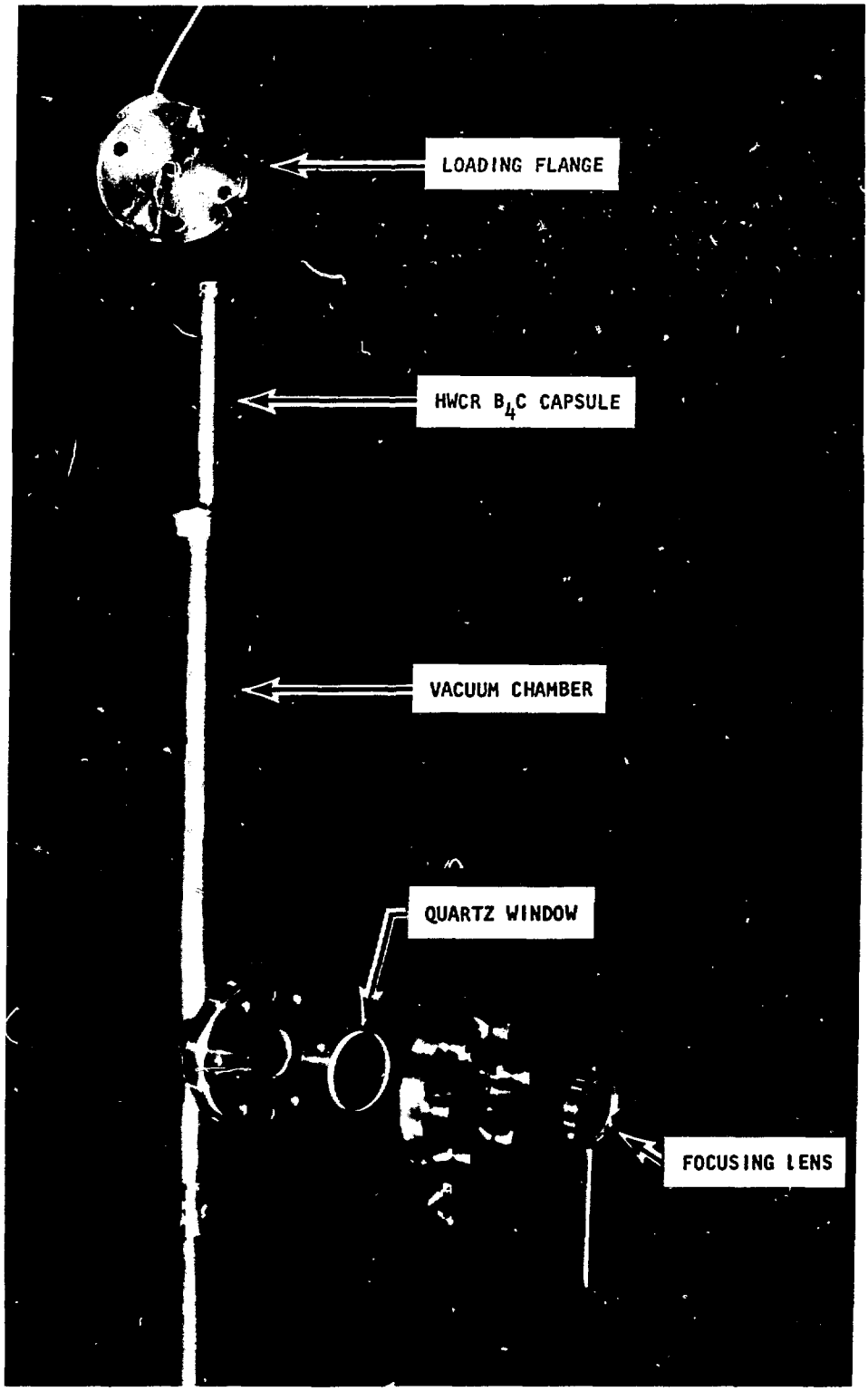

Fig. 8. Vacuum Chamber for Gas Sampling of HWCR Capsules, Exploded View

the vacuum line will be correctly oriented relative to the quartz window. Lipped flange halves, combined with the dowel pins, facilitated the remote assembly of the vacuum chamber. Essentially, the flange halves snap together and hold until the fastening cap screws are installed.

A 30-Joule neodymium-glass pulsed laser is used to pierce the cladding of the HWCR capsules. This laser is mounted on an optical bar immediately adjacent to the hot cell. A second 3-in.-dia penetration of the hot-cell wall is used for laser access. A helium-neon laser is used to visually establish the optical axis of the neodymium-glass laser, the focusing lens, the quartz window, and the capsule.

All gas-pressure measurements in the LGSS, except for the ionization-gauge monitoring of the vacuum system, are made with a Baratron* Model 77 Electronic Pressure Meter equipped with a 1000-Torr sensing head. The precision of measurements with this unit is within ± 0.05%.

2. Gas Sampling

Prior to the sampling of any capsules, the four basic components of the LGSS are assembled and tested. The vacuum integrity of the sampling chamber and vacuum line is checked. The focus adjustment of the 100-mm-focal-length lens is exactly set by test-firing the laser, using test specimens of the same diameter as the HWCR capsule. These tests are completed before installing the vacuum sample chamber in the hot cell.

Upon completion of testing, isolation valve 1 is closed and the vacuum line to the sampling chamber is disconnected. The top flange is removed from the vacuum chamber. The vacuum chamber and the top flange with attached vacuum line are transferred into the hot cell. The capsule to be gas-sampled is inserted into the vacuum chamber, plenum end up. The top flange is replaced and the assembled chamber placed on the stand provided, as shown in Fig. 7. The vacuum line now projects through the wall penetration, and the quartz window is in line with the second penetration used for the laser.

---

* MKS Instruments, Inc., Lexington, Mass.

The vacuum line, which now extends through the cell wall, is reconnected to the vacuum system at valve 1. The LGSS is evacuated by opening valves 1 and 2. After a few minutes, high vacuum (3×10^{-6} Torr) is achieved. Leak-testing of the LGSS is simply done by closing valve 1 and waiting 5 min before reopening. Sufficient vacuum integrity is obtained if the ionization-gauge reading changes less than 5% ($\sim 5 \times 10^{-7}$ Torr) with the gauge set at 1×10^{-5} Torr full scale.

After successful establishment of a leak-free system and a high vacuum of $\sim 3 \times 10^{-6}$ Torr, the volume of the vacuum-sampling chamber containing the unpunctured capsule is determined. Valve 2 is closed. The free volume is determined by expanding a known pressure of helium from a calibrated volume (Fig. 6) into the sampling chamber by opening valve 1, and then measuring the expanded pressure. The pressure drop is used to calculate the system volume. The complete procedure for determining free volume and plenum-gas pressure and volume is discussed in Appendix B. A derivation of the formulas used is also presented.

During the leak checking and prepuncturing volume determinations, the laser-system alignment is also checked to confirm that the optical axis of the laser extends through the focusing lens and the window of the sampling chamber.

Safety precautions are rigidly observed to prevent retinal damage to personnel from the laser operation. Provisions are made to contain stray light by erecting light barriers. The personnel that conduct the sampling are equipped with safety goggles designed to be opaque to the 1.02-μ wavelength of the neodymium-glass laser. Unnecessary personnel are excluded from the operating area.

The entire LGSS must be at high vacuum and leak-free in preparation for sampling. Valve 2 is closed. The Baratron meter is adjusted to zero at its highest sensitivity range. The sample cylinder attached to valve 3 must be evacuated and leak-free. Valve 3 must be closed.

The laser is fired with repeated shots until the HWCR capsule is punctured. The number of shots required depends upon the sharpness of focus of the laser and the energy applied to the laser. Normally, three or four pulses puncture the cladding and release the gas. Puncture is announced by a sudden dramatic response of the Baratron meter. At least 2 min elapse after puncture before equilibrium pressure conditions exist.

When equilibrium is reached, the pressure reading on the Baratron meter and the room temperature are recorded. Valve 3 is opened into the gas-sample cylinder. Five minutes are allowed to permit complete diffusion of the plenum gas into the sample cylinder. Valve 3 is now closed, and the sample cylinder is removed for mass-spectrometric analysis.

After the gas sample is removed, the LGSS is evacuated through valve 1. The system volume is redetermined as before laser puncturing to give a volume for the sample chamber plus punctured HWCR plenum. (See Appendix B for details.)

After completion of the postshot volume measurements, the vacuum-sampling chamber is vented to atmosphere through valve 1 and the vacuum system. The vacuum line is disconnected after closing valve 1, and the sample chamber is opened. A new capsule is loaded in preparation for the next measurement. The sampled capsule is returned to storage until it is disassembled to recover the B_4C pellets.

3. Analysis

A 21.4-cm-radius gas mass spectrometer is used to determine the composition of the plenum gas sample. The mass spectrometer is equipped with a molecular-flow sample inlet and electron-multiplier detector.

The mass spectrometer is routinely calibrated with pure gases so that quantitative gas measurements can be made. Input gas pressures versus signal output curves are prepared for the different gases analyzed, so that the partial pressures of the constituent gases in the sample gas can be determined.

The mass-spectrometer operating conditions were as follows: acceleration voltage, 3 keV; ionization voltage 70 eV; emission current, 300 μA; collector slit, 0.11 mm; source slit, 0.04 mm; resolution, 1100 (10% valley); inlet pressure, 0.10 Torr; inlet temperature, 100°C. The output of the mass spectrometer is recorded on a strip-chart recorder.

The plenum gas of HWCR capsules is readily sampled using the LGSS. A minimum of equipment is required. Only the chamber containing the capsule to be sampled needs to be inside a hot cell. All measuring and sampling equipment is located outside the hot cell. We have successfully sampled

the gas in the HWCR capsule, measured the gas pressure in the capsule, determined the capsule plenum volume, and removed a portion of the plenum gas for mass spectrometric analysis of its composition.

This method of gas sampling has also been adapted to plenum-gas sampling of irradiated fuel elements containing fission gas.

4. Results

Table II shows the results obtained by the puncture of six capsules from HWCR L-4008S and three capsules from HWCR L-4009S. The first column in Table II lists the laboratory that carried out the analysis. All the capsules examined by ANL were punctured by the technique described above. The plenum volume of 51 to 54 cm^3 agrees with the volume calculated from the dimensions of the component parts of the capsule. The measured gas pressures show that the helium released to the plenum as a result of the ^{10}B burnup is small, since the capsules were filled and sealed with helium at a pressure of approximately 15.7 psia.

Table III shows the composition of the gas sampled from the capsules, along with the laboratory that carried out the analysis. These results show that the plenum gas is predominantly helium, which is expected if the capsules are leak-free. The helium is generated predominantly from the $^{10}B(n, \alpha)\ ^{7}Li$ reaction. A small fraction of the helium (approximately 1%) is also generated from the $^{10}B(n, 2\alpha)\ ^{3}T$ reaction. A small quantity of tritium was detected in the plenum gas, as shown in Table III. The tritium that is generated in the $^{10}B\ (n, 2\alpha)\ ^{3}T$ reaction could either remain in the B_4C pellet or escape to the plenum, then rapidly diffuse through the stainless steel capsule wall. E. Ebersole (ANL) is now engaged in a study to determine the tritium concentration in the B_4C pellets and will report his results when obtained. The argon shown in the table comes from the argon cover gas used during the final closure weld.

D. Determination of ^{10}B Burnup in B_4C

The B_4C is analyzed isotopically for the boron isotopes with a thermal-ionization mass spectrometer. The ions produced in thermal ionization

TABLE II. Plenum-volume and Helium-pressure Measurements of B_4C Capsules from HWCR's

Lab	HWCR Number	Capsule	Plenum Volume, ml	Absolute Pressure at 24°C, psia[a]
WADCO	4008S	A	36[b]	22.3
WADCO	4008S	B	52	13.5
ANL	4008S	E	53.84	16.02
ANL	4008S	F	53.28	15.34
ORNL	4008S	G[c]		
ORNL	4008S	H	52.18	17.99
ANL	4009S	J	50.76	17.17
ANL	4009S	K	51.56	15.60
ANL	4009S	O	50.96	19.73

[a]Capsules were initially filled with helium and sealed at a pressure of 15.7 psia.

[b]Value is questionable because of the possibility of a leak in the system during the measurement.

[c]No results owing to system difficulties.

TABLE III. Gas Analyses on B_4C Capsules from HWCR L-4008S

Lab	Capsule	Gas Composition, mol %						Tritium, dis/sec per ml at STP
		He	O_2	N_2	A	CO_2	H_2	
WADCO	A	99.6	0.02	0.04	0.35	<0.01	<0.01	0.23
WADCO	B	99.8	<0.01	0.02	0.15	<0.01	<0.01	0.43
ANL	E	99.74	<0.01	0.06	0.21	--	--	--
ANL	F	97.90	0.40	0.63	1.08	<0.09	--	--
ORNL	G[a]							
ORNL	H	99.3	0.06	0.19	0.24	<0.02	0.03	

[a] No results owing to system difficulties

are $Na_2BO_2^+$ at masses 88 and 89 for the ^{10}B and ^{11}B isotopes respectively. These $Na_2BO_2^+$ ions are formed from the sodium tetraborate produced in sample preparation.

A sample from the irradiated B_4C pellet is obtained by fracturing the pellet with a hammer. The pellet is first carefully wrapped in a thick plastic bag to prevent scatter of the small shards produced during fracturing. This sampling is done in a hood to prevent the scatter of radioactive material. Similarly, samples are obtained from an unirradiated archive pellet.

The procedure for preparing these fractured B_4C chips for mass-spectrometric analysis is very simple. The chips require no ball milling, compositing, or extensive chemical treatment before analysis as described by Lerner,[4] Shields[5], or Abernathey[6].

Rhenium metal filaments 0.030 x 0.0012 in. are prebaked at 4 amps for 150 min in a vacuum bakeout device. One filament is used for each analysis. A drop, 0.050 ml, of reagent-grade 0.5M NaOH solution is placed on the filament. The NaOH solution is dried to a thick syrup by passing a current through the filament and slowly increasing the temperature. A small chip of the B_4C, ~1.5 mg, is placed on the filament in the syrupy NaOH with a pair of fine-tipped stainless steel tweezers. The filament is again slowly heated until the B_4C chip fuses with the NaOH. This sample is then introduced into the mass spectrometer for isotopic analysis.

The mass spectrometer is operated with an accelerating voltage of 12.5 keV and an electron-multiplier gain of 2×10^5. Stable ion emission is obtained after heating the filament containing the sample for 15 min to a temperature just below operating temperature before collecting data.

Identical conditions of analysis are maintained as closely as possible while determining the isotopic ratios of triplicate samples from each B_4C pellet. The results obtained by ANL are listed in the upper part of Table IV. The precision, which is shown for the ANL results, is also an indication of the homogeneity of the B_4C material. Isotopic ratios were corrected for the ^{17}O contribution to the mass-89 peak by the mass-88 ion. An electron-multiplier bias correction was also applied to the determined ratio.

The ^{10}B atom-percent burnup, A, is determined by the following equation:

TABLE IV. Analysis Results for ^{10}B Burnup in B_4C Pellets from HWCR's L-4008S and L-4009S

Sample[a]	At.% of Total Boron ^{10}B	At.% of Total Boron ^{11}B	Calculated ^{10}B Burnup, at.%
	ANL Results[b]		
Unirradiated Control	19.90	80.10	0
F - 2	19.77	80.23	0.8 ± 0.2
F - 7	19.69	80.31	1.3 ± 0.2
F - 13	19.62	80.38	1.7 ± 0.2
Unirradiated Control	19.87	80.13	0
0 - 2	19.68	80.32	1.2 ± 0.2
0 - 7	19.64	80.36	1.4 ± 0.2
0 - 13	19.63	80.37	1.5 ± 0.2
	ORNL Results		
Unirradiated Control	19.81	80.19	0
G - 4	19.61	80.39	1.26
G - 9	19.67	80.33	0.86
G-13 (average of three specimens)	19.54	80.46	1.72
H - 2	19.61	80.39	1.26
H - 7	19.57	80.43	1.51
H - 14	19.55	80.45	1.62

WADCO results on capsules A and B are summarized by the following relationship that was fit to 18 ^{10}B burnup analyses on B_4C pellets from capsules A and B.

$$\text{At. \% burnup of } ^{10}B = 1.34 \exp(-4.8 \times 10^{-2} X)$$

where X is the distance from the bottom of the B_4C stack in cm.

[a] Letter designates capsule; numeral designates the B_4C pellet location in the capsule.

[b] Error is ± one standard deviation.

$$A = 100 \left[\frac{(\text{atom \% } {}^{10}B)U - (\text{atom \% } {}^{10}B)I}{(\text{atom \% } {}^{10}B)U} \right] \quad (1)$$

where I is irradiated B_4C sample
U is unirradiated B_4C sample.

If we divide both the numerator and the denominator of Eq. (1) by the atom percent ^{11}B determined in the unirradiated-sample analyses, we can simplify the above equation so that corrected isotopic ratios can be used. The resulting equation is

$$A = 100 \left[1 - \frac{R_I}{R_U} \right] \quad (2)$$

where R_I is the $^{10}B/^{11}B$ irradiated ratio
R_U is the $^{10}B/^{11}B$ unirradiated ratio.

Table IV and Fig. 9 summarize the results of ^{10}B burnup analyses carried out by ORNL, WADCO, and ANL on B_4C pellets from HWCR L-4008S and pellets from capsule O of HWCR L-4009S. The results obtained by ANL on B_4C pellets from capsule F are comparable to the results obtained by ORNL on pellets from capsules G and H. The results obtained by WADCO on capsules A and B are somewhat lower. This trend is qualitatively explained by considering the reactor location of the capsules. The B_4C pellets from capsules A and B should have the lowest ^{10}B burnup, since these capsules were located farthest from the core center.

Integration of the ^{10}B burnup profiles in Fig. 9 results in an estimate of the quantity of helium generated during irradiation. Table V shows the moles of helium generated for capsules A, B, F, H, and O. The data from capsule G were not integrated. Also shown in Table V is the helium pressure in the capsule at 24°C, if 100% gas release had occurred. Since the measured helium pressures, after irradiation, were near the fill pressure of 15.7 psia, the percentage of gas release was small.

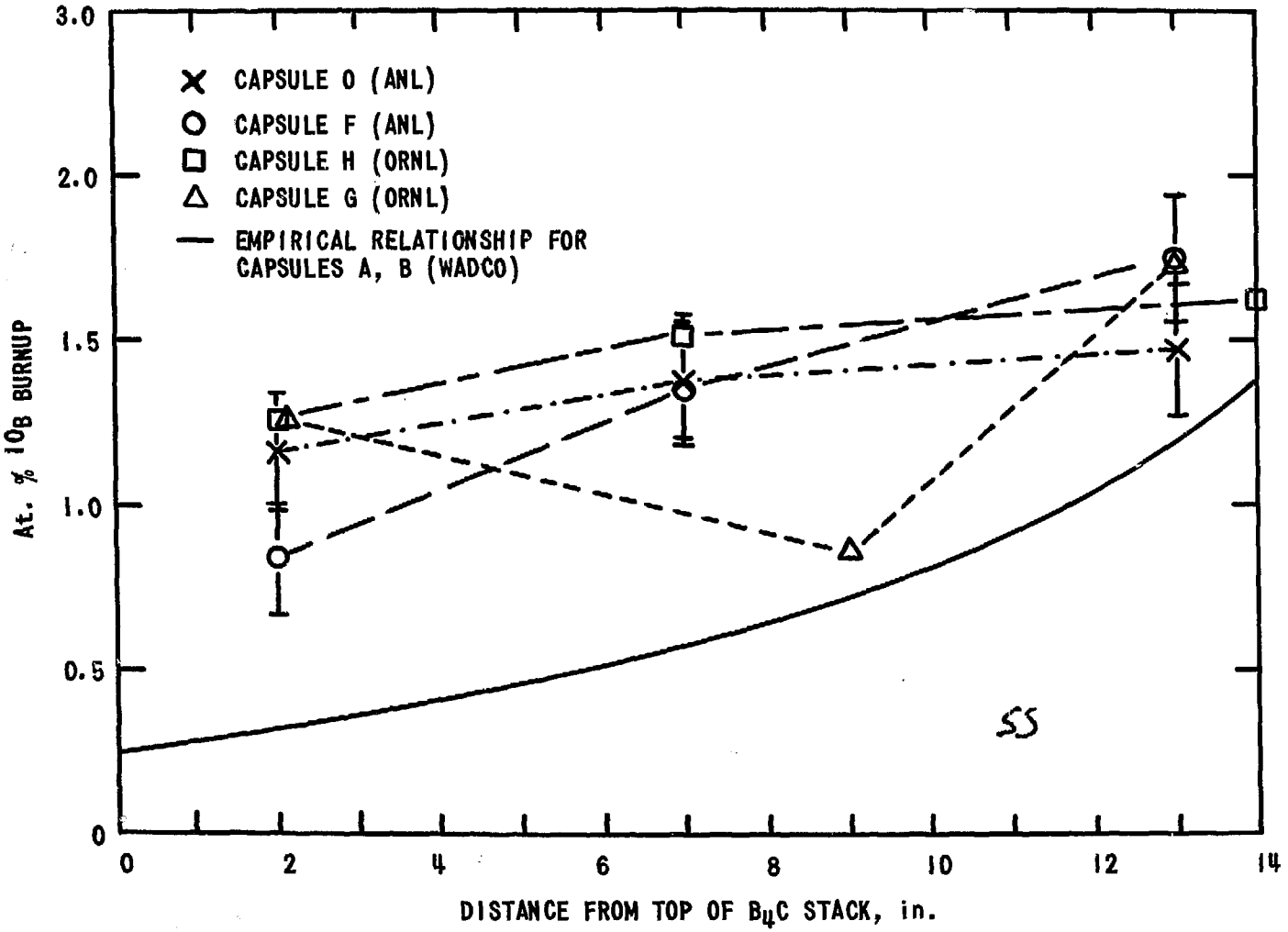

Fig. 9. Profiles for ^{10}B Burnup in B_4C Pellets from HWCR's L-4008S and L-4009S

TABLE V. Helium Generation in B_4C Capsules from HWCR's L-4008S and L-4009S

Capsule	He Generated, 10^{-2} moles	Plenum Volume, ml	Pressure at 24°C, psia[a]
F	2.33	53.84	170.7
H	2.61	52.18	194.7
A or B	1.17	52	96.4
O	2.49	50.96	175.8

[a] Assuming 100% gas release.

E. Retained Helium in B_4C Pellets

The results given above in Sections C and D showed that the B_4C pellets retained nearly 100% of the helium generated in ^{10}B burnup. However, we had no direct proof of near-100% helium retention. The question arose as to the possibility of leaks in the capsules so that helium was lost while the capsules were in the reactor, implying that the B_4C did not retain nearly all the helium generated due to ^{10}B burnup. The likelihood seemed small for leaks because, prior to puncture, the capsule was placed in a chamber that was then evacuated. If a leak existed, the helium in the capsule would be pumped out prior to the puncture step.

To resolve the question of leaks, the concentration of helium in the B_4C pellets was determined. Dr. R. R. Hobbins of the Materials Research Section, Aerojet Nuclear Company, carried out the experiments to determine the quantity of helium retained in the B_4C pellets. Hobbins devised a technique that involved heating the B_4C in a flux of iron and tantalum at 2000°C. The helium released from the B_4C was monitored by a mass spectrometer as a function of time at temperature. Approximately 95% of the gas collected was released within 45 min at the temperature of 2000°C.

Samples from the same B_4C pellets from capsule F that were used for ^{10}B burnup analysis were used for this helium-retention experiment. Table VI compares the results of the helium-retention experiments with the calculated helium concentrations, based on the ^{10}B burnup analysis. The table shows excellent agreement between the calculated and measured helium concentrations. It can therefore be concluded that virtually all the helium generated by ^{10}B burnup is retained in the B_4C pellets.

The helium-retention experiments, in addition to serving as proof for the nonexistence of leaks, were the last step in the mass balance on helium. We thus measured the helium by three methods: calculation of generation due to ^{10}B burnup, determination of liberated helium by pressure measurements and gas analysis, and finally the determination of retained helium. The agreement between the three different experiments lends confidence to each individual experiment.

TABLE VI. Helium Retention in B_4C Pellets from HWCR's L-4008S and L-4009S

Sample No.	Helium Concentration (Measured), ppm atomic	Helium Concentration (Calculated), ppm atomic
F - 2	$(7.0 \pm 0.7) \times 10^3$	$(6.4 \pm 0.2) \times 10^3$
F - 7	$(9.6 \pm 0.5) \times 10^3$	$(10.4 \pm 0.2) \times 10^3$
F - 13	$(13.3 \pm 0.5) \times 10^3$	$(13.6 \pm 0.3) \times 10^3$

Error is ± one standard deviation.

F. Dimensions and Immersion-density Results for B_4C Pellets

Postirradiation measurements of diameter and length were obtained with the Bausch and Lomb DR-25 remote optical gauge (± 0.0002-in. measurement error) on the 14 B_4C pellets from capsule F of HWCR L-4008S and the 14 B_4C pellets from capsule O of HWCR L-4009S. Preirradiation measurements were also available for these pellets. Tables VII and VIII show the pre- and postirradiation dimensions for the individual pellets. Summarized below are the maximum, average, and minimum diameters for the stack of 14 pellets from each capsule:

	Minimum Dia, in.		Maximum Dia, in.		Average Dia, in.	
Capsule	Pre	Post	Pre	Post	Pre	Post
F	0.534	0.536	0.547	0.545	0.539	0.540
O	0.532	0.534	0.545	0.546	0.539	0.540

The original gap between the capsule wall and the B_4C pellets of 4 mils was decreased by, at most, 0.5 mils. (Note that only the increase in maximum pellet diameter is significant here.) The B_4C pellets did slide freely from the capsules upon removal during postirradiation examination. Thus, no additional stress was produced on the capsule wall by swelling of the B_4C pellets. The results in Tables VII and VIII show no definite trend with relation to the location of the B_4C pellets in the stack (i.e., it is not apparent that the highest-burnup pellets had the largest diameter increases).

The preirradiated length of the stack of 14 B_4C pellets from capsule F was 13.997 in., and the postirradiated length was 14.024 in. The preirradiated length of the stack of 14 B_4C pellets from capsule O was 14.015 in. and the postirradiated length was 14.033 in. The length increases of 27 and 18 mils, respectively, produce a negligible decrease in the capsule plenum volume.

TABLE VII. Dimensions, Weights, and Immersion-density Results for B_4C Pellets from Capsule F of HWCR L-4008S

Pellet Number	Preirradiation Results			Postirradiation Results						
	Minimum Diameter, in.	Maximum Diameter, in.	Length, in.	Minimum Diameter, in.	Maximum Diameter, in.	Average Diameter, in.	Length, in.	Weight, g	Density g/cm^3	Density % of Theoretical
1	.536	.540	1.046	.5386	.5390	.5388	1.0472	9.3948	2.4526	97.3
2	.540	.547	0.908	.5437	.5448	.5443	0.9090	8.4334	2.4722	98.1
3	.538	.543	0.908	.5380	.5413	.5397	0.9089	8.3746	2.4814	98.5
4	.535	.540	1.011	.5365	.5406	.5386	1.0119	8.9927	2.4233	96.2
5	.534	.542	1.038	.5368	.5371	.5370	1.0400	9.1634	2.4496	97.2
6	.536	.543	1.038	.5385	.5394	.5390	1.0396	9.4271	2.4661	97.9
7	.535	.543	1.038	.5371	.5387	.5379	1.0394	9.3792	2.4654	97.8
8	.535	.543	1.038	.5388	.5388	.5388	1.0394	9.3026	2.4615	97.7
9	.535	.543	1.046	.5378	.5384	.5381	1.0478	9.4102	2.4632	97.7
10	.535	.542	1.038	.5386	.5400	.5393	1.0396	9.1590	2.4535	97.4
11	.534	.540	1.046	.5357	.5383	.5370	1.0483	9.1447	2.4413	96.9
12	.540	.545	0.889	.5447	.5456	.5452	0.8938	8.3558	2.4885	98.8
13	.534	.539	1.046	.5358	.5375	.5367	1.0481	9.4146	2.4604	97.6
14	.542	.545	0.907	.5424	.5438	.5431	0.9109	8.4412	2.4799	98.4
								Total Weight 126.39	Average	97.7

Total Preirradiation Weight = 126.45 g

TABLE VIII. Dimensions, Weights, and Immersion-density Results for B_4C Pellets from Capsule O of HWCR L-4009S

Pellet Number	Preirradiation Results			Postirradiation Results						
	Minimum Diameter, in.	Maximum Diameter, in.	Length, in.	Minimum Diameter, in.	Maximum Diameter, in.	Average Diameter, in.	Length, in.	Weight, g	Density	
									g/cm^3	% of Theoretical
1	.534	.537	0.998	.5376	.5384	.53800	0.9990	8.9738	2.453	97.3
2	.540	.545	0.997	.5394	.5437	.54155	1.0001	9.3579	2.501	99.3
3	.539	.542	0.999	.5392	.5409	.54005	1.0004	9.2789	2.499	99.2
4	.539	.544	0.997	.5402	.5413	.54075	1.0004	9.3191	2.500	99.2
5	.538	.543	1.004	.5397	.5419	.54080	1.0044	9.3829	2.499	99.2
6	.538	.543	0.999	.5402	.5408	.54050	1.0007	9.3410	2.499	99.2
7	.536	.537	1.003	.5370	.5380	.53750	1.0055	9.2127	2.490	98.8
8	.534	.537	--	.5359	.5394	.53765	1.0008	9.0128	2.461	97.7
9	.538	.541	1.000	.5419	.5459	.54390	1.0028	9.3228	2.497	99.1
10	.540	.543	1.003	.5432	.5447	.54395	1.0058	9.4071	2.496	99.1
11	.532	.538	0.999	.5341	.5363	.53520	1.0023	8.9583	2.446	97.1
12	.537	.539	1.001	.5394	.5406	.54000	1.0042	9.2323	2.482	98.5
13	.538	.543	0.998	.5387	.5442	.54145	1.0029	9.3064	2.492	98.9
14	.538	.539	0.999	.5390	.5401	.53955	1.0039	9.2105	2.485	98.6
	Total Stack Weight (g) = 129.31					Total Weight =		129.32	Average =	98.7

Also shown in Tables VII and VIII are the postirradiation immersion-density results for capsules F and O. The immersion fluid was water. During the density measurements, it was found that the weight increased with time, which indicates that the B_4C was absorbing the fluid. All the results shown in Tables VII and VIII were thus the measurements obtained after the B_4C pellet had been immersed in the fluid for 1 hr. Early measurements on the first few pellets showed that after 1 hr the weight became constant. This same absorption phenomenon was observed during unirradiated immersion-density measurements[3]. The unirradiated immersion-density results were not obtained on pellets that were later irradiated, but rather on pellets from the same manufacturing batch, and thus no direct pre- and postirradiation comparison can be made. However, the preirradiation density measurements showed densities that ranged between 92.8% and 99.8% of the theoretical density, which is taken as 2.52 g/cm^3 (see Ref. 3). The postirradiation densities from capsules F and O ranged between 96.2% and 99.3% of the theoretical density. Thus, no substantial density change took place. From the density results shown in Tables VII and VIII, no trend could be established that would relate density to pellet location.

The two tables also show the pre- and postirradiation total weight of the B_4C stack. For both capsules F and O, the pre- and postirradiation stack weights agreed within experimental error.

The dimensional measurements on the B_4C pellets and the immersion-density results discussed above were confirmed by similar measurements carried out by ORNL on B_4C pellets from capsules G and H of HWCR L-4008S (Ref. 7) and by WADCO on B_4C pellets from capsules A and B of HWCR L-4008S (Ref. 8).

G. Metallography of the Irradiated Type 304L Stainless Steel Capsules That Contained the B_4C Pellets

Metallographic specimens were obtained from capsule F of HWCR L-4008S and capsule O of HWCR L-4009S. On each stainless steel capsule, a specimen 3/8 in. long was obtained at an axial distance of 1 in. from the bottom of the capsule (high-fluence region), and another 3/8-in.-long specimen was obtained 7.5 in. from the bottom of the capsule.

On each of the four samples, the transverse surface that faced toward the bottom of the capsule was polished and etched according to the following procedure: the sample was potted in epoxy and polished on the remote polishing wheel through the following stages: 120 grit - 15 min, 240 grit - 15 min, 400 grit - 15 min, repot to avoid relief effects, 400 grit - 5 min, 600 grit - 15 min, 1-μ diamond paste - 30 min, and finally, 0.05 Alumina-water slurry - 60 min. A low force was exerted on the sample for all polishing steps. The sample was then electroetched for 20 sec in a 10% oxalic acid solution at 6 V.

Figure 10 shows representative micrographs of each of four samples at a magnification of 500X. Each micrograph shows a portion of the inner circumference. On all four specimens, moderate sensitization was observed, with carbides precipitated along the grain boundaries. This degree of sensitization is comparable to that observed on fuel cladding that has been irradiated to low fluences. The sensitization was uniform across the capsule walls. On the inside walls, there was no evidence of a zone of interaction between the B_4C pellets and the stainless steel cladding.

H. Compatibility of the Irradiated B_4C Pellets with Liquid Sodium

B_4C pellets were exposed to low-velocity liquid sodium. Initial testing consisted of the exposure of unirradiated B_4C pellets (0.54 in. OD x 1.0 in. long) from two commercial sources (Cerac Inc. and Carborundum Co.) for periods of 1 day and 8 days to flowing sodium at a temperature of 1110°F. The sodium flow velocity was approximately 0.1 ft/min. Table IX shows that the unirradiated pellets had only slight weight losses during these short exposures.

Irradiated B_4C pellets Nos. 13 and 14 (the pellets with highest ^{10}B burnup) from capsule E of HWCR L-4008S were then tested. These pellets were exposed directly to sodium in a pumped and cold-trapped stainless steel loop. The sodium velocity past the test pellets was 0.5 to 1.0 ft/min; the concentration of oxygen in sodium was about 0.3 ppm.

Pellet 13 was immersed in sodium in a series of scoping tests, which resulted in the following exposures:

1 day - 700°F
1 day - 850°F
14 days - 1000°F.

a. Top Sample (Low Fluence) from Capsule F, HWCR L-4008S

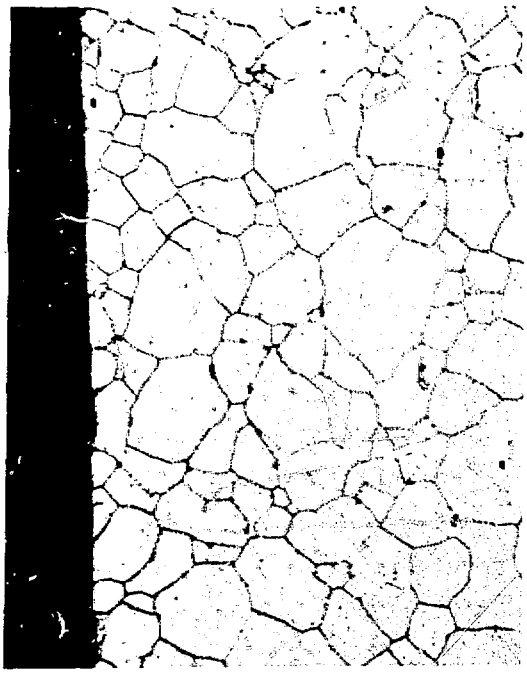

b. Bottom Sample (High Fluence) from Capsule F, HWCR L-4008S

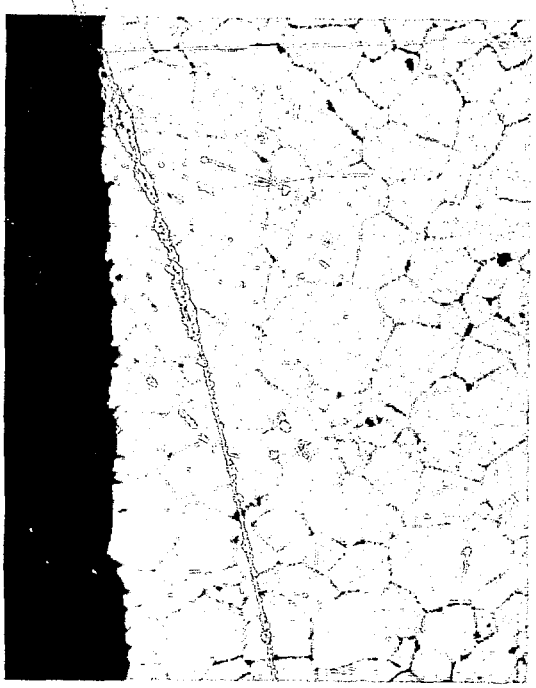

c. Top Sample (Low Fluence) from Capsule O, HWCR L-4009S

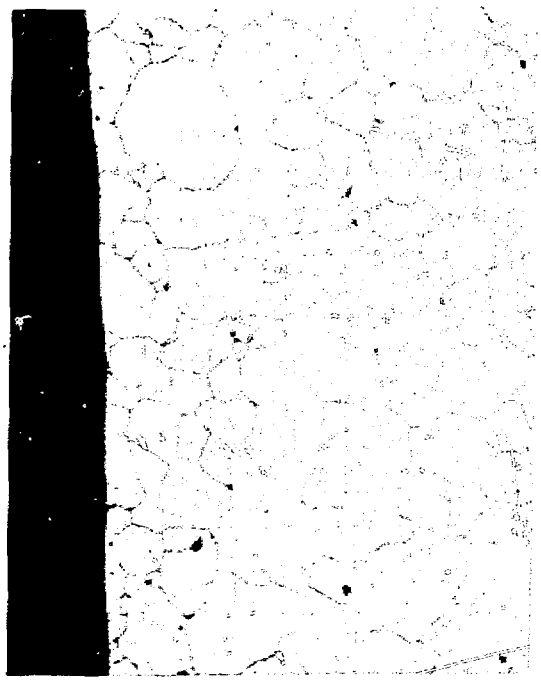

d. Bottom Sample (High Fluence) from Capsule O, HWCR L-4009S

Fig. 10. Micrographs of Inside Walls of Type 304L Stainless Steel Capsules That Contained B_4C Pellets; Magnification 500X.

TABLE IX. Weight Loss (mg/cm^2) of Unirradiated Boron Carbide Pellets Exposed to 1110°F Sodium[a]

	Days of Exposure	
Manufacturer	1	8
Cerac Inc.	0.12	0.45
Carborundum Co.	0.17	0.86

[a] Velocity, ∿0.1 fpm; cold-trap temperature, 230°F.

Following these sodium-exposure tests, adherent sodium was removed from pellet 13 by washing first in ethyl alcohol and then in water. The pellet was then reweighed. The overall weight loss was 30 mg/cm^2 (4.5% of the initial pellet). This was substantially larger than the losses in the pre-irradiated tests (Table IX).

Pellet 14 was exposed only to 1000°F sodium. An unirradiated B_4C pellet was included in the same test to determine if some abnormal sodium impurity had caused the large weight loss observed for pellet 13. The pellets were removed at 6 days and again at 13 days. In both examinations, the sodium was removed by washing in alcohol, followed by water. The irradiated pellet released a large cloud of black particles into the liquid at each cleaning. A small number of particles was also released by the unirradiated control pellet. The black particles from both pellets remained in suspension for several hours in the alcohol, suggesting that they were almost colloidal in size. Even after extensive washing, the irradiated pellet retained enough sodium beneath its surface to continue to show tiny bubbles of hydrogen forming in wet areas. Figure 11 shows the unirradiated and irradiated pellets before and after exposure to liquid sodium.

The weight losses for the unirradiated control pellet and for pellet 14 are shown in Table X. The weight loss for the unirradiated control pellet for the first six days is high in relation to the unirradiated values shown in Table IX. It is suspected that a weighing error was made when the unirradiated control pellet was initially weighed in the hot cell.

The high-temperature sodium apparently found paths for penetrating deeply into the irradiated pellets. In this low-velocity test (low-velocity compared to flowrate in EBR-II) the pellet did not disintegrate to any extent in the sodium. The gentle bubbling in the alcohol and the dissolution of the metallic sodium "gluing" the particles together caused most of the observed loss of material. The fragile nature of the sodium-penetrated pellet suggests that it might be eroded quickly in rapidly flowing sodium.

TABLE X. Weight Loss (%) of Boron Carbide upon Exposure to 1000°F Sodium[a]

Specimen	Days of Exposure	
	6	13
Irradiated (Pellet No. 14)	5.2	11.2
Unirradiated Control	0.75	0.75

[a] Velocity, 0.5 fpm; cold-trap temperature, 265-275°F.

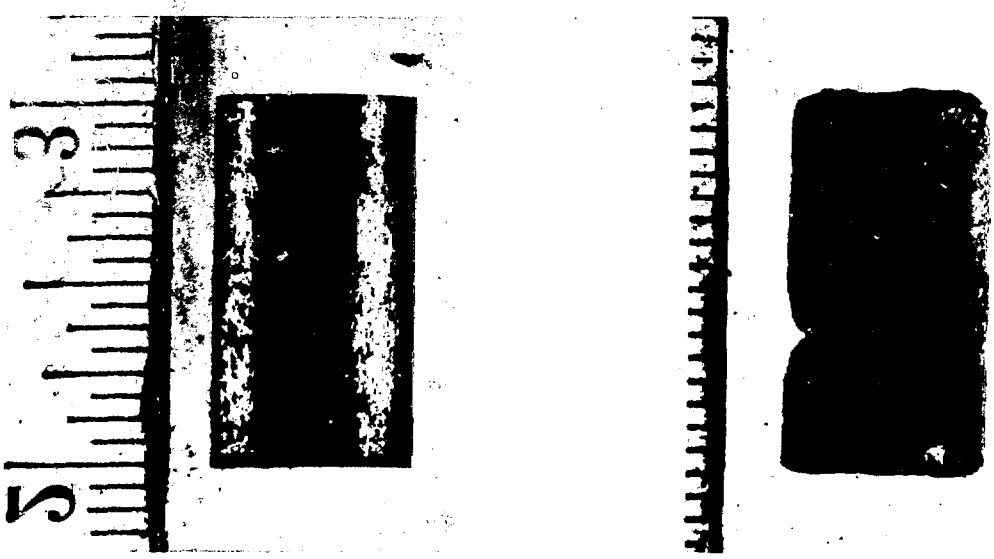

BEFORE EXPOSURE AFTER EXPOSURE

IRRADIATED (PELLET NO. 14)

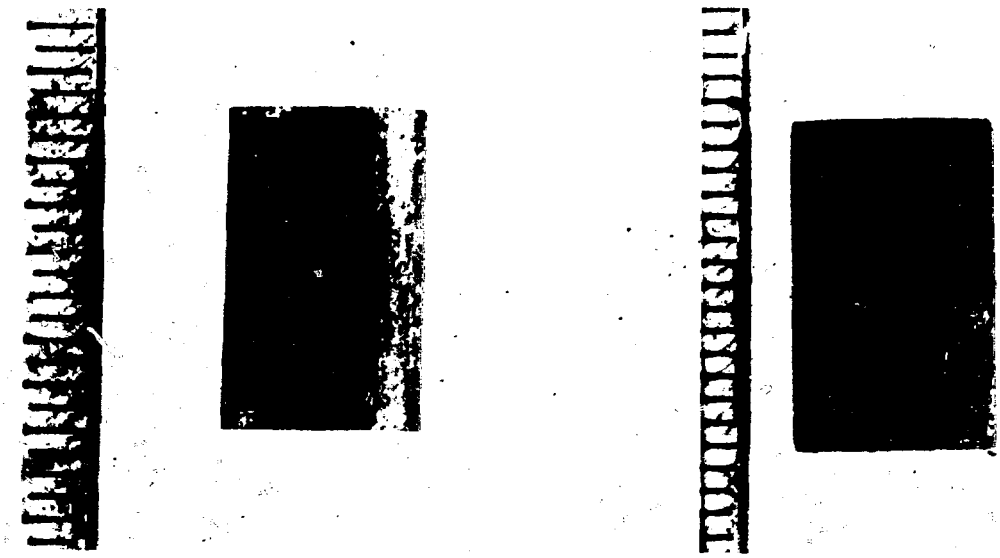

BEFORE EXPOSURE AFTER EXPOSURE

UNIRRADIATED

Fig. 11. Effect of Exposure of Irradiated and Unirradiated Boron Carbide Pellets to 1000°F Sodium for 13 Days; Magnification 2X

I. Summary of Additional Experiments and Observations from ORNL and WADCO on Irradiated B_4C Pellets from HWCR L-4008S

The detailed results from ORNL are given in Refs. 7, 9, and 11, and the detailed results from WADCO are given in Refs. 8 and 10. This section of the present report is not intended to supply a detailed account of their experiments but rather a summary of their observations.

ORNL carried out the following examinations on B_4C pellets from capsules G and H of HWCR L-4008S:

(1) Plenum-gas analysis
(2) Visual examination
(3) Length, diameter, and weight measurements
(4) Burnup determination by $^{10}B/^{11}B$ isotopic analysis
(5) Metallography on B_4C pellets
(6) Transmission electron microscopy on B_4C pellets
(7) Scanning electron microscopy of fractured surfaces
(8) X-ray diffraction to determine lattice parameters
(9) Measurement of retained gas by vacuum fusion analysis.

Items (1), (3), and (4) have been discussed and compared with results from ANL in previous sections of the present report. The ORNL visual examination showed that the irradiated pellets were in excellent condition with no observed cracks or other irregularities attributable to irradiation. The pellets slid freely from the Type 304L stainless steel capsule.

The metallography examination revealed "a microstructure which is typical of carbon rich hot-pressed B_4C with some free graphite in the grain boundaries, a typical amount of twinning, some metallic appearing impurities, some intergranular porosity, and a small amount of intragranular porosity."[9]

The transmission electron microscopy of the irradiated B_4C pellets showed a microstructure that was "characterized by a high density of black spot defects. There is a grain boundary denuded zone of defects but twin boundaries do not exhibit denuding. The grown-in lattice defects, twins and stacking faults, are still present after irradiation. Thus, to a first glance, the radiation damage structure closely resembles that in metals where defect clusters formed by the aggregation of point defects caused by displacements are the main evidence of damage for irradiation

temperatures below about 0.3 T_m, where T_m is the melting point in °K. For B_4C, with T_m about 2450°C, the temperature range investigated, about 500 - 730°C, represents 0.28 - 0.36 T_m. . .

"The scanning electron microscopy results showed that the irradiated B_4C pellets fractured in a predominant transgranular fashion. After annealing at 1150°C for 1 hr, the fracture is clearly intergranular. After annealing at 2000°C, the fracture appears to be of mixed mode."[7]

X-ray-diffraction Debye-Scherrer powder patterns were obtained on powdered samples from the irradiated B_4C pellets. "The as-irradiated lattice parameters show a unit cell volume increase of about 0.3% through an increase in the rhombohedral a parameter and a slight decrease in the angle α. The lattice parameter change during annealing showed that the a parameter first increased, then decreased with increasing annealing temperature. The angle α first showed a marked decrease and then a rapid increase with annealing temperature. The volume again changed uniformly with annealing temperature and returned to about the unirradiated value around 1300°C."[9]

The vacuum-fusion results (comparable to ANL's helium-retention experiments) on pellet 14 from capsule H showed that 8.1 ± 4.6% of the helium gas generated due to ^{10}B burnup was released during irradiation. Further vacuum-fusion experiments are in progress at ORNL.

WADCO carried out the following examination on B_4C pellets from capsules A and B of HWCR L-4008S.

(1) Plenum gas analysis
(2) Length, diameter, and weight measurements
(3) Immersion density measurements
(4) Burnup determination by $^{10}B/^{11}B$ isotopic analysis
(5) Thermal conductivity studies.

Items (1) through (4) have been discussed and compared with results from ANL in previous sections of the present report.

The thermal-conductivity studies showed that low-level exposure to radiation reduces the conductivity by 50%. The reduction saturates at a burnup of 1×10^{20} captures/cm^3, which is equal to approximately 0.46 at.% ^{10}B burnup.

"The thermal conductivity decrease is attributed to lattice damage and to the formation of plate-like porosity within the boron carbide matrix,

both of which introduce scattering centers that decrease the average phonon mean-free-path."[10]

IV. CONCLUSIONS

The following are the conclusions of this study:

(1) No galling or chafing was observed on the surfaces of the stainless steel capsules that contained the B_4C pellets.

(2) No significant diameter increases or bow was observed on the stainless steel capsules that contained the B_4C pellets.

(3) The B_4C pellets retained most of the helium generated from ^{10}B burnup, and therefore, the additional stress produced from helium release was negligible.

(4) No additional stress was imposed on the stainless steel capsule by swelling of the B_4C pellets.

(5) Metallographic examination showed no interaction of the B_4C pellets with the Type 304L stainless steel capsule.

(6) The B_4C pellets appeared in good condition after irradiation, with no observed disintegration due to crack formation.

(7) The sodium-compatibility experiments showed that B_4C pellets did not disintegrate to any extent in low-velocity flowing sodium but did disingegrate during the alcohol and water wash after removal from the sodium.

On the basis of this postirradiation examination, it is concluded that higher-worth control rods of the present design can be safely used in EBR-II up to the maximum Mark-IA fuel burnup limit of 1.8 at.%.

APPENDIX A

Diameter Profiles and Bow Measurements of B_4C Capsules

Figures 12 through 39 show the pre- and postirradiation diameter profiles of the B_4C capsules from HWCR's L-4008S and L-4009S.

Figures 40 through 55 show the direction and amount of bow for each of the capsules in the two HWCR's. Capsule L from HWCR L-4009S had the maximum bow (0.029 in.). The bow for all capsules was insignificant, and no correlation could be made between the direction of bow and the reactor core center.

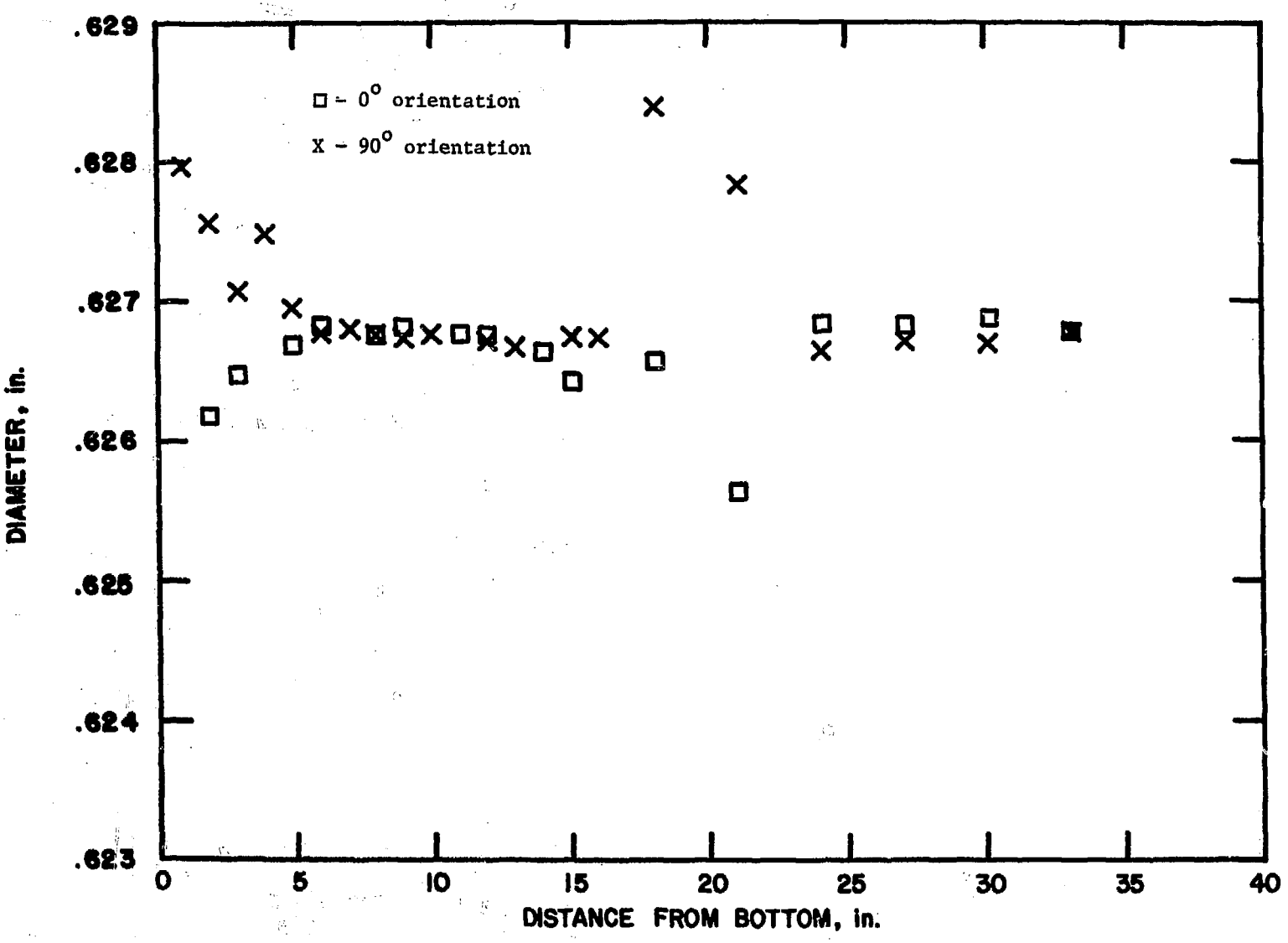

Fig. 12. Preirradiation Diameter Profile of Capsule A (L-4008S)

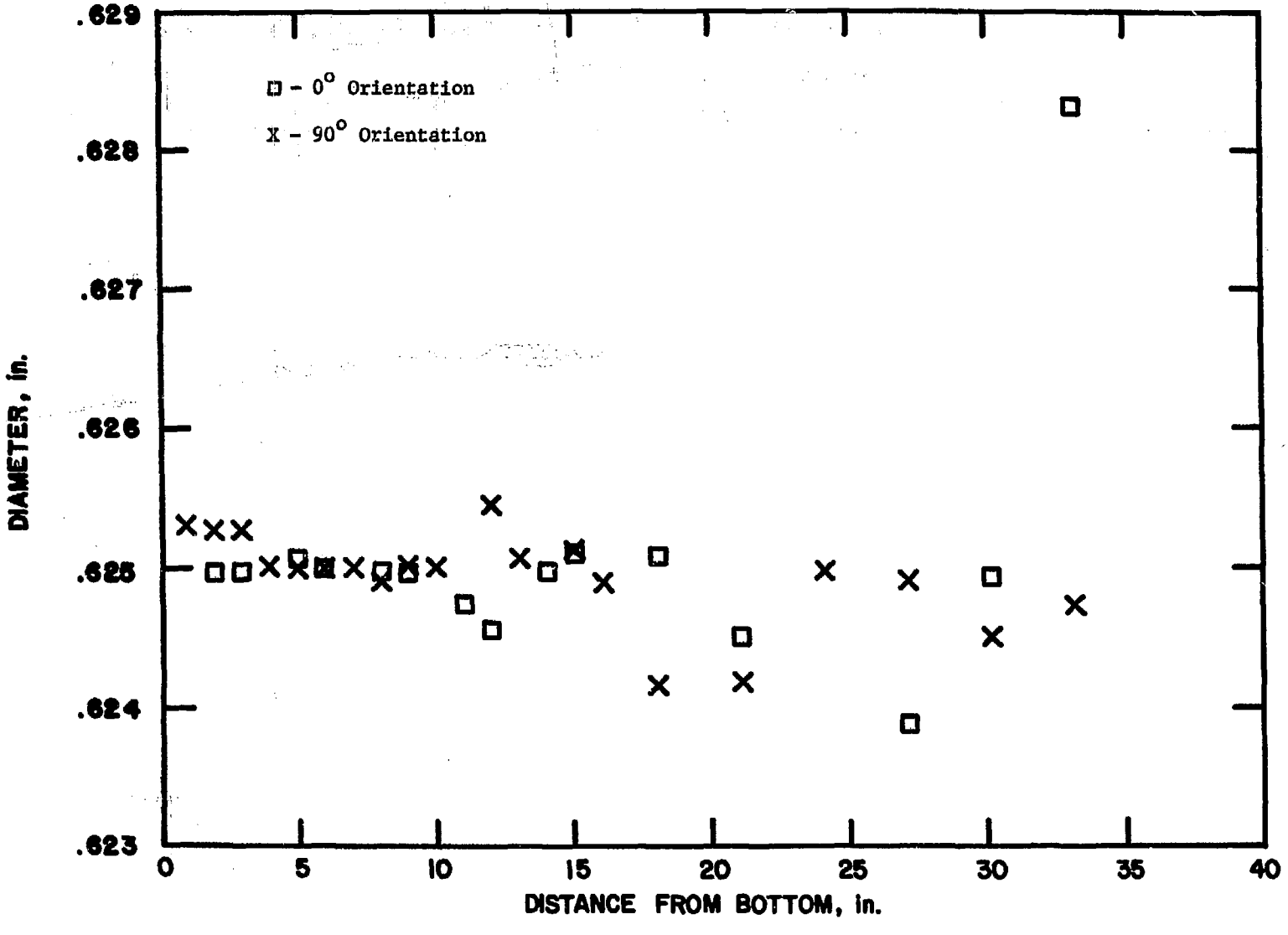

Fig. 13. Postirradiation Diameter Profile of Capsule A (L-4008S)

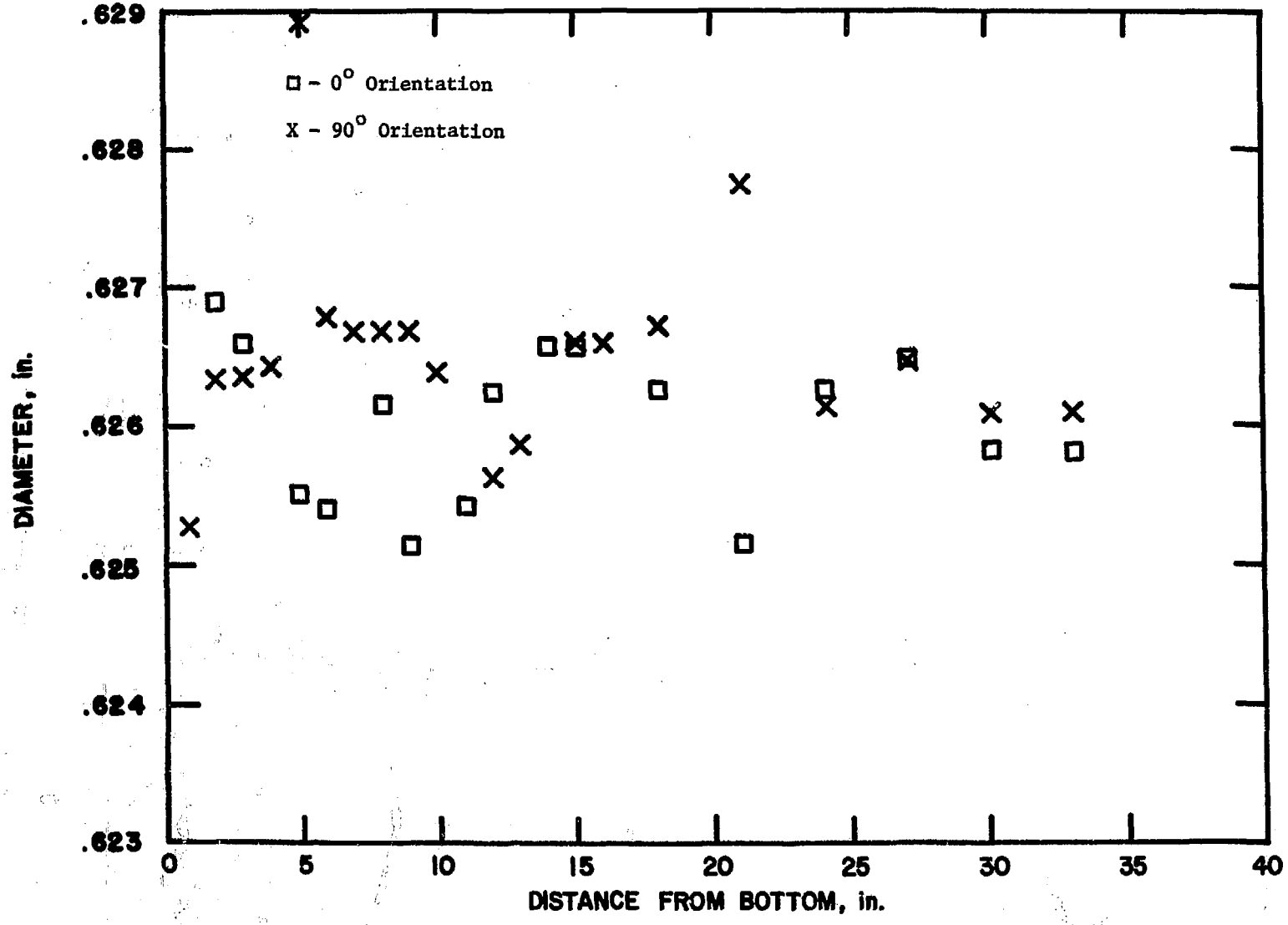

Fig. 14. Preirradiation Diameter Profile of Capsule B (L-4008S)

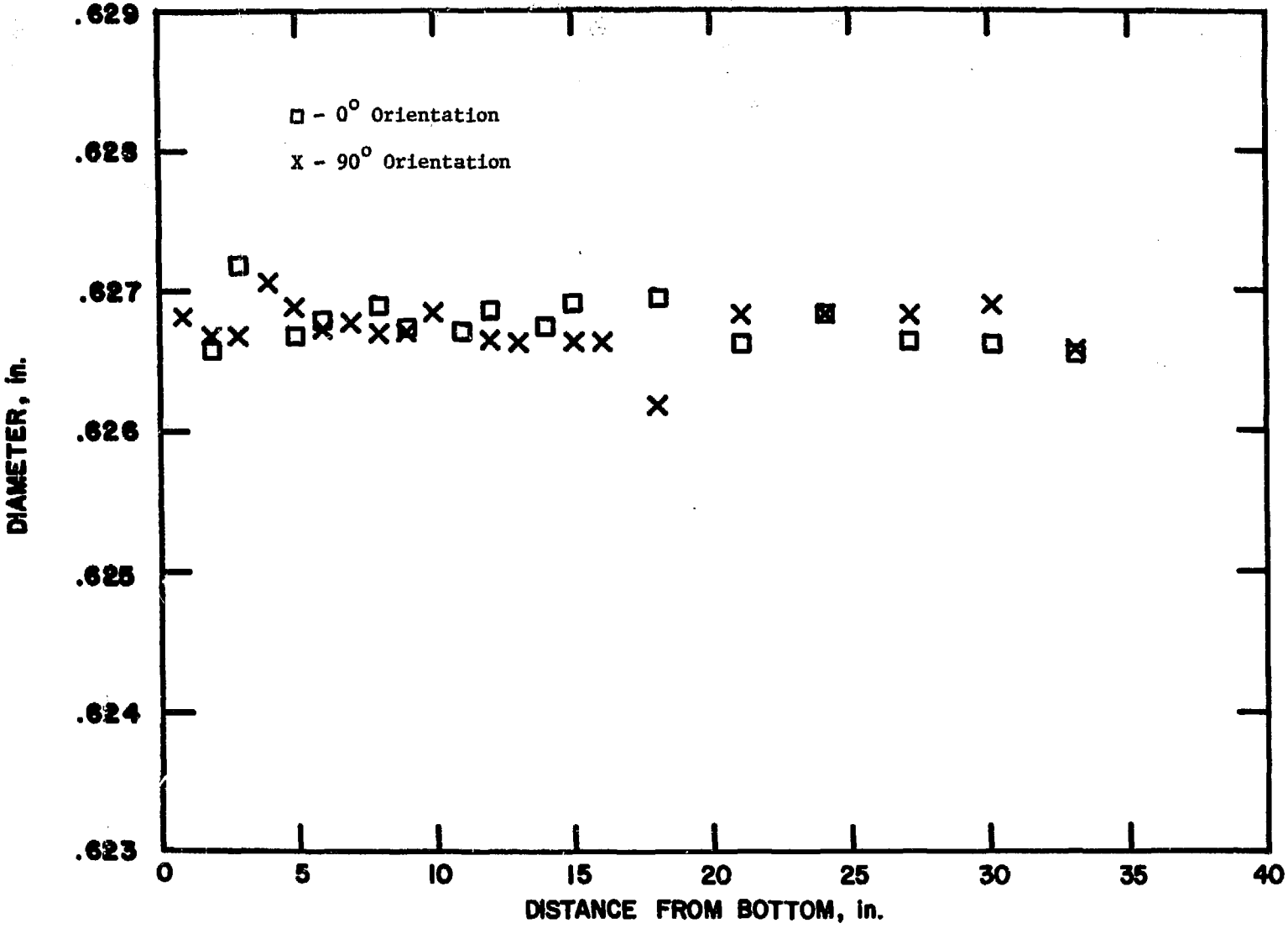

Fig. 15. Postirradiation Diameter Profile of Capsule B (L-4008S)

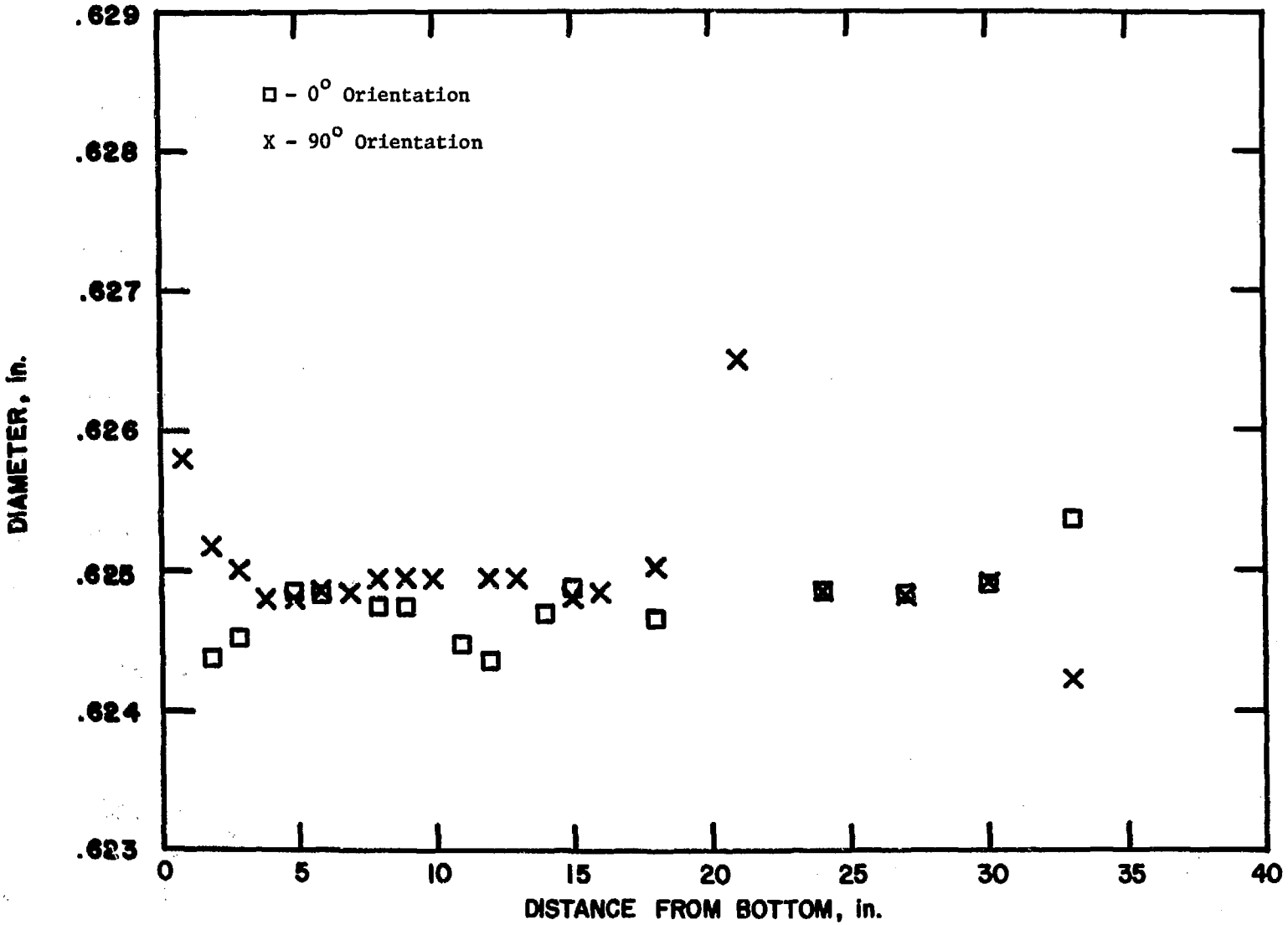

Fig. 16. Preirradiation Diameter Profile of Capsule C (L-4008S)

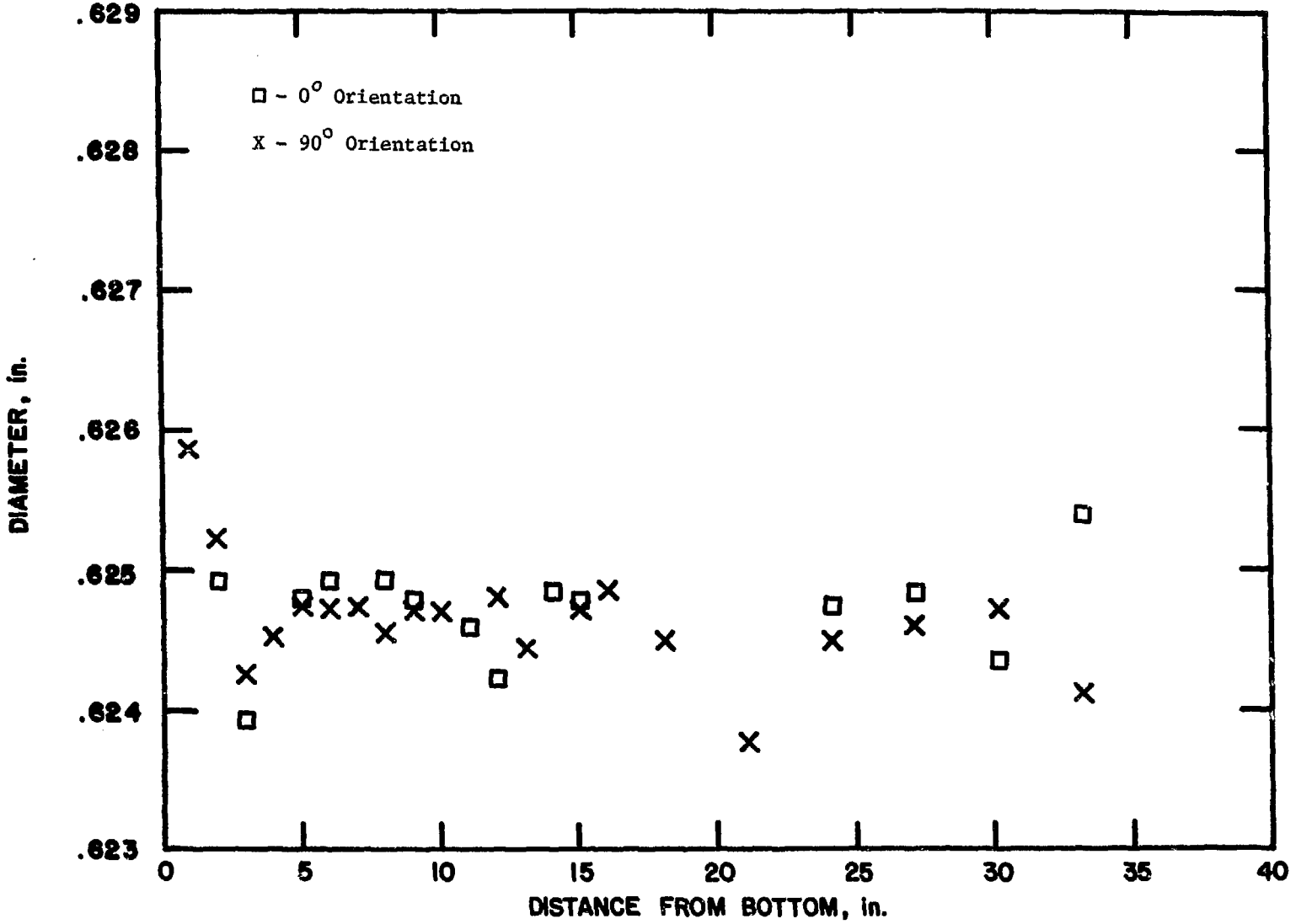

Fig. 17. Postirradiation Diameter Profile of Capsule C (L-4008S)

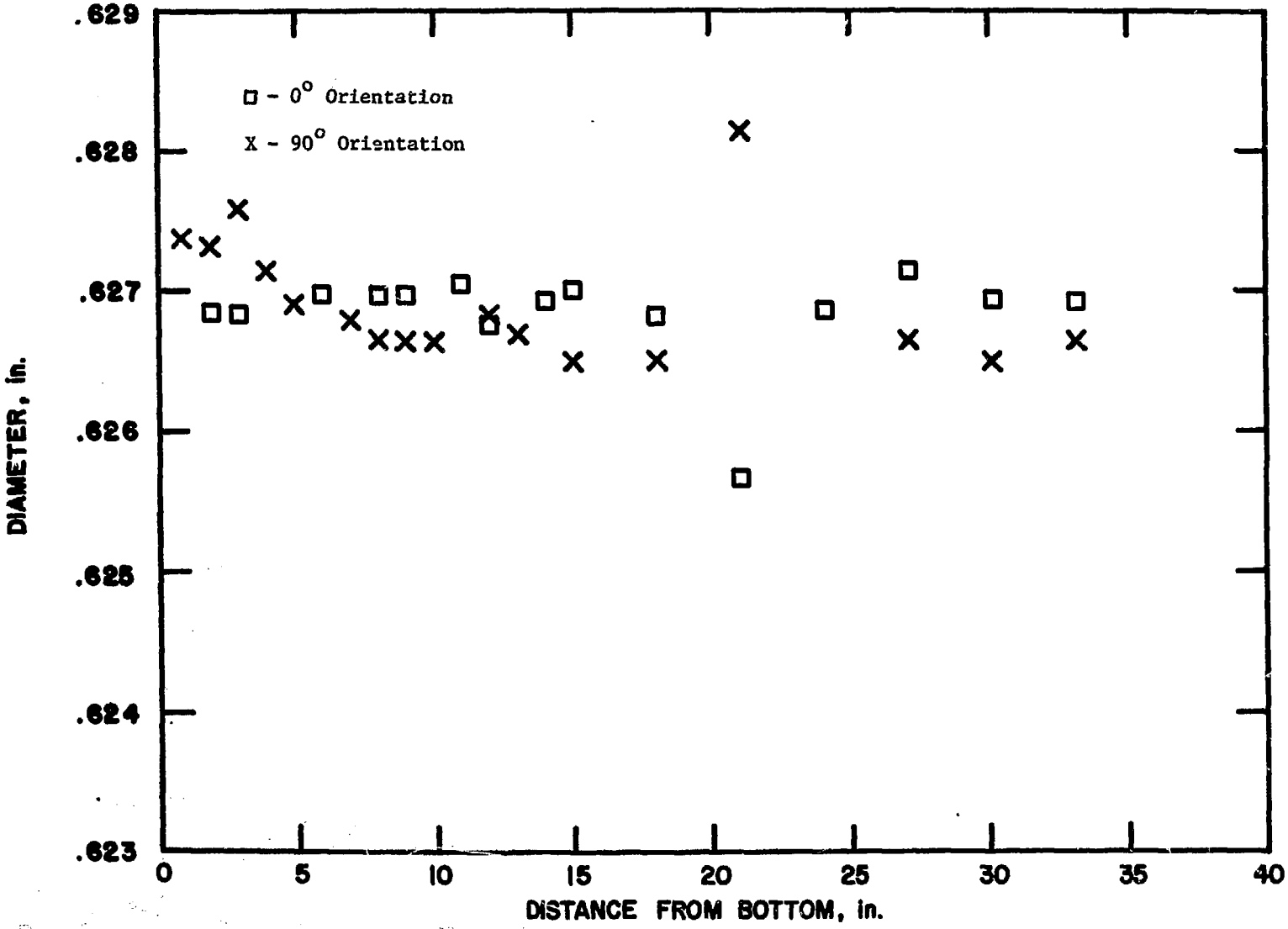

Fig. 18. Preirradiation Diameter Profile of Capsule E (L-4008S)

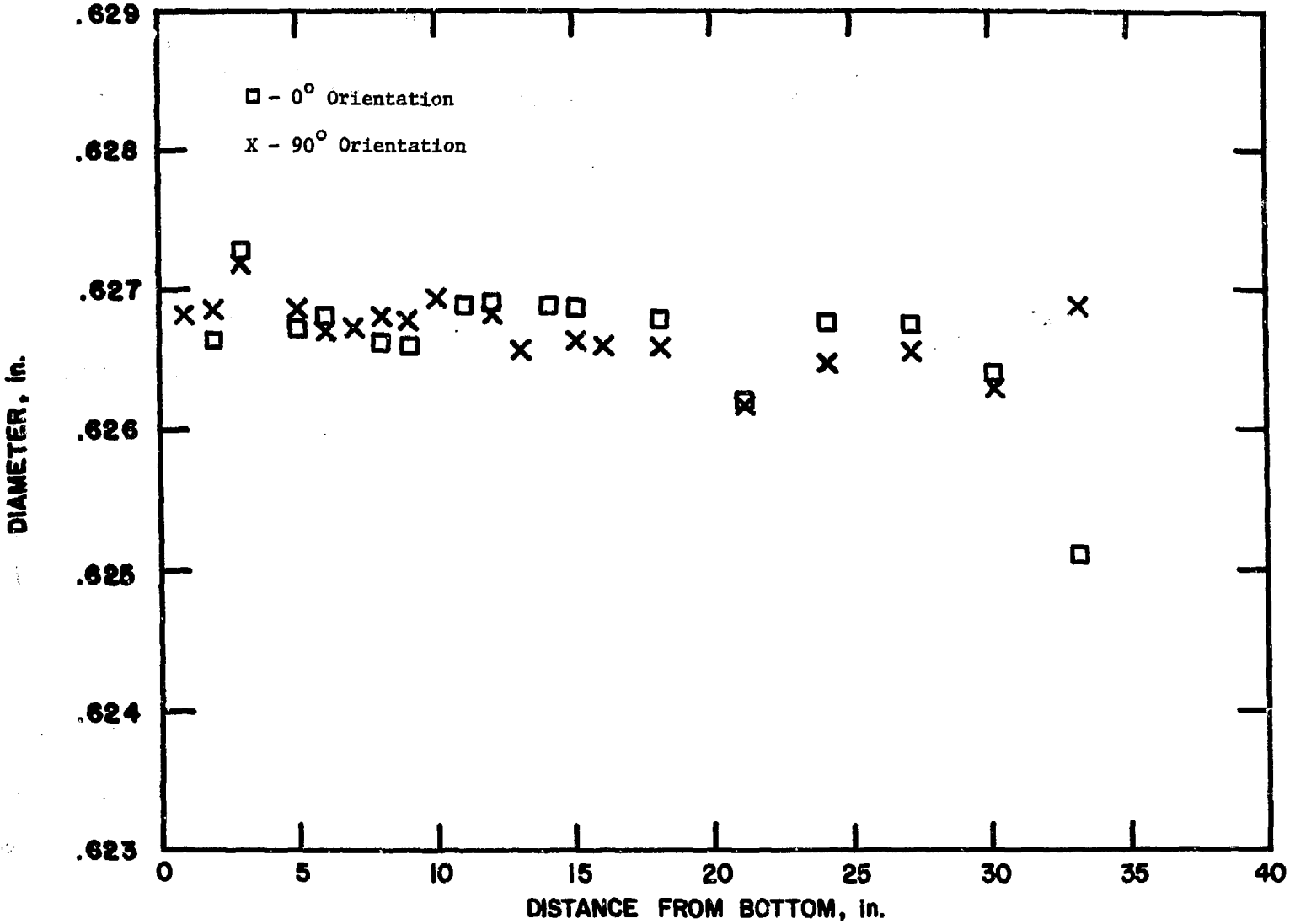

Fig. 19. Postirradiation Diameter Profile of Capsule E (L-4008S)

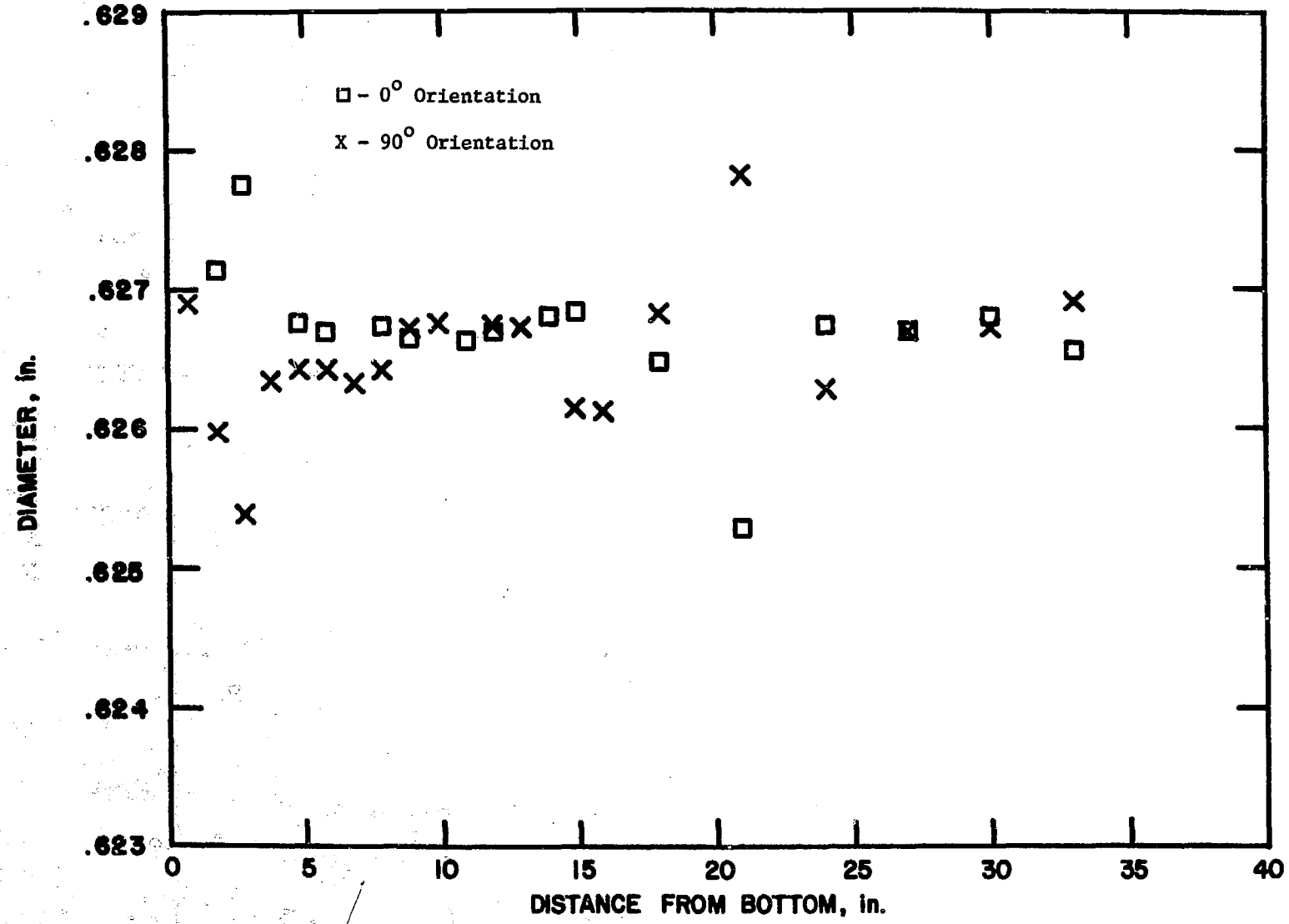

Fig. 20. Preirradiation Diameter Profile of Capsule F (L-4008S)

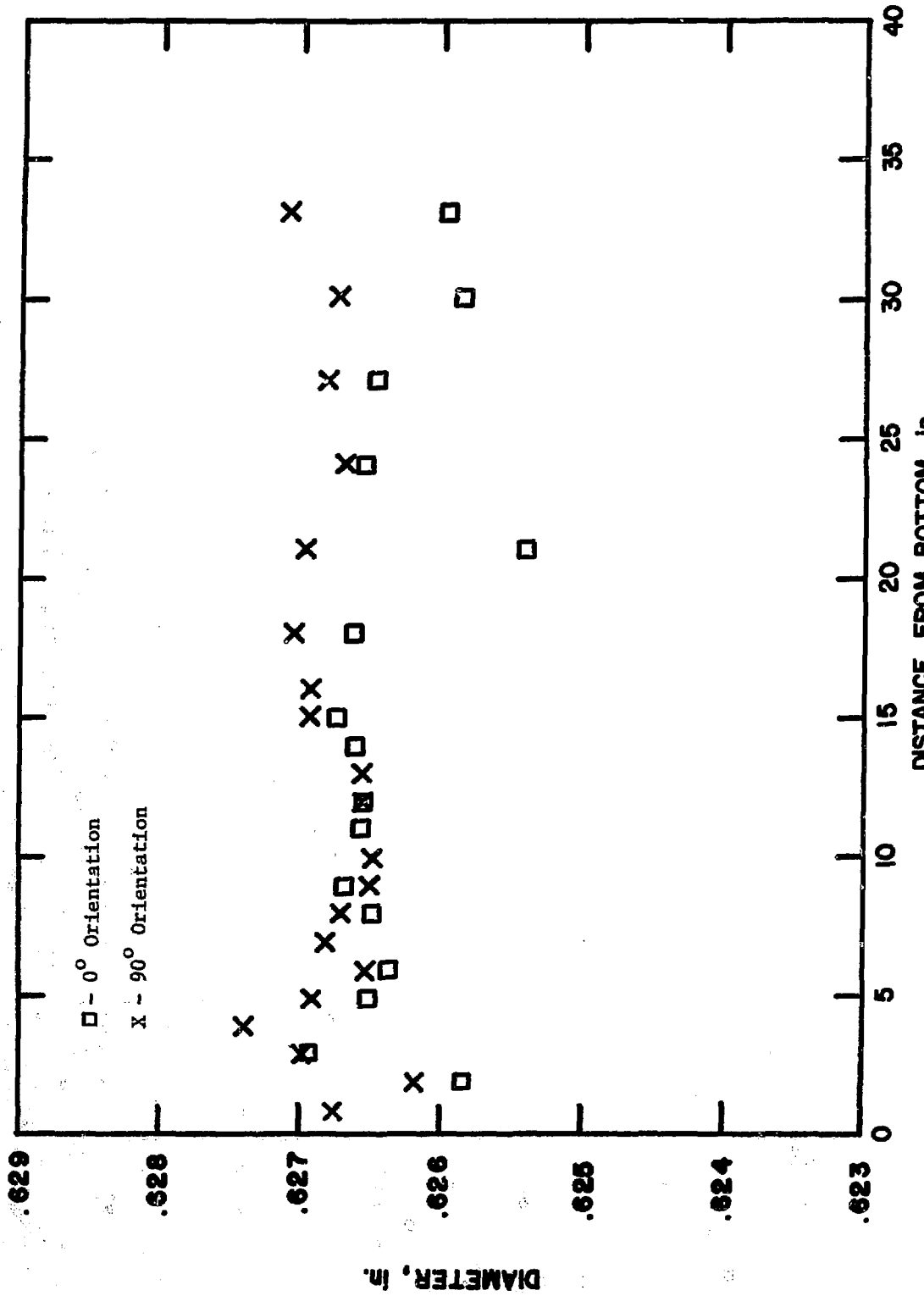

Fig. 21. Postirradiation Diameter Profile of Capsule F (L-4008S)

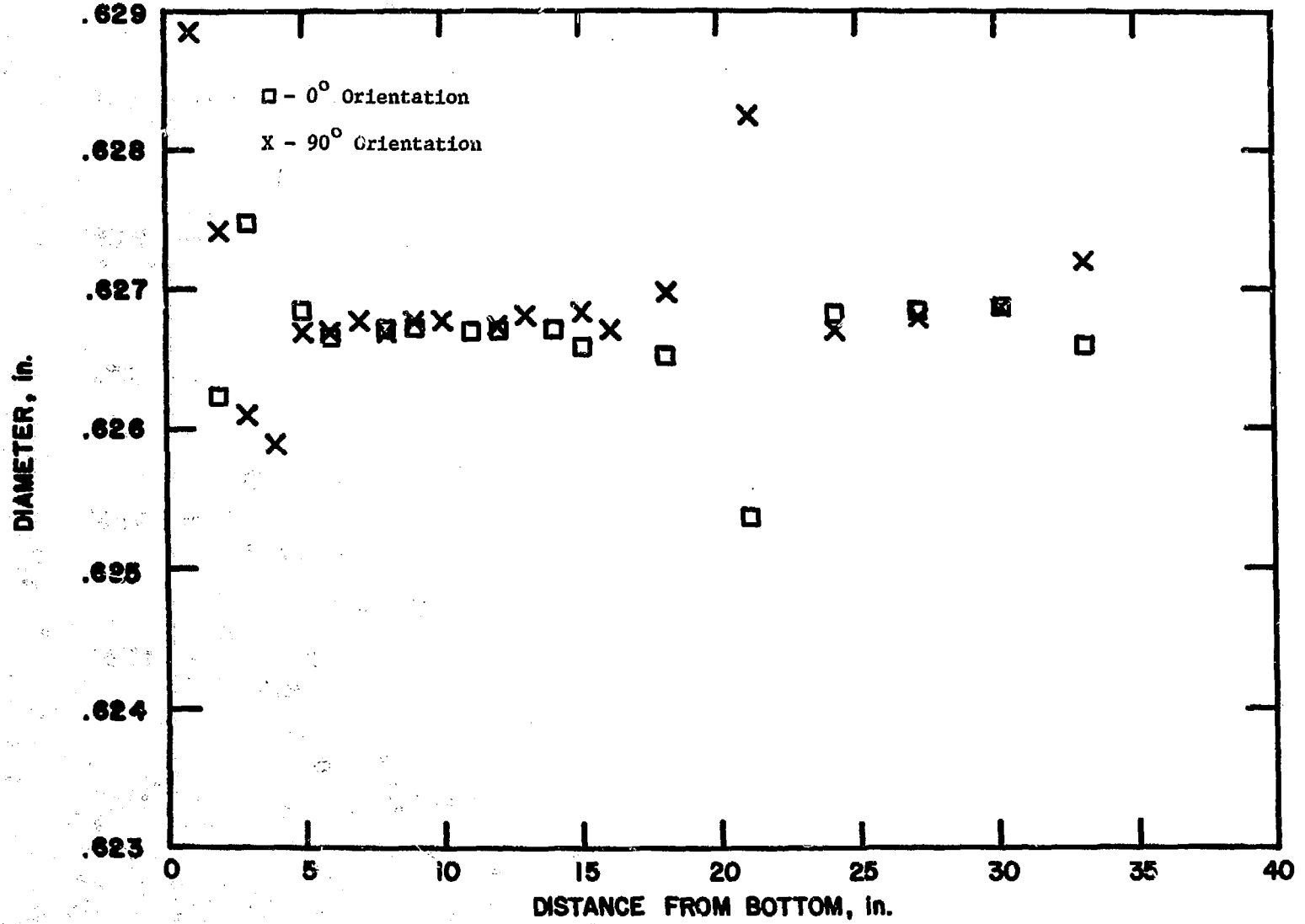

Fig. 22. Preirradiation Diameter Profile of Capsule G (L-4008S)

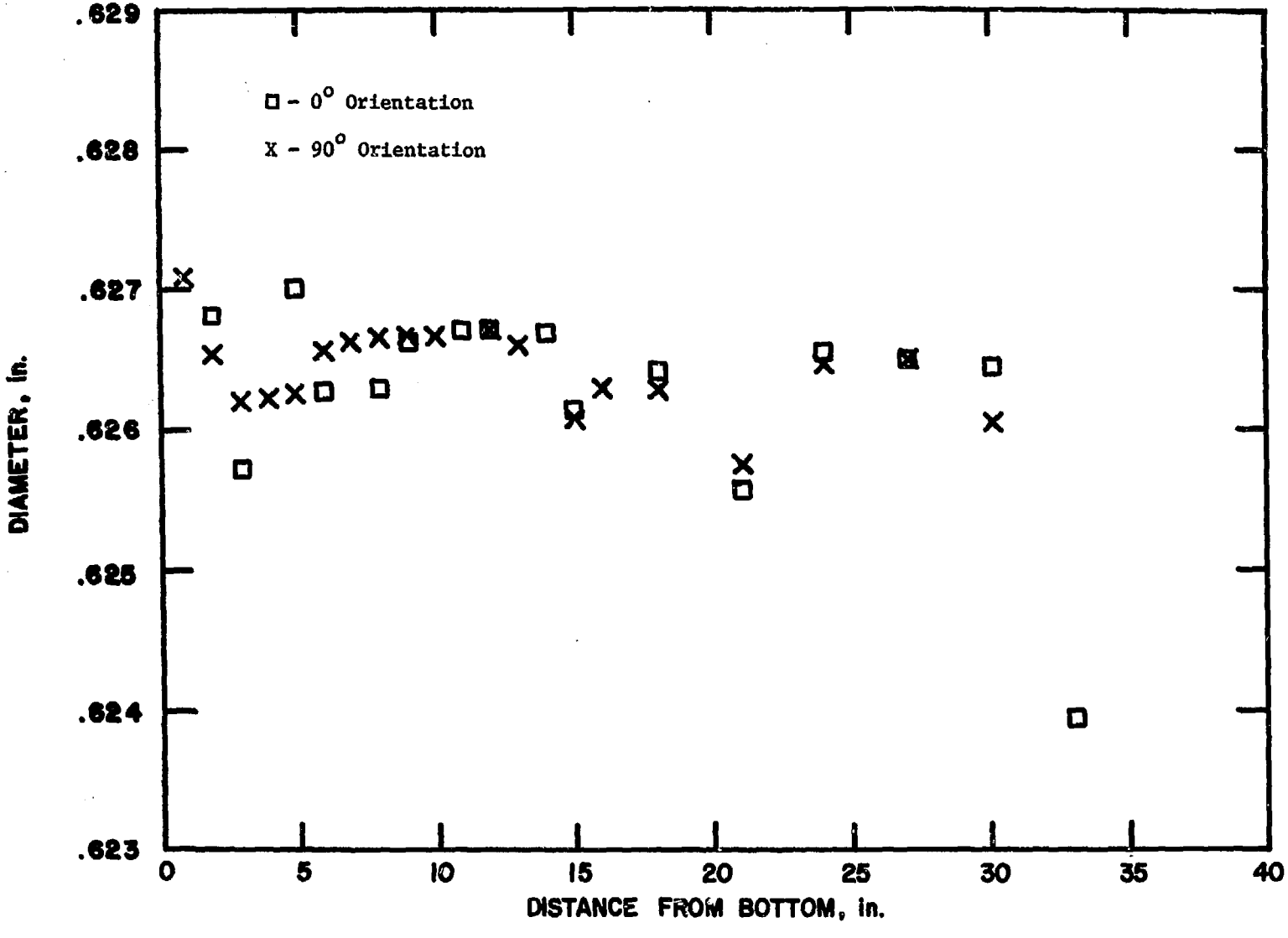

Fig. 23. Postirradiation Diameter Profile of Capsule G (L-4008S)

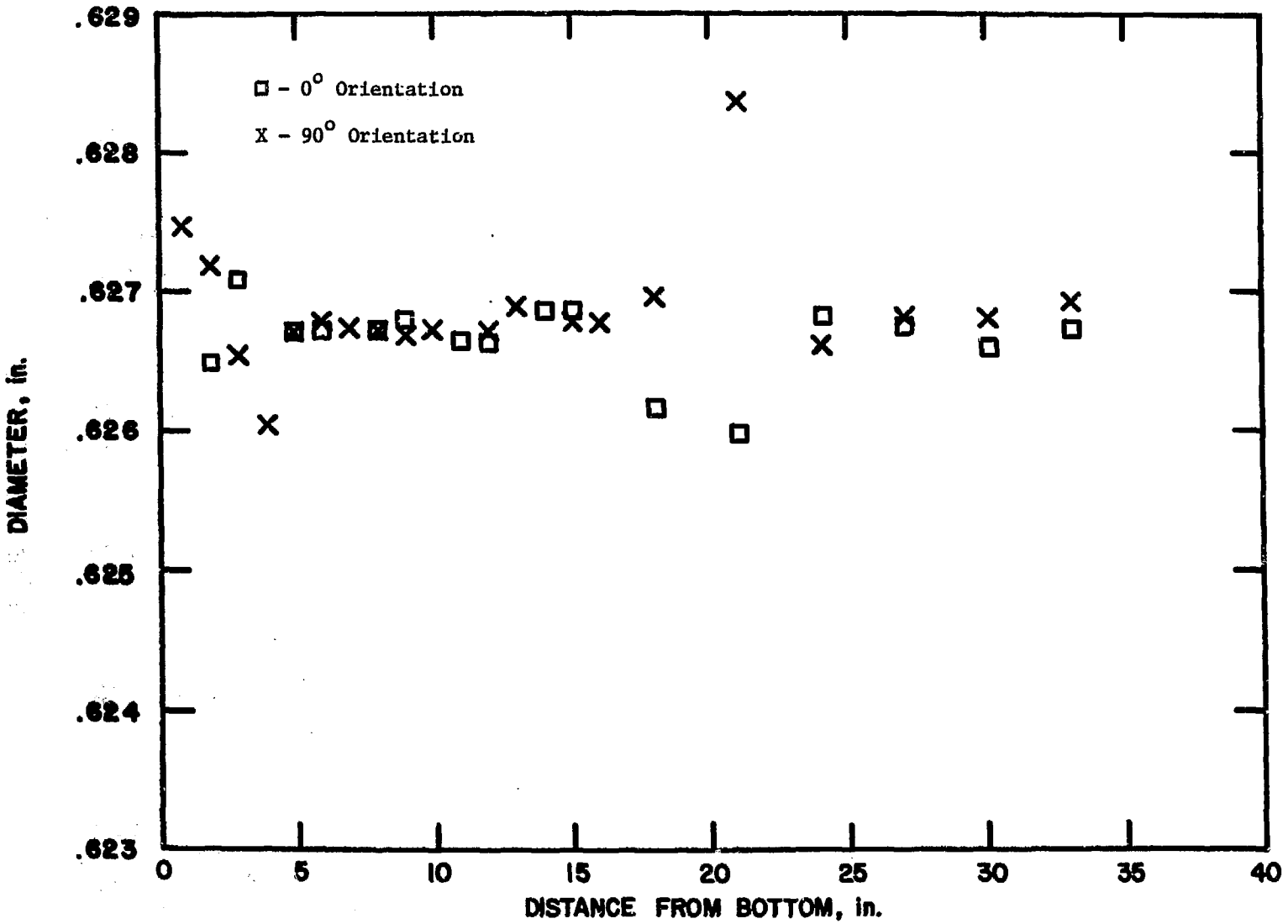

Fig. 24. Preirradiation Diameter Profile of Capsule H (L-4008S)

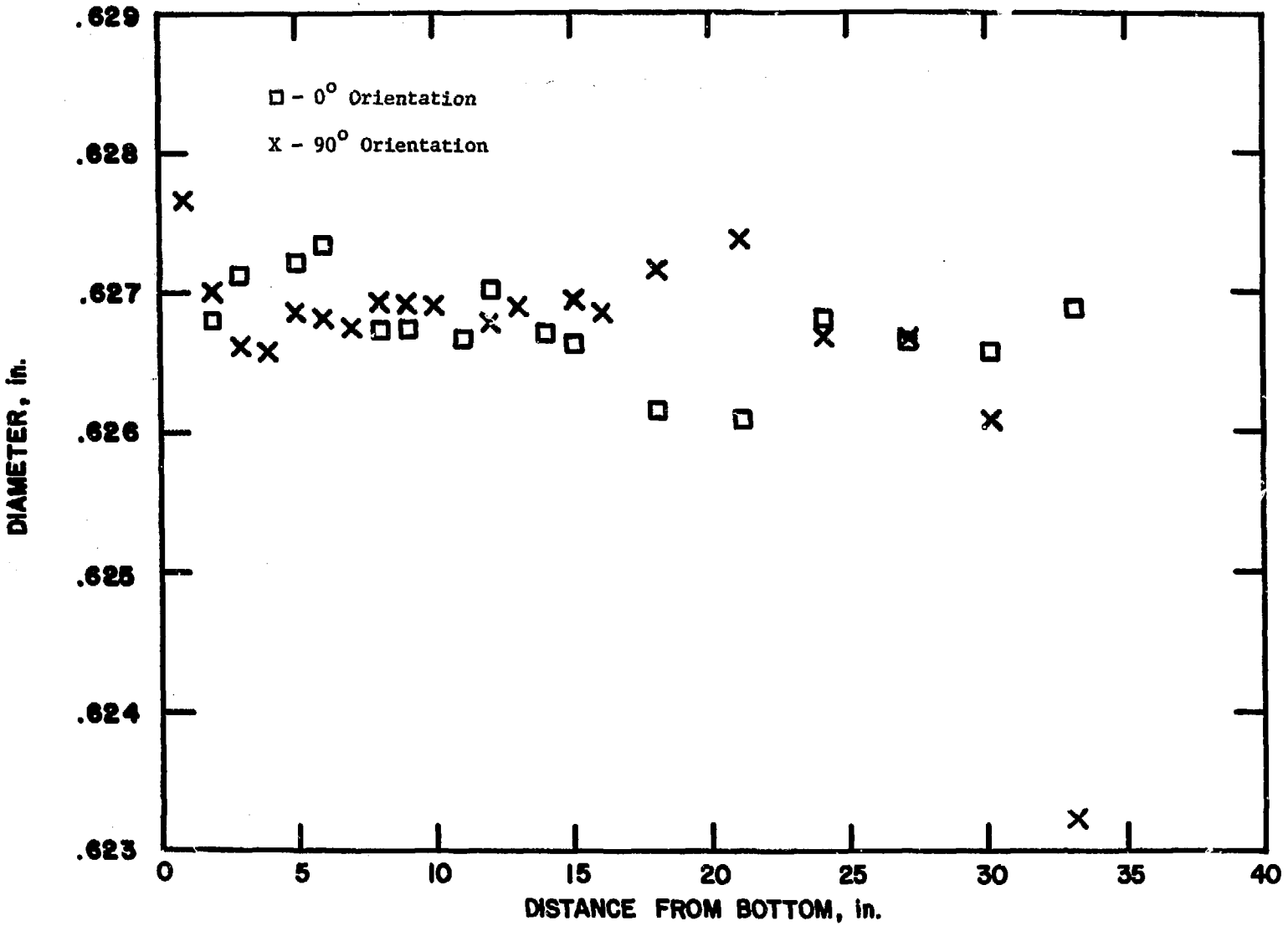

Fig. 25. Postirradiation Diameter Profile of Capsule H (L-4008S)

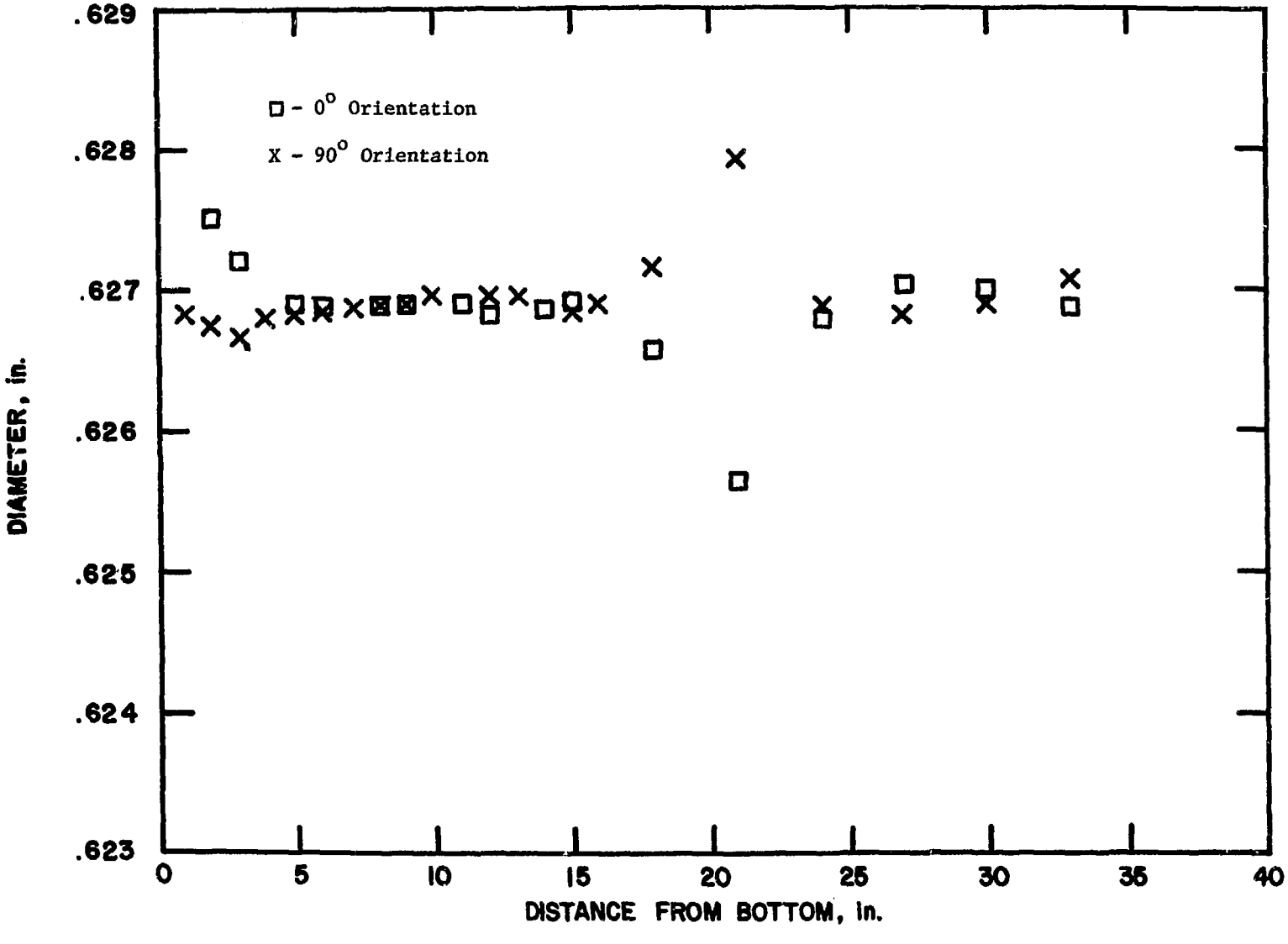

Fig. 26. Preirradiation Diameter Profile of Capsule D (L-4009S)

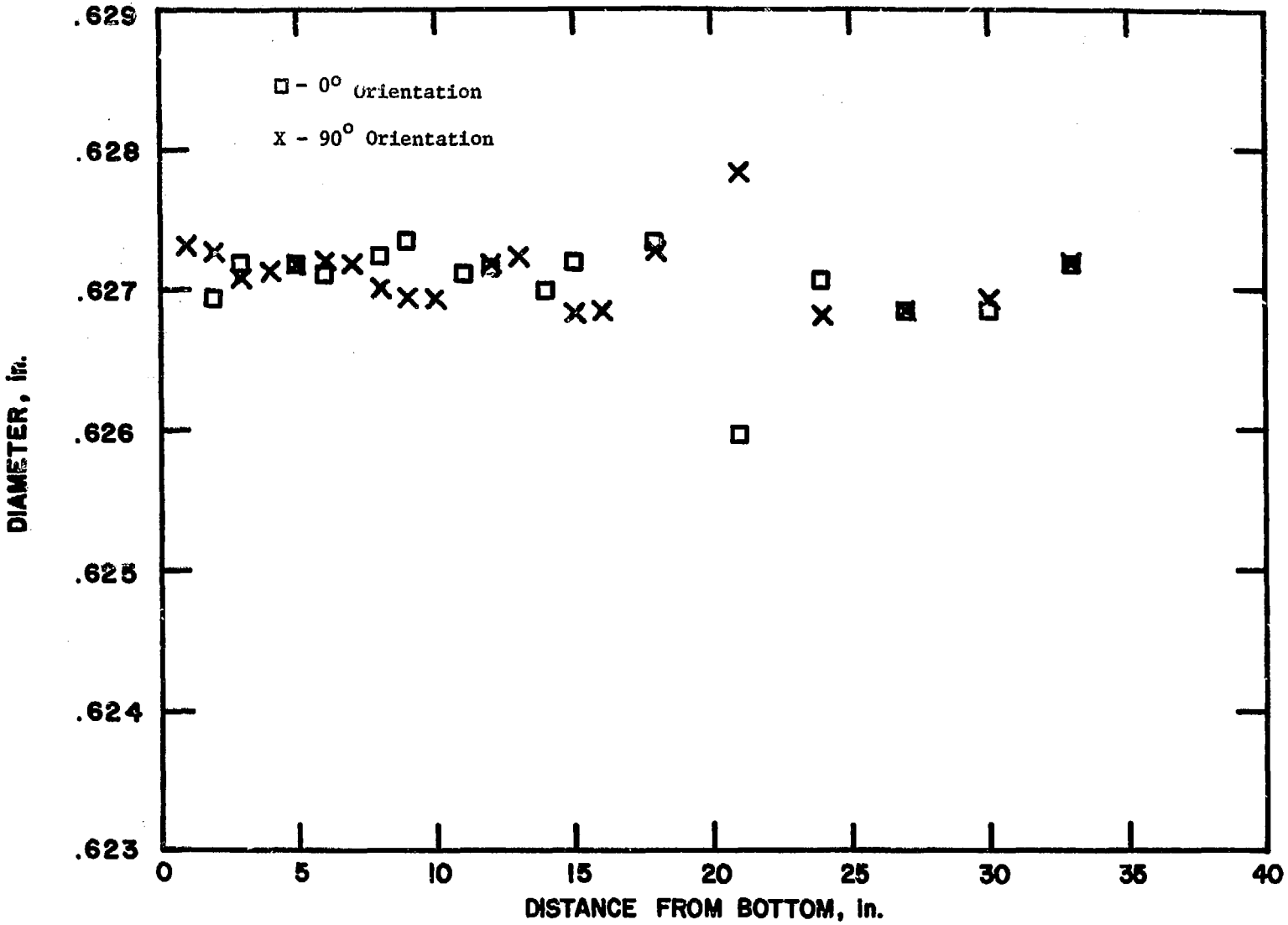

Fig. 27. Postirradiation Diameter Profile of Capsule D (L-4009S)

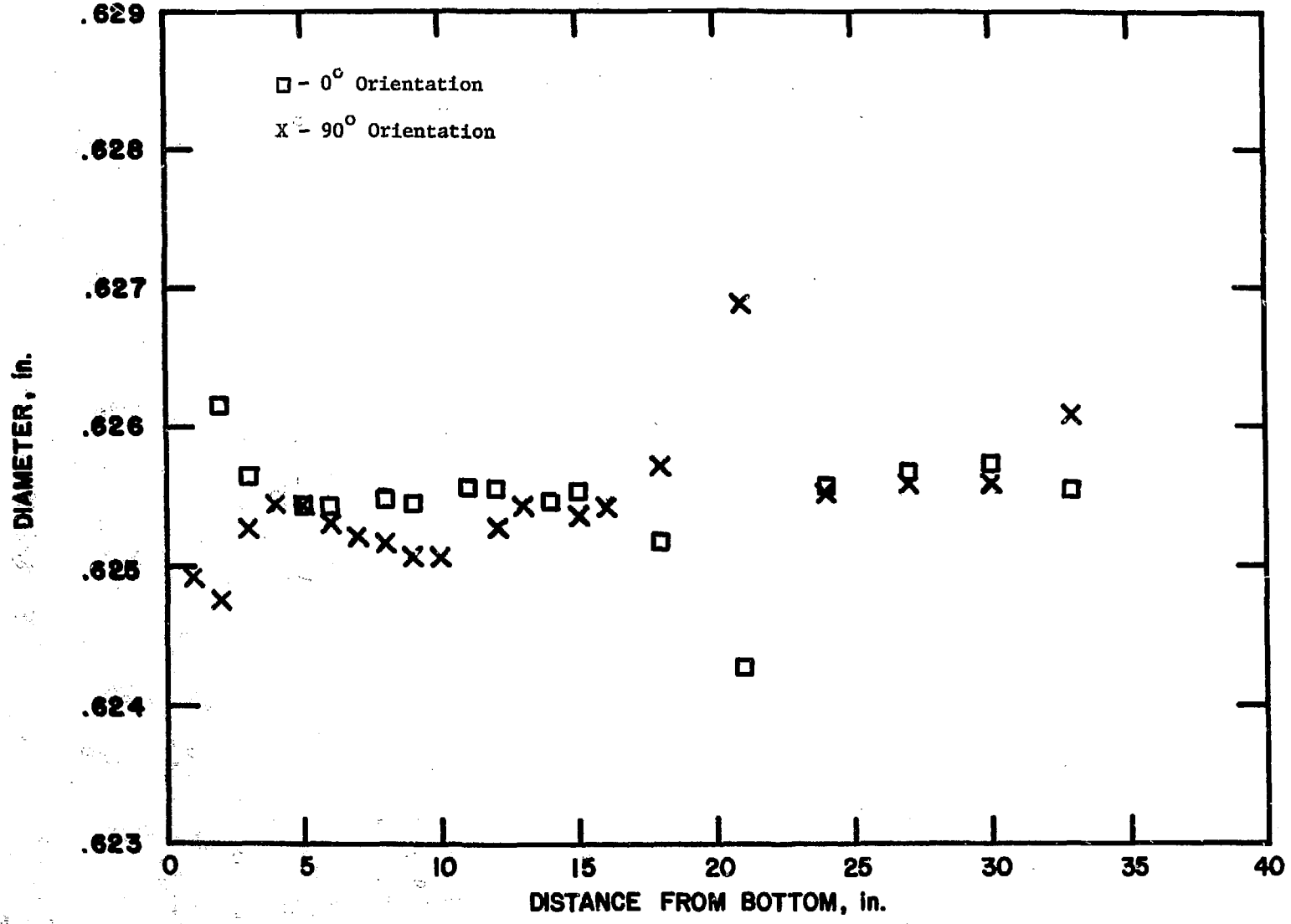

Fig. 28. Preirradiation Diameter Profile of Capsule J (L-4009S)

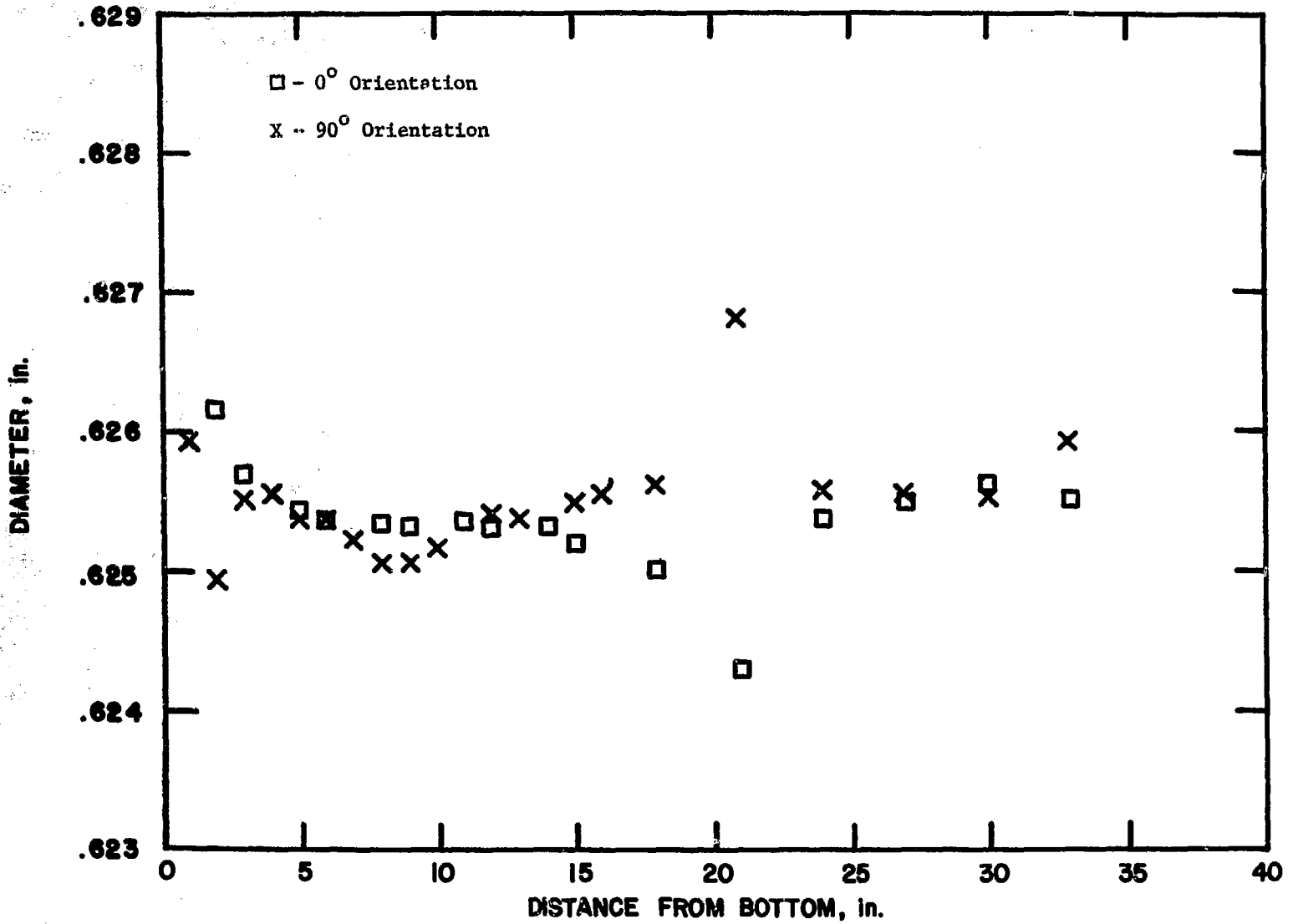

Fig. 29. Postirradiation Diameter Profile of Capsule J (L-4009S)

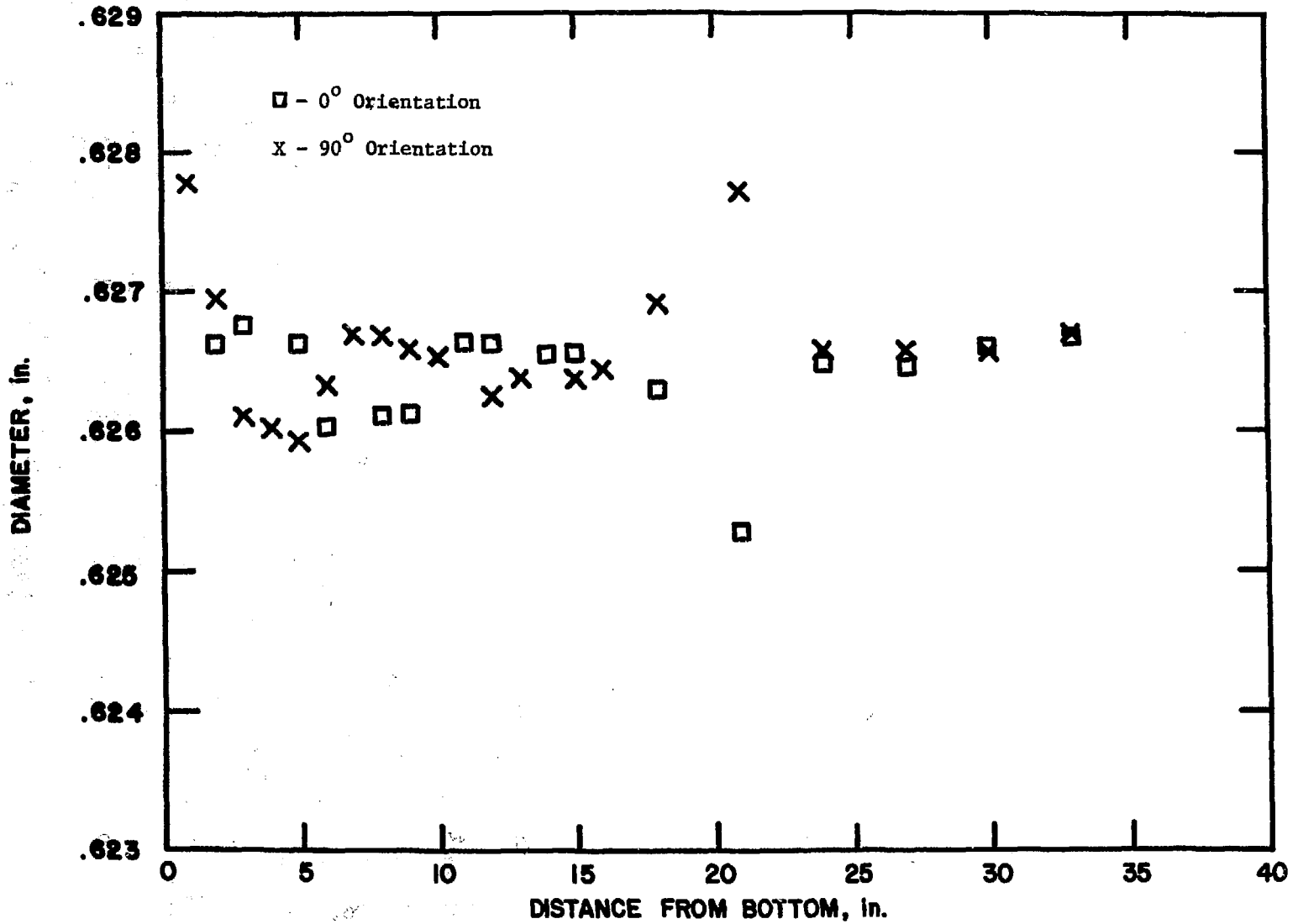

Fig. 30. Preirradiation Diameter Profile of Capsule K (L-4009S)

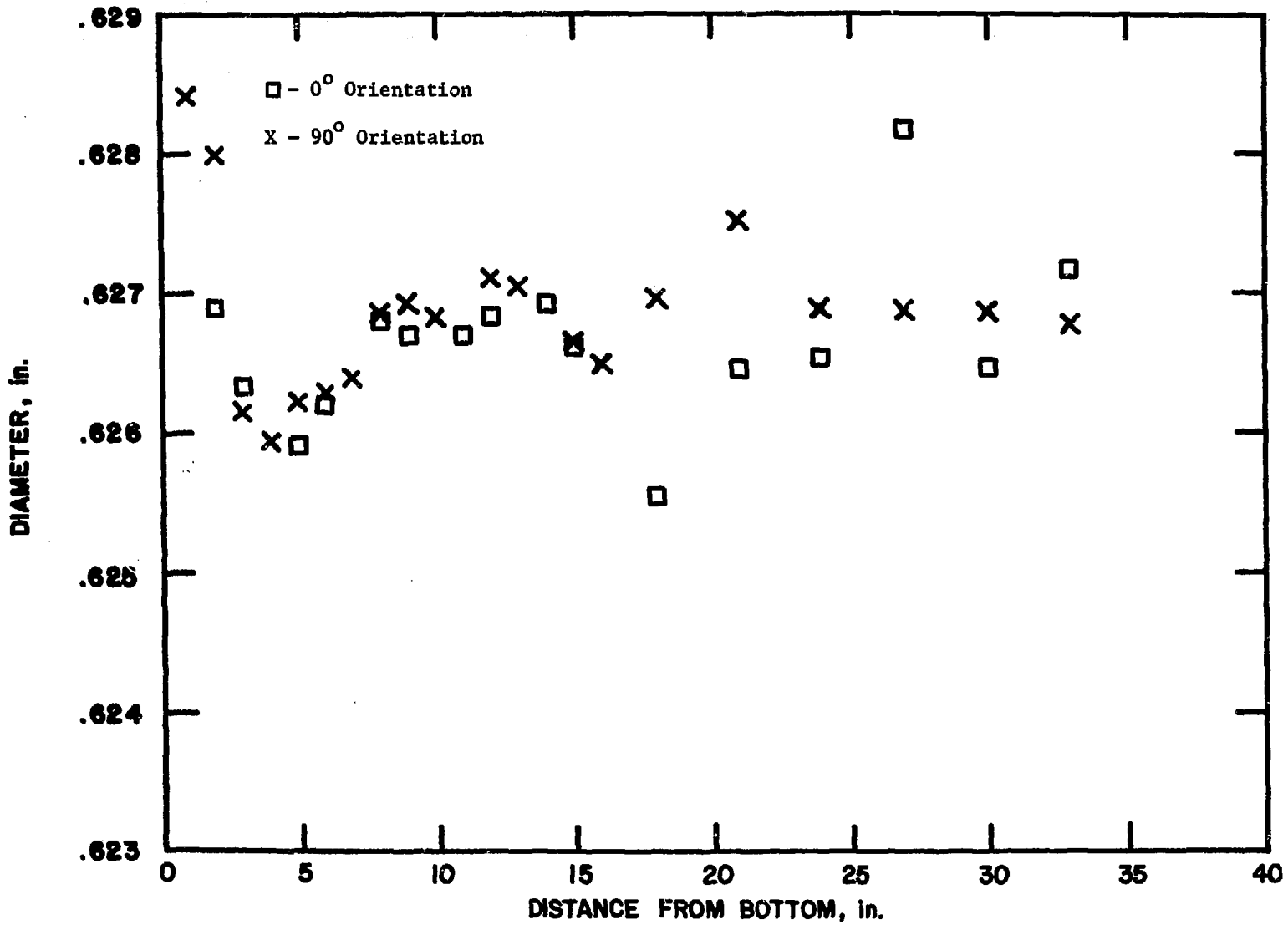

Fig. 31. Postirradiation Diameter Profile of Capsule K (L-4009S)

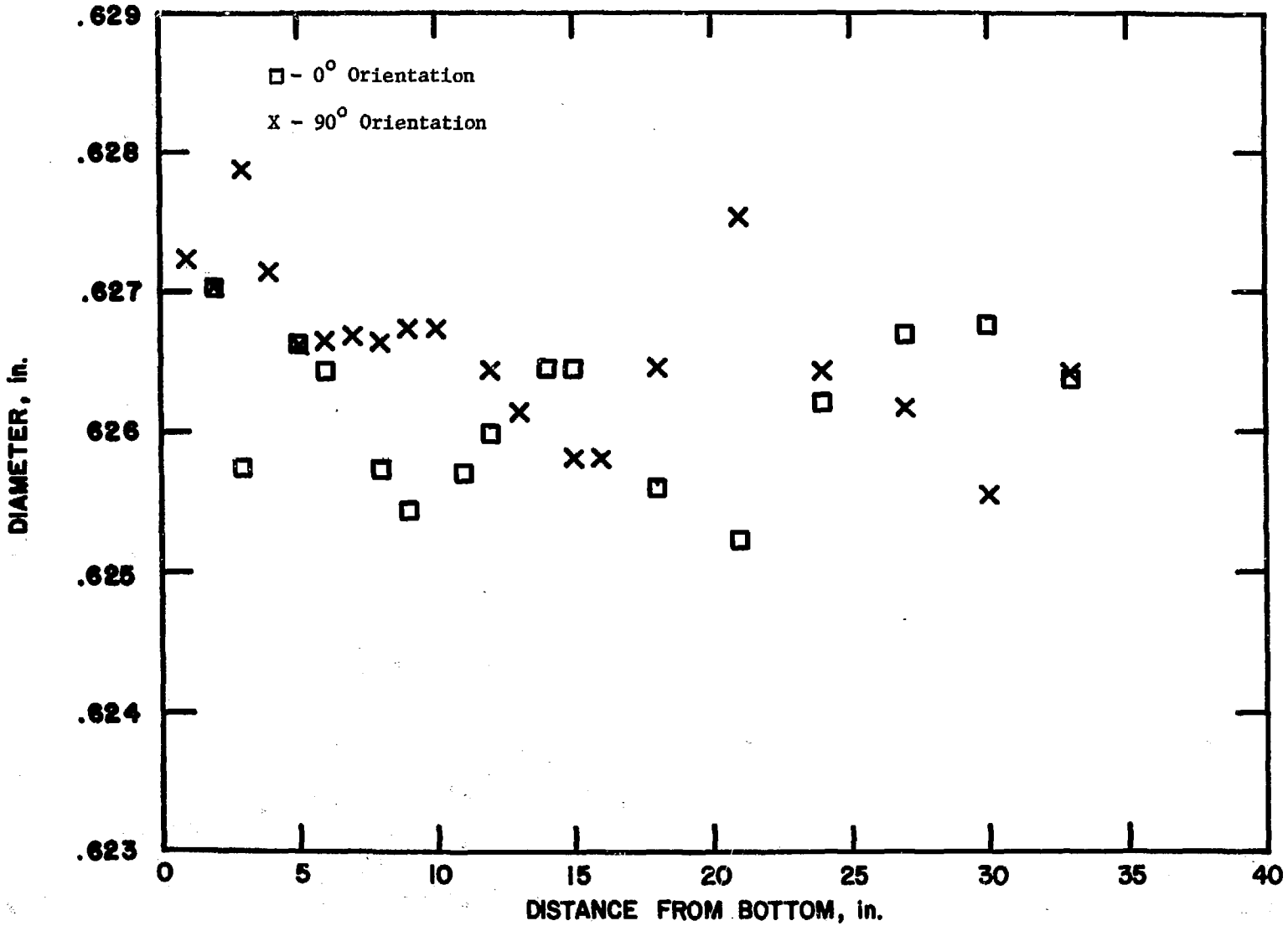

Fig. 32. Preirradiation Diameter Profile of Capsule L (L-4009S)

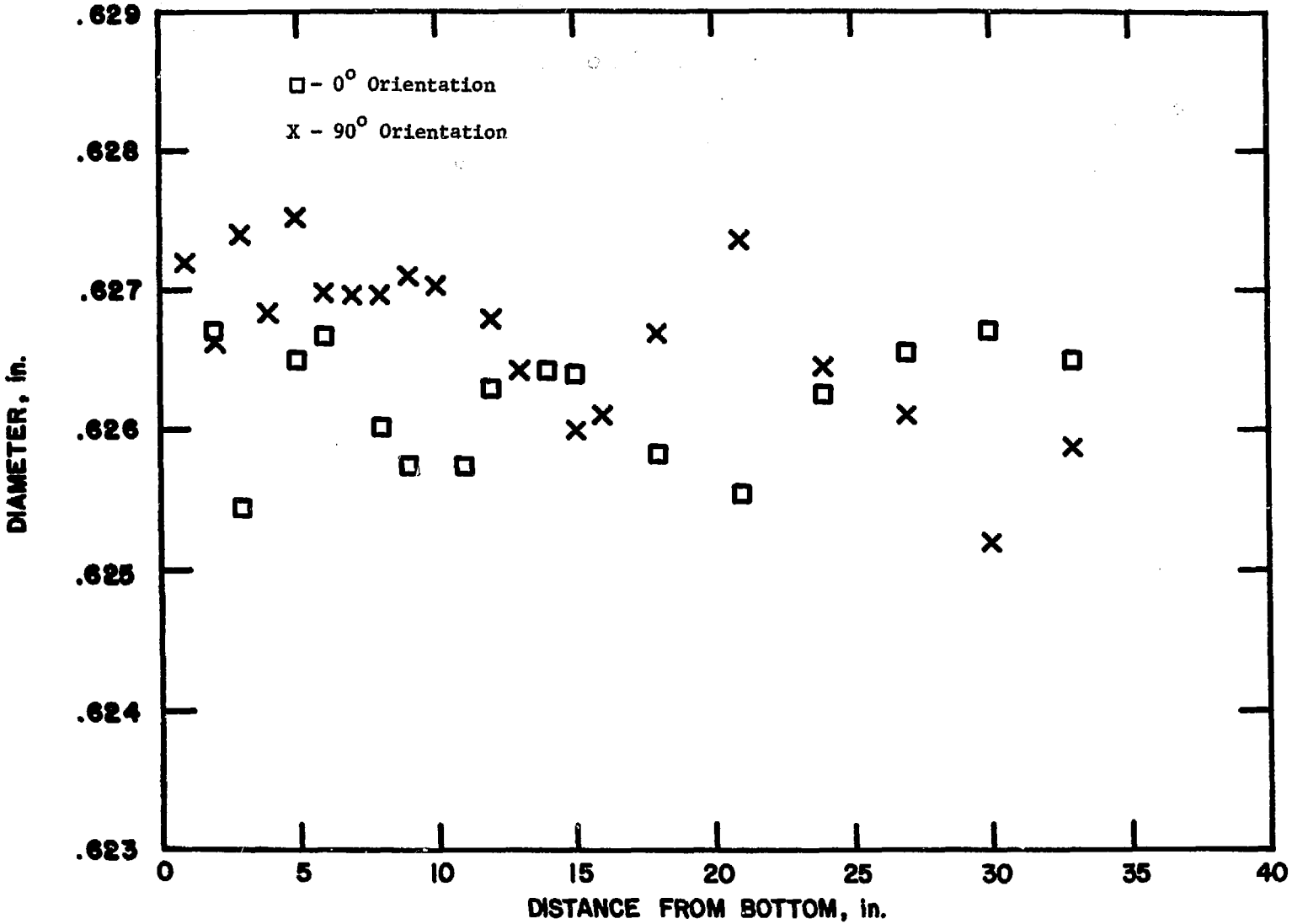

Fig. 33. Postirradiation Diameter Profile of Capsule L (L-4009S)

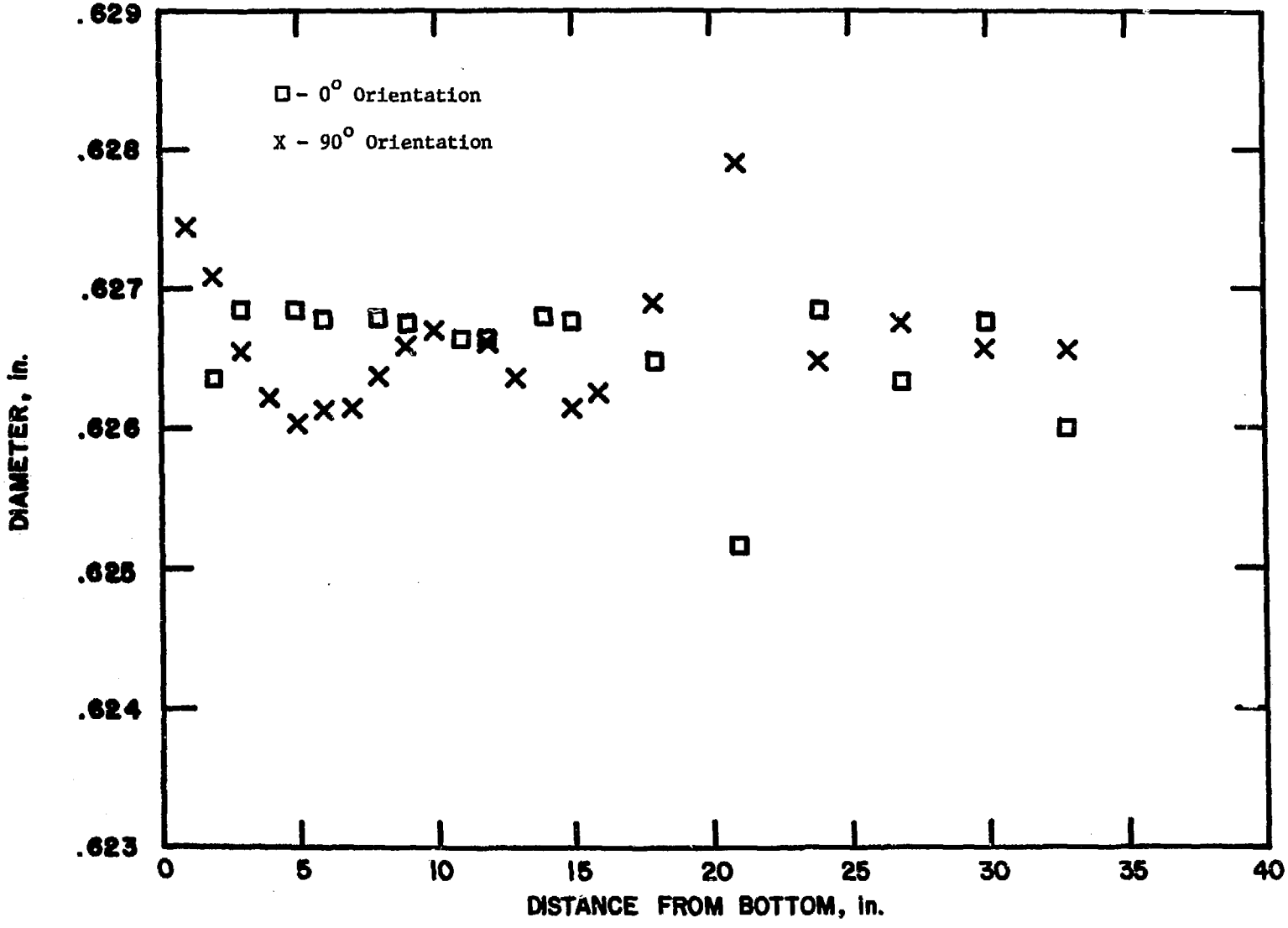

Fig. 34. Preirradiation Diameter Profile of Capsule M (L-4009S)

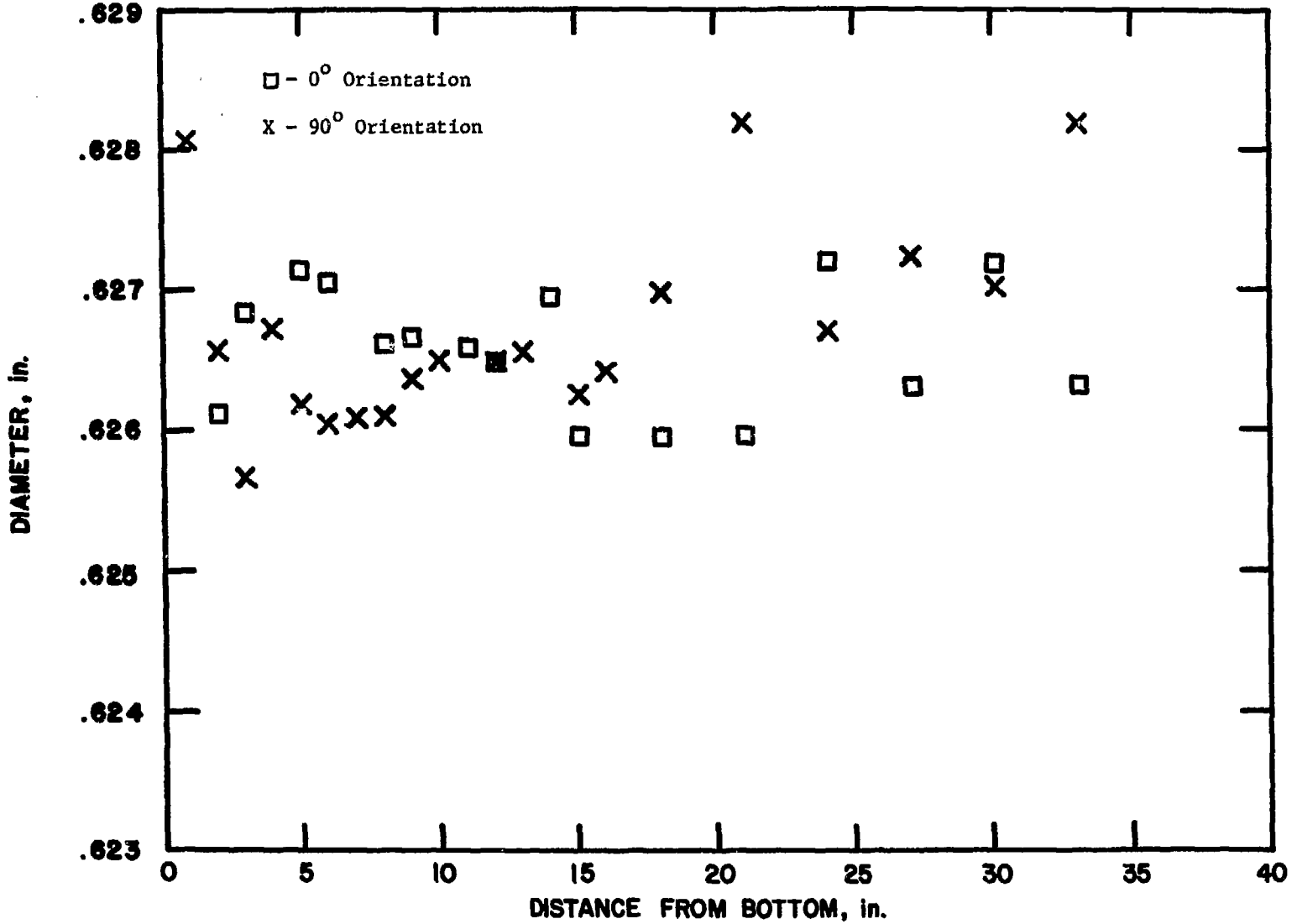

Fig. 35. Postirradiation Diameter Profile of Capsule M (L-4009S)

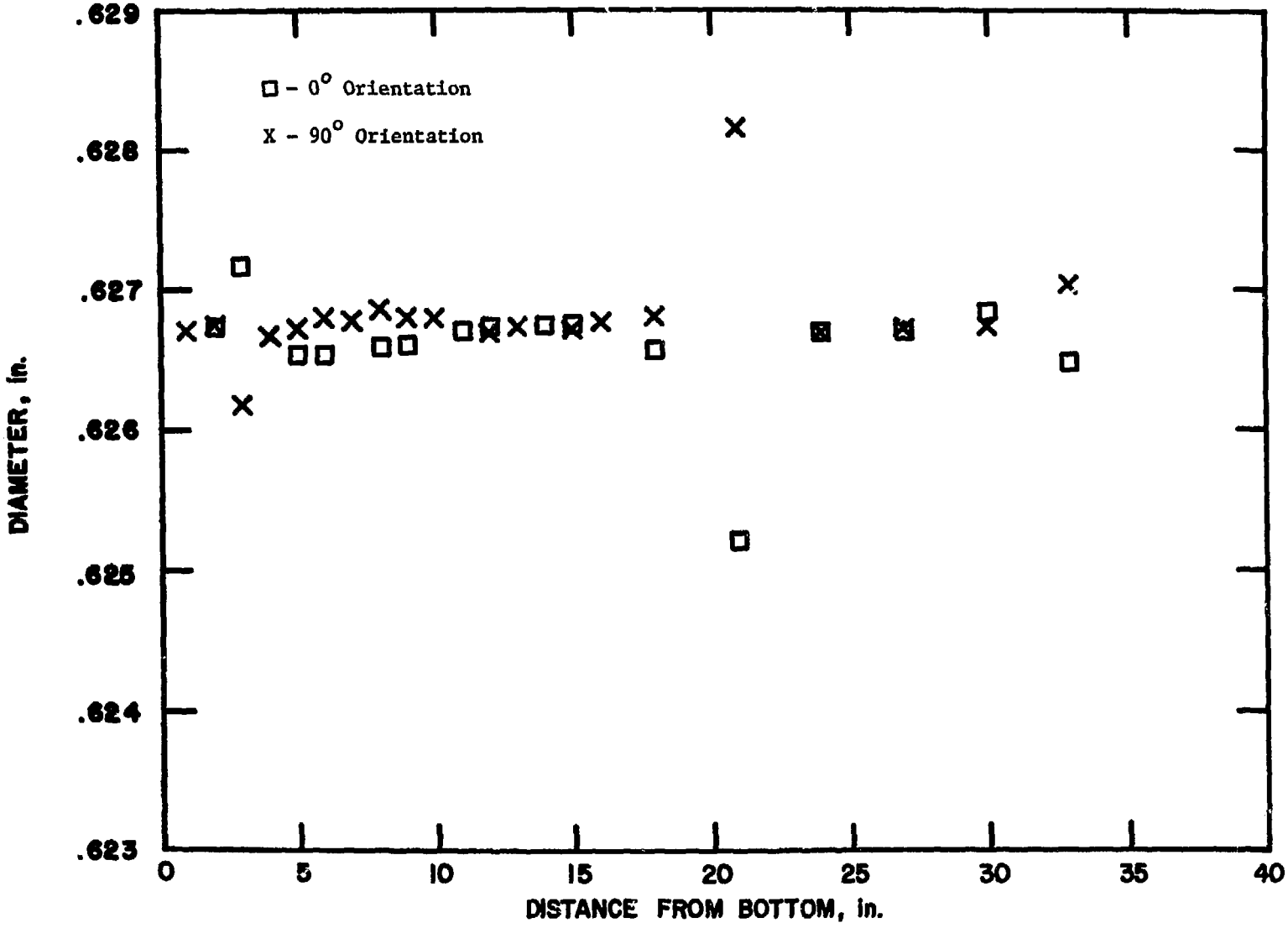

Fig. 36. Preirradiation Diameter Profile of Capsule N (L-4009S)

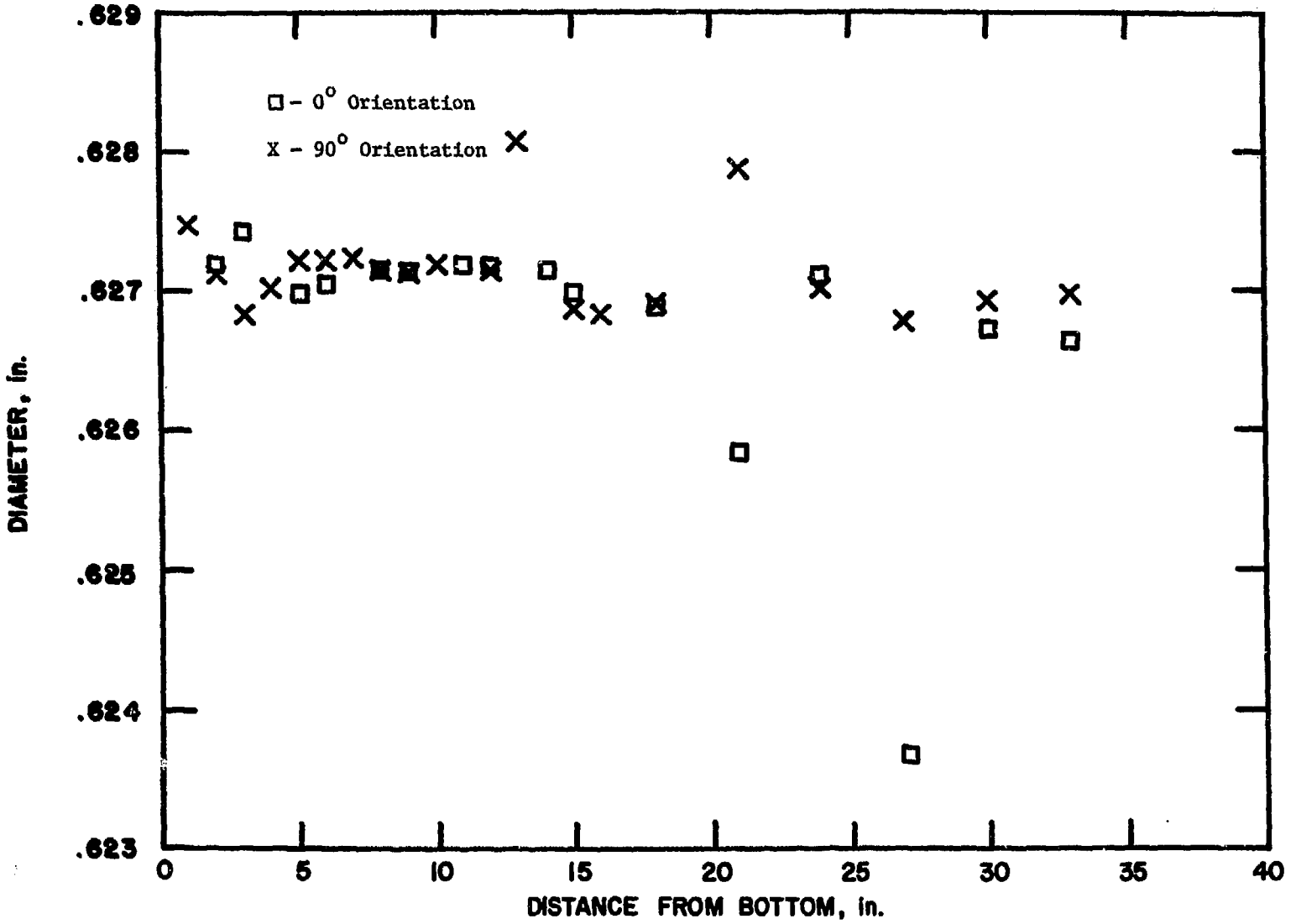

Fig. 37. Postirradiation Diameter Profile of Capsule N (L-4009S)

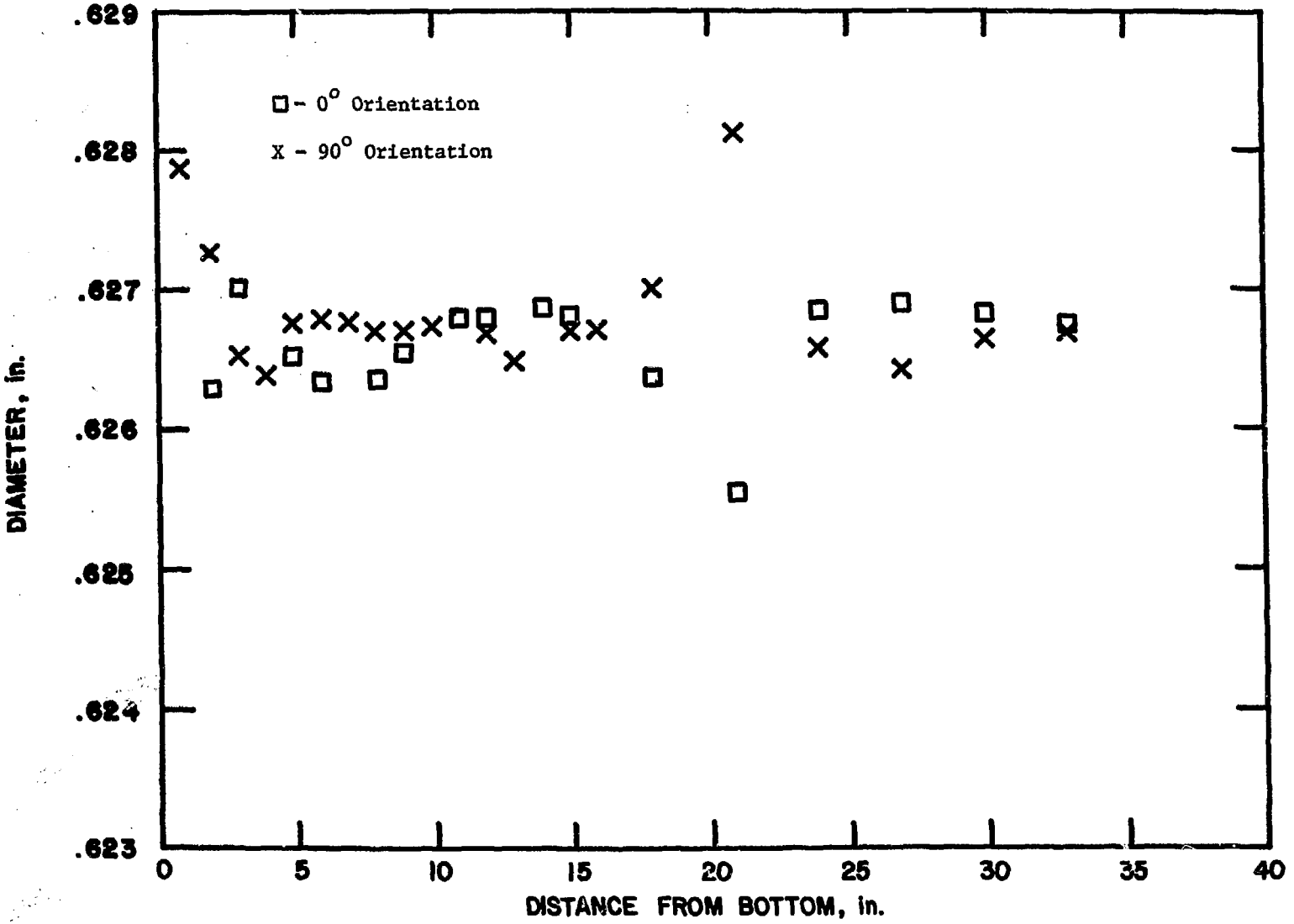

Fig. 38. Preirradiation Diameter Profile of Capsule O(L-4009S)

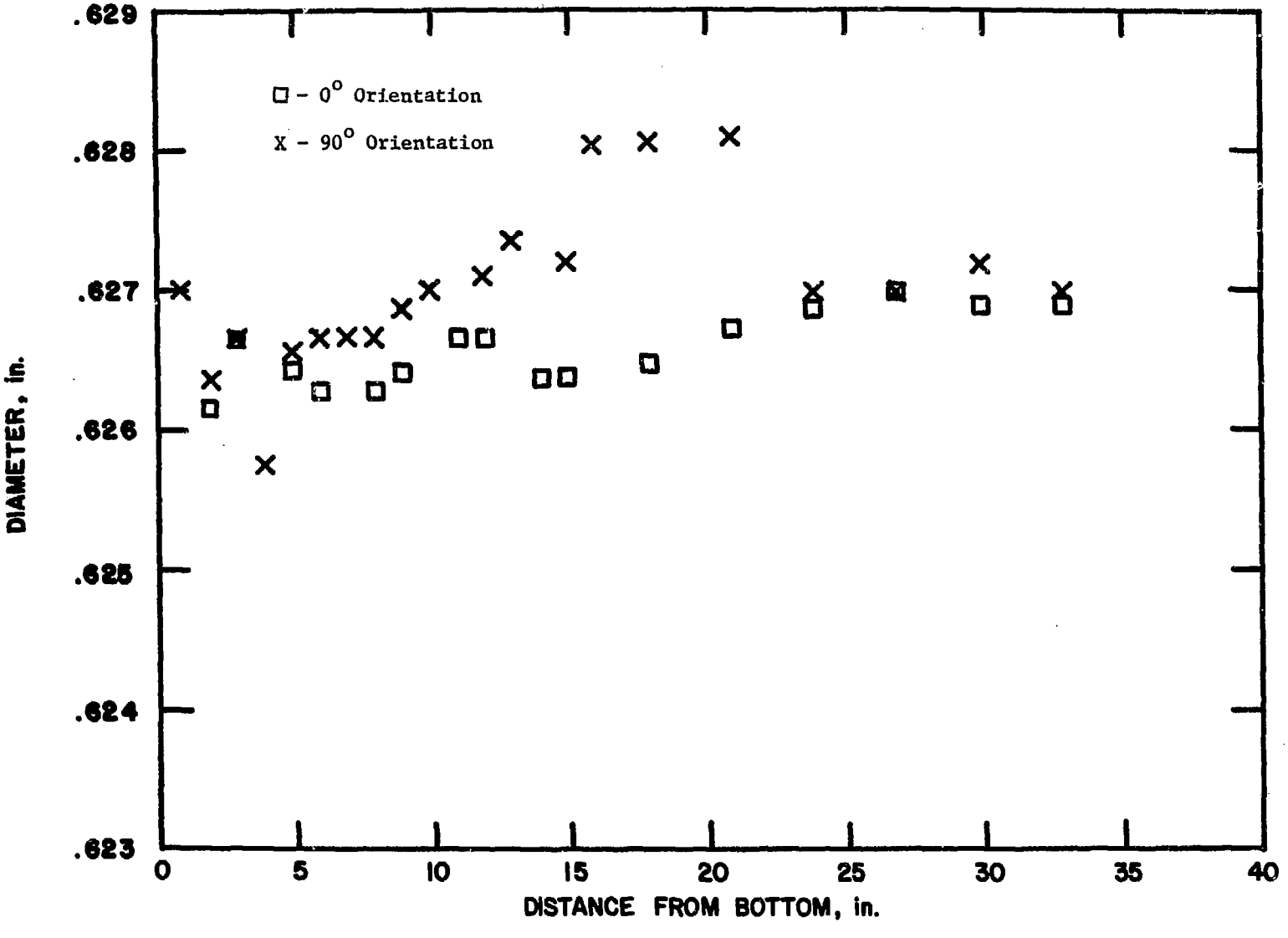

Fig. 39. Postirradiation Diameter Profile of Capsule O(L-4009S)

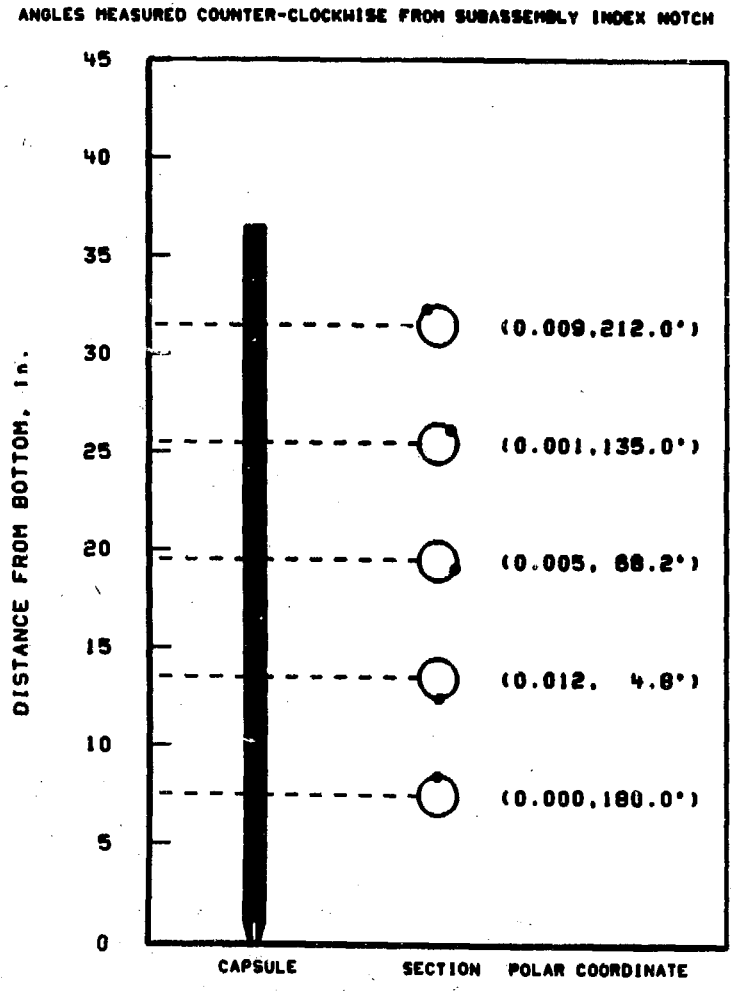

Fig. 40. Bow Results for Capsule A
(L-4008S)

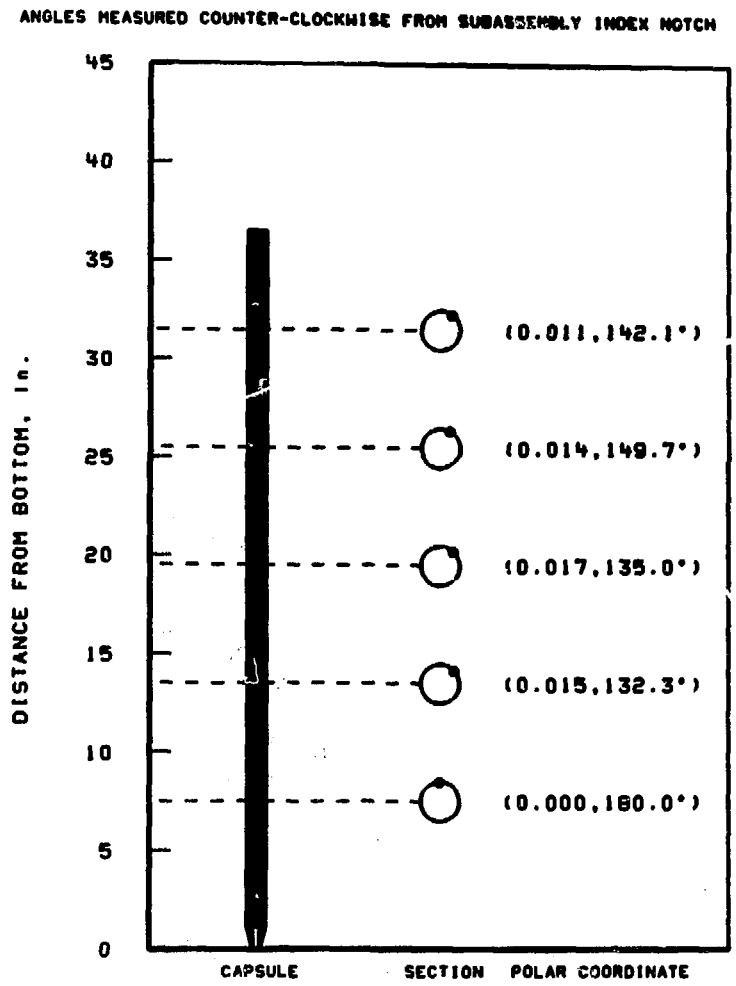

Fig. 41. Bow Results for Capsule B
(L-4008S)

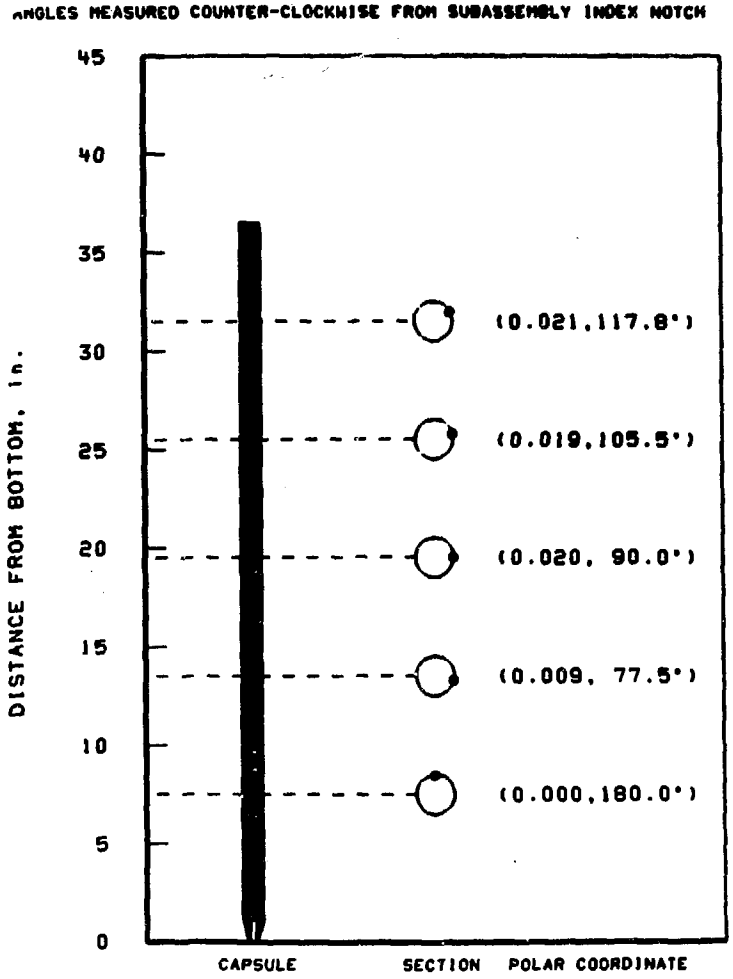

Fig. 42. Bow Results for Capsule C
(L-4008S)

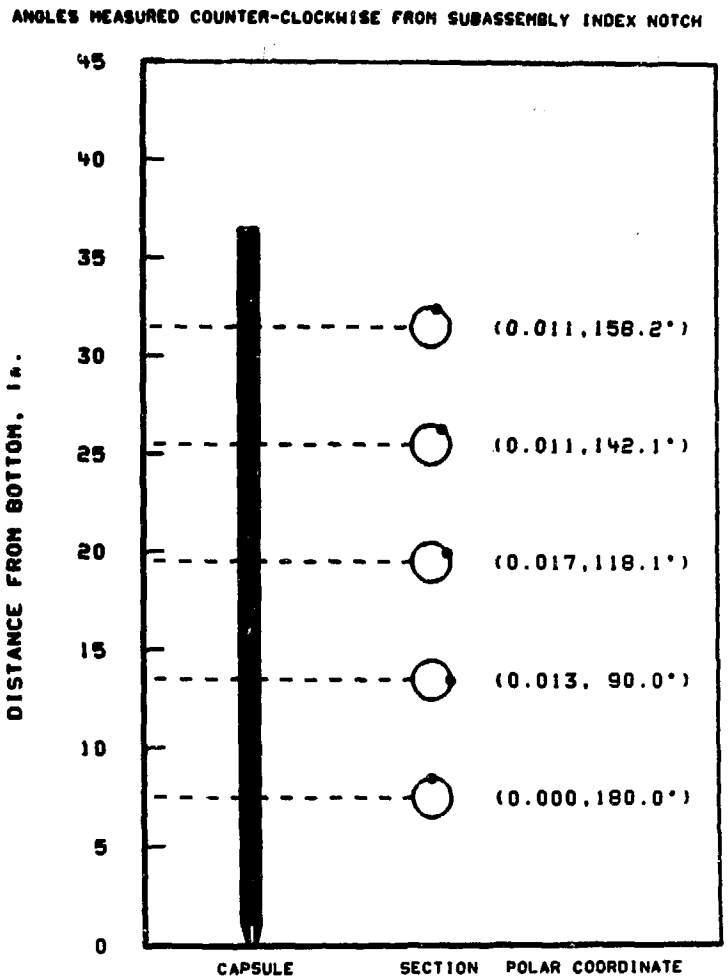

Fig. 43. Bow Results for Capsule E
(L-4008S)

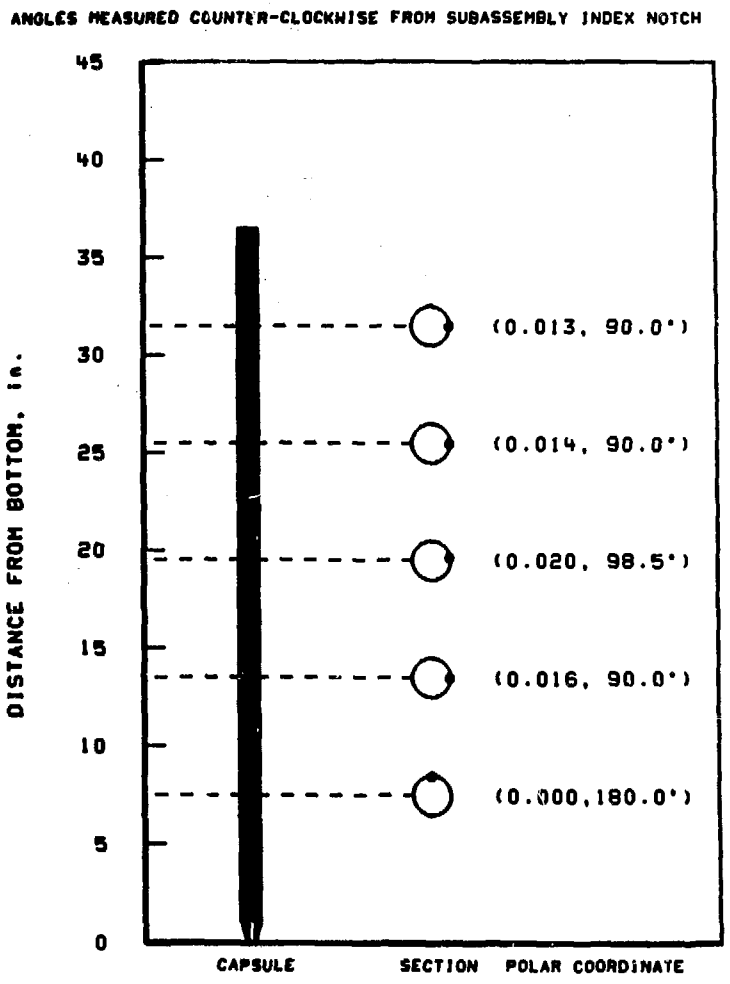

Fig. 44. Bow Results for Capsule F
(L-4008S)

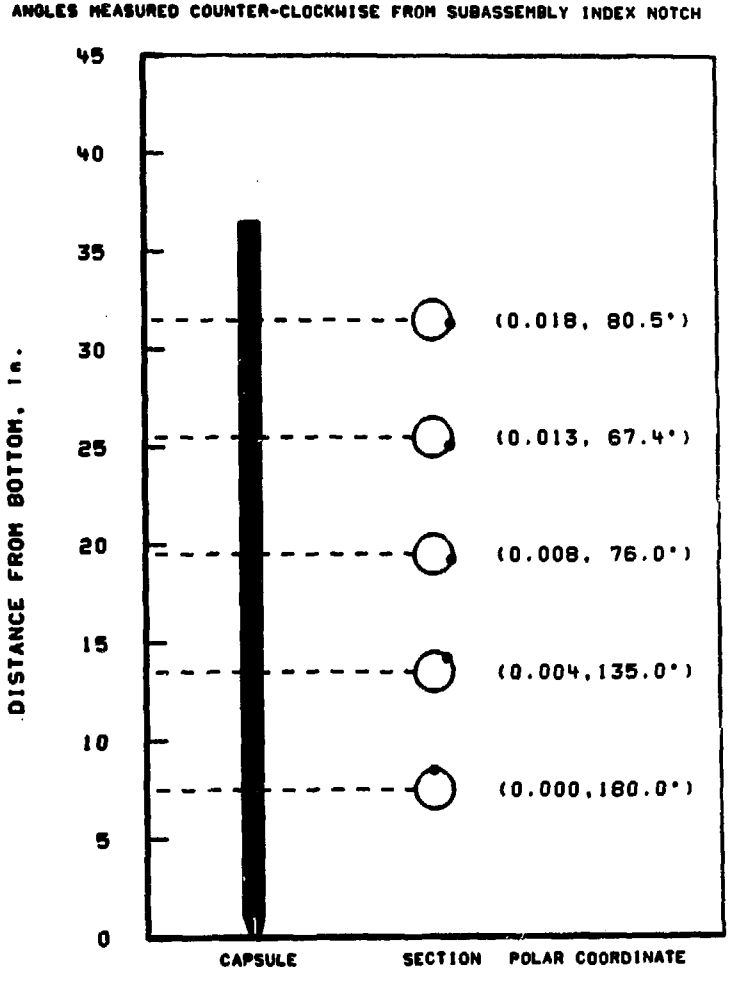

Fig. 45. Bow Results for Capsule G
(L-4008S)

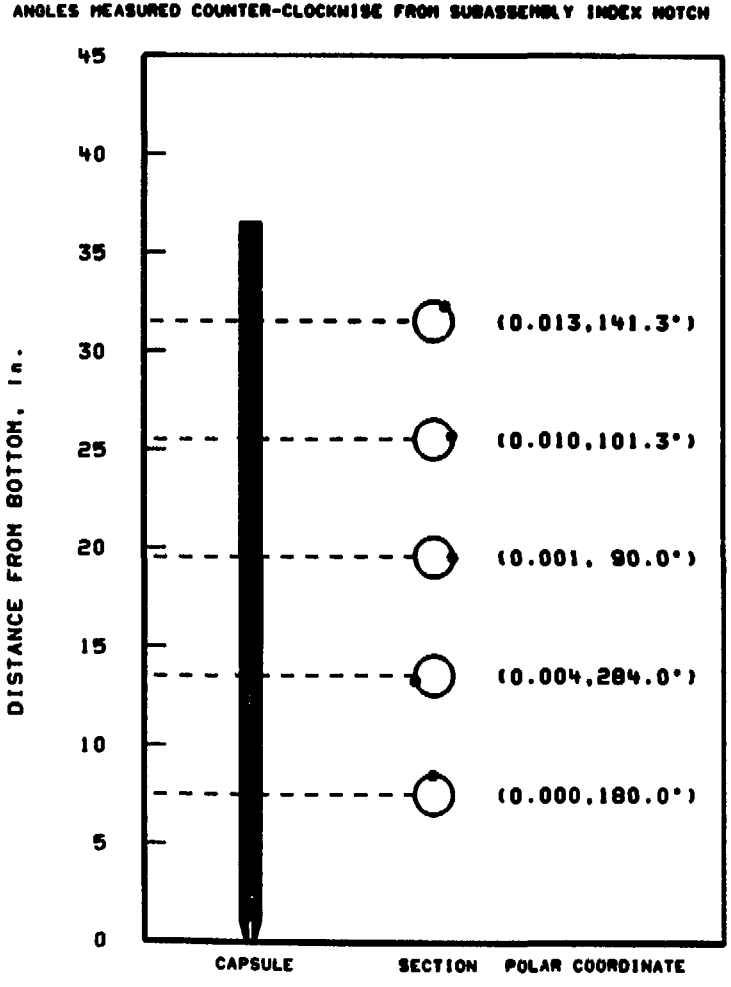

Fig. 46. Bow Results for Capsule H
(L-4008S)

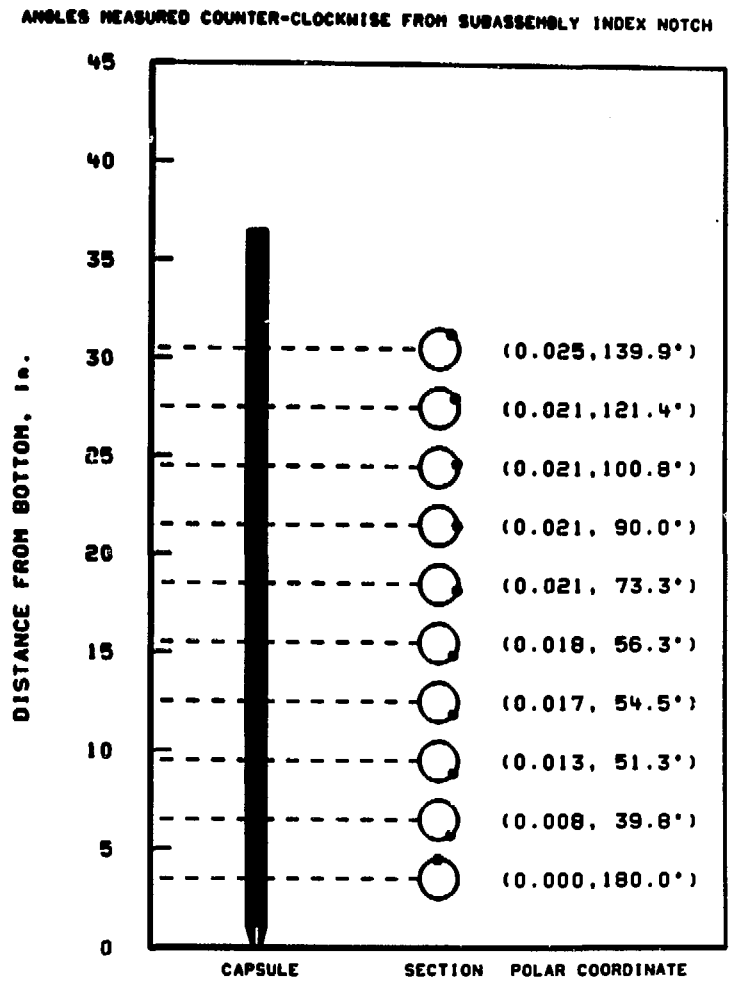

Fig. 47. Bow Results for Capsule D
(L-4009S)

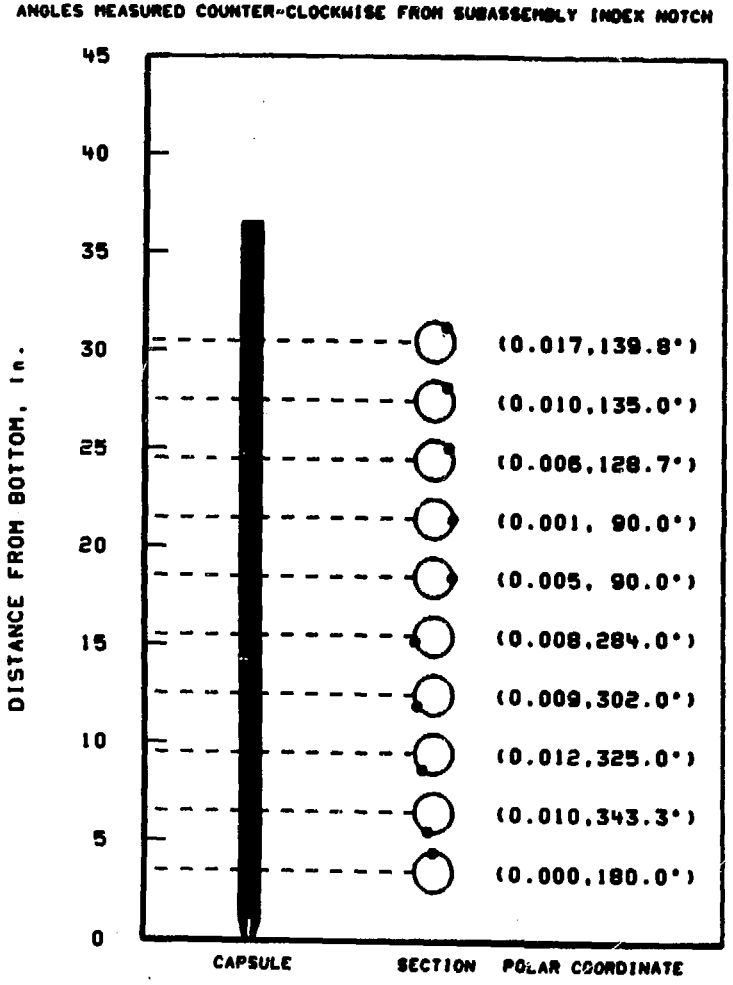

Fig. 48. Bow Results for Capsule J
(L-4009S)

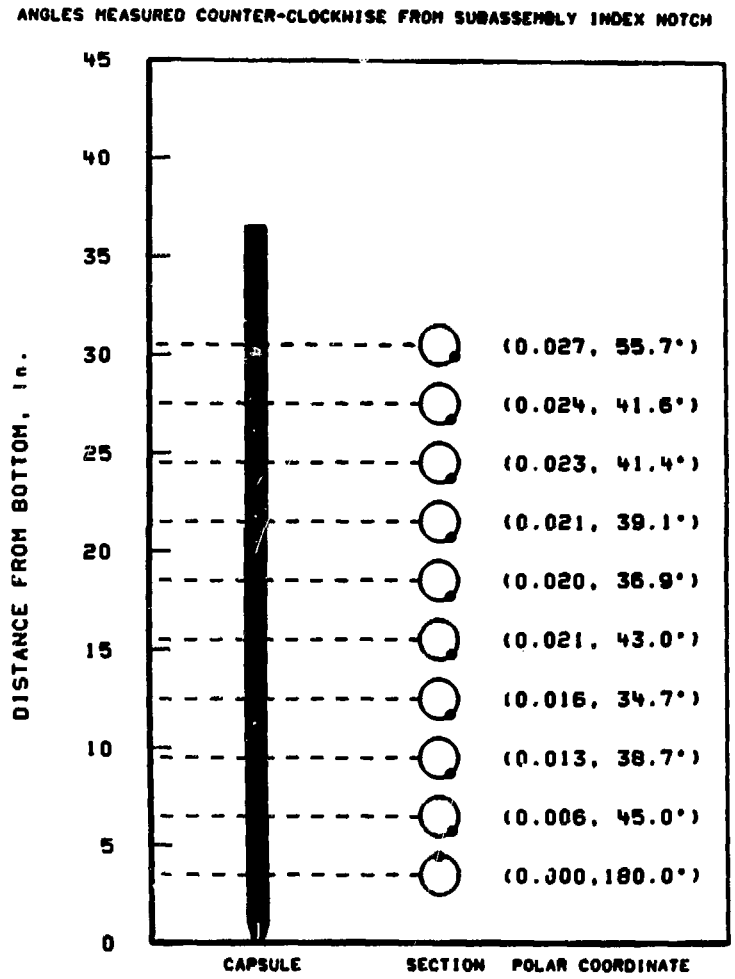

Fig. 49. Bow Results for Capsule K
(L-4009S)

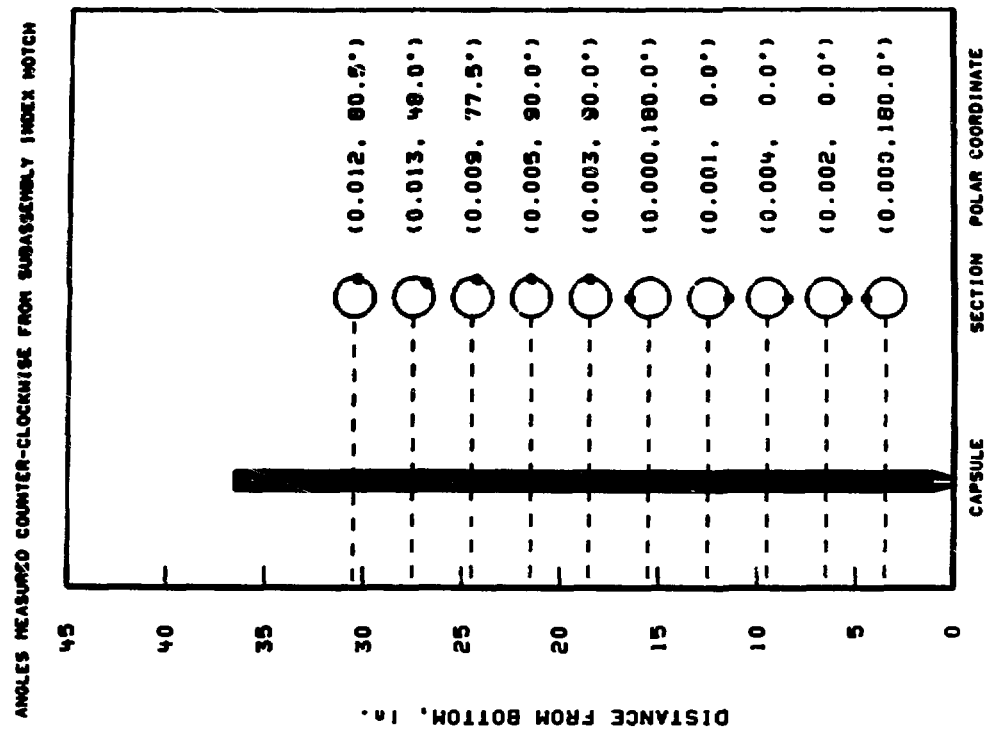

Fig. 51. Bow Results for Capsule M (L-4009S)

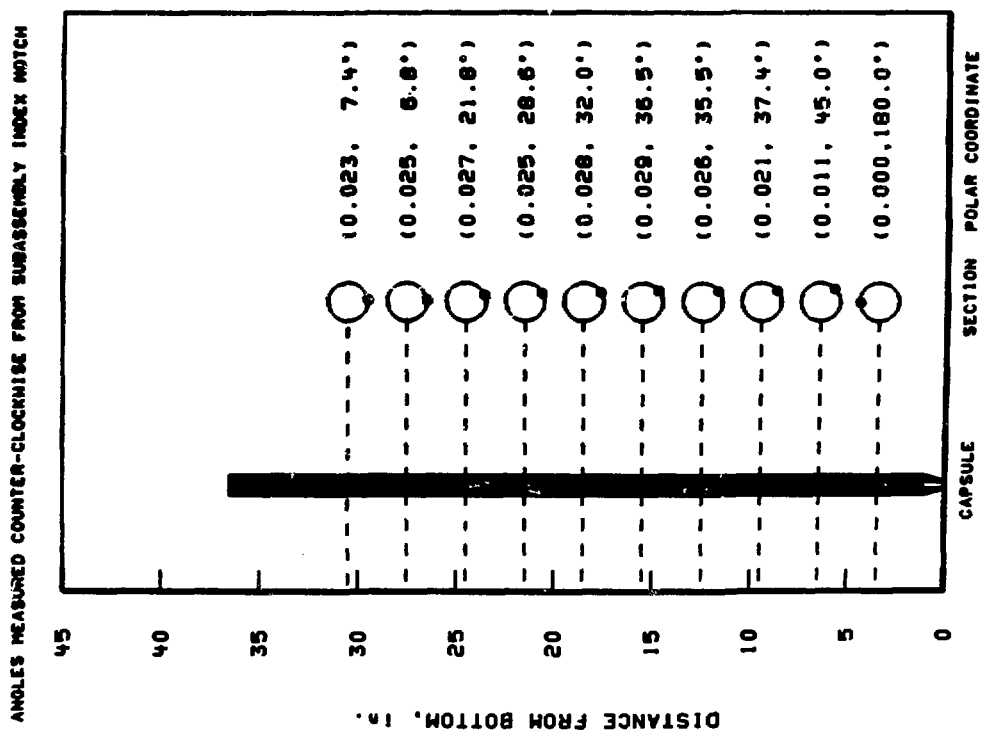

Fig. 50. Bow Results for Capsule L (L-4009S)

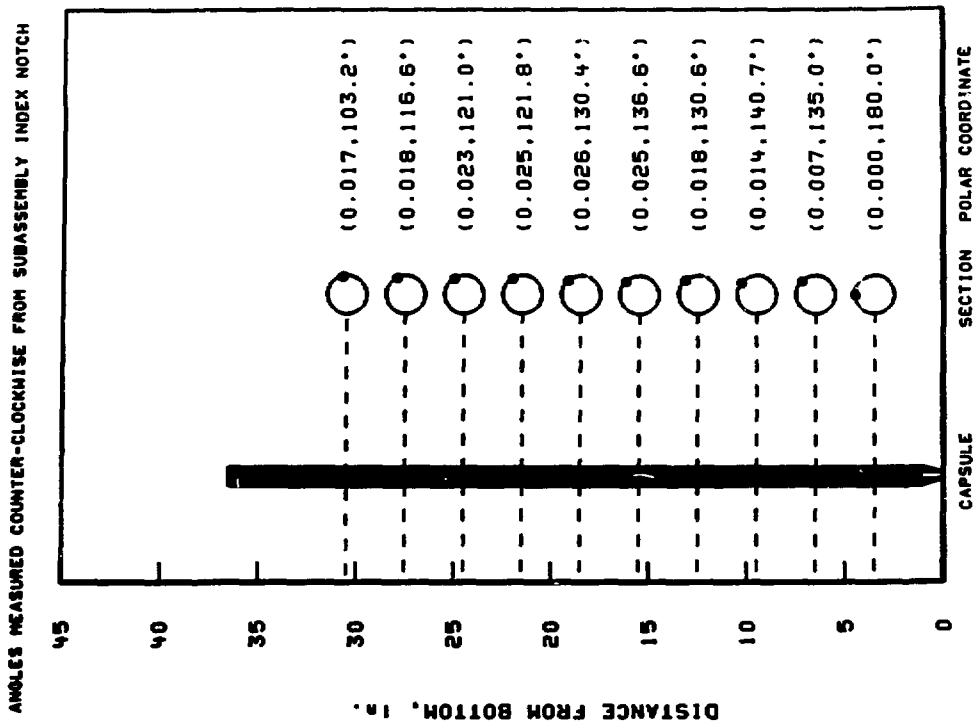

Fig. 53. Bow Results for Capsule O
(L-4009S)

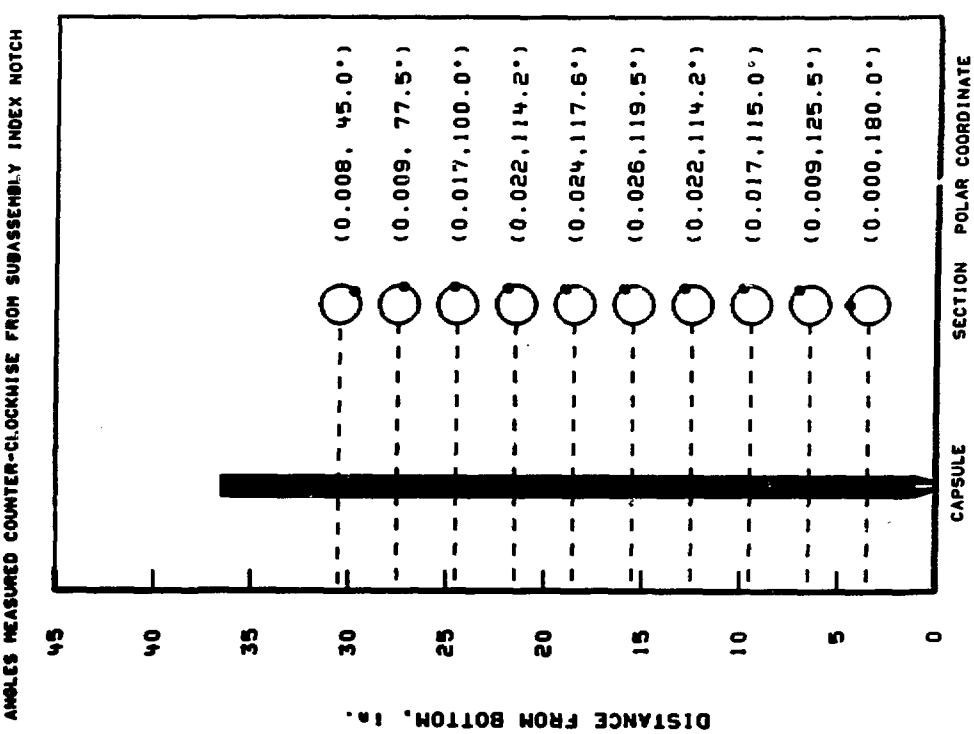

Fig. 52. Bow Results for Capsule N
(L-4009S)

SYMBOL '•' INDICATES DIRECTION OF BOW

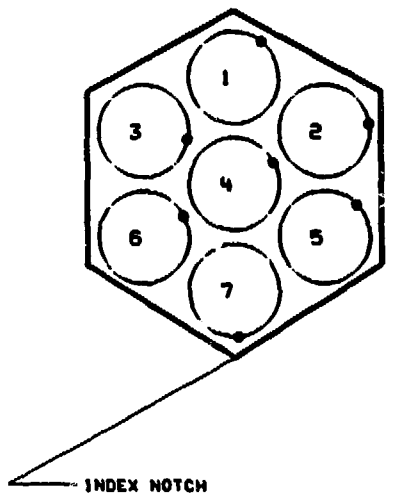

SUBASSEMBLY L4008S
(AT POINT OF MAX BOW ON EACH CAPSULE)

POSITION	CAPSULE	BOW, in.	DIRECTION, deg.	AXIAL POS, in.
6	C	0.021	117.8	31.5
3	G	0.018	80.5	31.5
7	A	0.012	4.8	13.5
4	E	0.017	118.1	19.5
1	H	0.013	141.3	31.5
2	F	0.020	98.5	19.5
5	B	0.017	135.0	19.5

(ANGLES MEASURED COUNTER-CLOCKWISE FROM SUBASSEMBLY INDEX NOTCH)

Fig. 54. Summary of Bow Data for B_4C Capsules from HWCR L-4008S

SYMBOL '•' INDICATES DIRECTION OF BOW

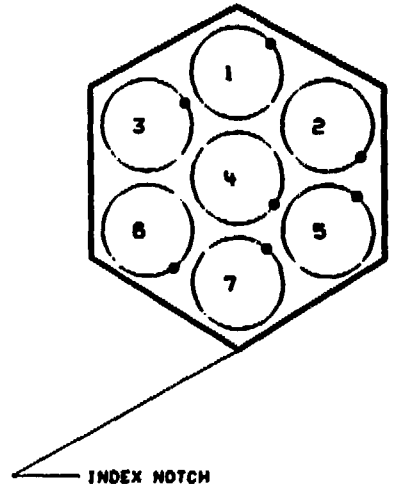

SUBASSEMBLY L4009S
(AT POINT OF MAX BOW ON EACH CAPSULE)

POSITION	CAPSULE	BOW, in.	DIRECTION, deg.	AXIAL POS, in.
5	J	0.017	139.8	30.5
3	N	0.026	119.5	15.5
2	M	0.013	48.0	27.5
7	D	0.025	139.9	30.5
6	L	0.029	36.5	15.5
1	O	0.026	130.4	18.5
4	K	0.027	55.7	30.5

(ANGLES MEASURED COUNTER-CLOCKWISE FROM SUBASSEMBLY INDEX NOTCH)

Fig. 55. Summary of Bow Data for B_4C Capsules from HWCR L-4009S

APPENDIX B

Procedure for Calibrating LGSS Volumes, and Derivation of the Equations to Calculate the Plenum Pressure and Volume

Description of the Procedure

The volume V_A represents the portion of the vacuum system that is located outside of the hot cell. V_A is isolated from the vacuum chamber V_B that contains the capsule to be punctured, designated by V_C. Valve 1 isolates V_A from V_B, and valve 4 represents the puncture that is made in the capsule V_C. The volume V_A is accurately calibrated by a series of gas expansions from a known volume and pressure into V_A.

LGSS CALIBRATION SYSTEM

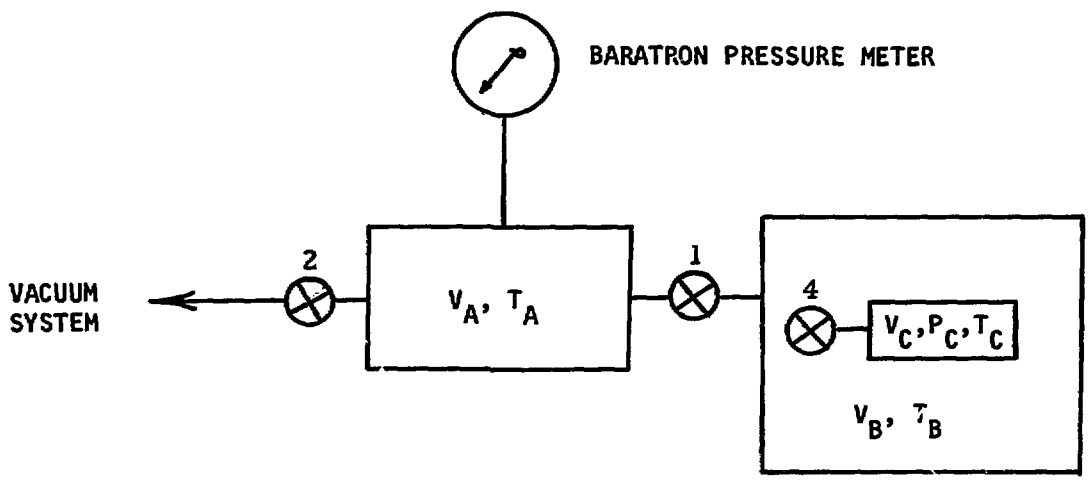

With valve 1 closed, a helium gas pressure of P_o is introduced through valve 2 into V_A. Valve 1 is then opened and the gas expanded into V_B with a final pressure in V_A and V_B of P_f. Thus,

$$\frac{P_o V_A}{T_A} = P_f\left(\frac{V_A}{T_A} + \frac{V_B}{T_B}\right)$$

and

$$V_B = V_A\left(\frac{T_B}{T_A}\right)\left(\frac{P_o}{P_f} - 1\right) \tag{1}$$

Equation (1) is the equation used to calculate the volume of the system before puncture.

Now with valve 1 open, the volumes V_A and V_B are evacuated and valve 2 then closed. The capsule is now punctured, which is represented by valve 4 being opened. The final pressure P_p is then measured for the entire system. P_p is the equilibrium pressure due entirely to the gas released from V_C. We thus have the following relationship.

$$\frac{P_C V_C}{T_C} = P_p\left(\frac{V_A}{T_A} + \frac{V_B}{T_B} + \frac{V_C}{T_C}\right) \tag{2}$$

Of course, we want to determine the capsule plenum pressure P_C and plenum volume V_C.

The next step is to evacuate the entire system (V_A, V_B, and V_C), then close valves 1 and 2. A helium gas pressure P_x is now introduced into volume V_A and V_C by opening valve 1. The final pressure is P_y. The following relationship results:

$$\frac{P_x V_A}{T_A} = P_y\left(\frac{V_A}{T_A} + \frac{V_B}{T_B} + \frac{V_C}{T_C}\right) \tag{3}$$

By substituting equation (1) into equation (3) for V_B we have the following expression for V_C, with all parameters measured:

$$V_C = V_A\left(\frac{T_A}{T_C}\right)\left[\frac{P_x}{P_y} - \frac{P_o}{P_p}\right] \tag{4}$$

The expression for V_C in Eq. (4) is now substituted for V_C in Eq. (2). This now results in the following expression for the plenum pressure, P_C, with all parameters measured:

$$P_C = \frac{P_p P_x P_f}{P_x P_f - P_o P_y} \tag{5}$$

In practice, it was found desirable to repeat the expansions $P_o \rightarrow P_f$ and $P_x \rightarrow P_y$ three times in order to increase the accuracy of the determination. Thus, the values for P_o, P_f, P_x, and P_y are averages of these determinations.

It should be noted that Eq. (5) is independent of temperature, but Eq. (4) for the plenum volume V_C is dependent on the out-of-hot-cell system temperature T_A and the temperature of the capsule T_C. For this report, T_A was considered equal to T_C because the hot cell used was in the work-area air-flow system. The correction for the ratios of the absolute temperatures could thus be ignored.

ACKNOWLEDGMENTS

The authors gratefully acknowledge the efforts, advice, and assistance given by the following individuals: Dr. R. R. Hobbins (ANC; the rest ANL), M. H. Williamson, R. B. Holdsworth, R. W. Swanson (density), R. M. Coleman (cap puncturing, gas composition), H. E. Keckler (^{10}B burnup), and the HFEF operating personnel.

REFERENCES

1. Argonne National Laboratory, Reactor Development Program Progress Report: July 1968, ANL-7478, pp. 57-59 (Aug. 28, 1968).
2. R. A. Cushman, B. R. Sehgal, and V. W. Lowery, Prospectus for Operating EBR-II with High-Worth Control Rods, ANL/EBR-066 (Sept. 1972).
3. D. E. Walker, Preirradiation Characterization of B_4C Pellets Used in Experiment on High-Worth Control Rods, ANL/EBR-051 (Jan. 1972).
4. M. W. Lerner, The Analysis of Elemental Boron, TID-25190, Section 5-3 (1970).
5. E. J. Catanzaro, C. E. Champion, E. L. Garner, G. Marinenko, K. M. Sappenfield, and W. R. Shields, Boric Acid; Isotopic and Assay Standard Reference Materials, NBS Spec. Publ. 260-17 (1970)
6. J. E. Rein and R. M. Abernathey, Rapid Mass-Spectrometric Determination of Boron Isotopic Distribution in Boron Carbide, Talanta 19, pp. 857-862 (1972).
7. Oak Ridge National Laboratory, Fuels and Materials Development Program Quarterly Progress Report for Period Ending December 31, 1971, ORNL-TM-3703, p. 38 (March 1972).
8. D. Mahagin, Hanford Engineering Development Laboratory, private communication (Jan. 1972).
9. Oak Ridge National Laboratory, Fuels and Materials Development Program Quarterly Progress Report for Period Ending March 31, 1972, ORNL-TM-3797, p. 42 (June 1972).
10. J. A. Bashajian, A. L. Pitner, D. E. Mahagin, H. C. F. Ripfel, and D. E. Baker, Irradiation Effects in Boron Carbide Pellets Irradiated in Fast Neutron Spectra, J. Nuclear Technology, 16, (1), p. 238 (Oct. 1972).
11. A. Jostons and C. I. H. Dubose, Microstructure of Boron Carbide After Fast Neutron Irradiation, J. Nuc. Mat. 44, p. 91 (July 1972).